Analysis of the Performance of Ganged Operation of Smoke and Heat Vents with Sprinklers and Draft Curtains

Prepared for

AAMA
Smoke and Heat Vent Task Group
Paul Simony, Chairman

Prepared by

Hughes Associates, Inc.
3610 Commerce Drive, Suite 817
Baltimore, MD 21227-1652 USA
Phone +1.410.737.8677
FAX +1.410.737.8688

18 February 2008

Table of Contents

Section		Page
1.0	Introduction	13
2.0	Computational Fluid Dynamics	14
2.1	Computational Domain	15
2.2	Initial and Boundary Conditions	16
2.3	Growth Rate in Four-Tier Rack-Mounted Plastic Commodities	17
2.4	Heat Release Rate	21
2.5	Configuration for Burning Racks	24
2.6	Smoke and Heat Vents	25
2.7	Makeup Air	25
2.8	Sprinklers	25
2.9	Draft Curtain	26
2.10	Structural Elements	26
2.11	Visibility	27
2.12	Simulation Matrix	29
3.0	Results	30
3.1	Validations	30
3.2	HRR1 Fire Source	32
3.2.1	Run #1 (HRR1SHV0DC0): HRR1 without Smoke and Heat Vents and without Draft Curtains	32
3.2.2	Run #2 (HRR1SHV1DC0): HRR1 with Smoke and Heat Vents and without Draft Curtains	34
3.2.3	Run #3 (HRR1SHV1DC1): HRR1 with Smoke and Heat Vents and with Draft Curtain	36
3.3	HRR2 Fire Source	42
3.3.1	Run #4 (HRR2SHV0DC0): HRR2 without Smoke and Heat Vents and without Draft Curtains	43
3.3.2	Run #5 (HRR2SHV1DC0): HRR2 with Smoke and Heat Vents and without Draft Curtains	44
3.3.3	Run #6 (HRR2SHV1DC1): HRR2 with Smoke and Heat Vents and with Draft Curtain	46
3.4	HRR3 Fire Source	52

3.4.1 Run #7 (HRR3SHV0DC0): HRR3 without Smoke and Heat Vents and without Draft Curtains 53
3.4.2 Run #8 (HRR3SHV1DC0): HRR3 with Smoke and Heat Vents and without Draft Curtains 54
3.4.3 Run #9 (HRR3SHV1DC1): HRR3 with Smoke and Heat Vents and with Draft Curtain ... 56
3.5 Ceiling-Mounted Support Beams 62
3.6 HRR4 Fire Source 68
3.6.1 Run #11 (HRR4SHV0DC0): HRR4 without Smoke and Heat Vents and without Draft Curtains 68
3.6.2 Run #11 (HRR4SHV1DC1): HRR4 With Smoke and Heat Vents and Draft Curtain 70
3.7 Run #13 (HRR3SHV1DC1R): Burning Racks Centered on Row Farthest away from the Draft Curtain 77
3.8 Run #14 (HRR3SHV1DC1RC): Burning Racks Located on Corner Farthest away from the Draft Curtain 81
3.9 Burning Racks Located on Corner Nearest to the Draft Curtain Location 83
3.9.1 Run #15 (HRR3SHV1DC0FC): With Smoke and Heat Vents and Without Draft Curtains 84
3.9.2 Run #16 (HRR3SHV1DC1FC): With Smoke and Heat Vents and Draft Curtain 86
4.0 Discussion 91
5.0 Conclusions 92

List of Figure Captions

Caption **Page**

Figure 1. View of a computational domain with smoke and heat vents and a curtain..... 16

Figure 2. View of a computational domain without vents or curtains. 16

Figure 3. Burning rate of the standard plastic commodity – two, three, and four tiers high. Figure from [Zalosh, 2003], based on the work of [Kung, Spaulding, & You, 1984]. 18

Figure 4. Plastic commodity convective heat release rates from FMRC experiments and from IFS simulations (Figure 47 of [McGrattan, Hamins, & Stroup, 1998])..... 20

Figure 5. The four heat release rate curves used in this study differed in their maximum attained rates and in the duration of their steady burn and decay periods. 20

Figure 6. Example of fire growth methodology for one quarter of the commodity racks that define the flue. The commodities are shown in outline format. Cells that contribute to the heat release rate are marked with an ×. Each cell has a heat release rate per unit area similar to the one shown above. The length of the steady burn period varies from cell to cell. The durations of the ramps vary with heat release rate number. 23

Figure 7. Vents used in simulations with smoke and heat vents..... 24

Figure 8. Comparison of the computed heat release rate for Run 1 (HRR1SHV0DC0) with the HRR1 curve. 32

Figure 9. Comparison of the heat release rate and the sprinkler activation times for Run 1 (HRR1SHV0DC0): HRR1 without smoke and heat vents and without draft curtains. . 33

Figure 10. Sprinkler activation map for Run 1 (HRR1SHV0DC0): HRR1 without smoke and heat vents and without draft curtains. 34

Figure 11. Comparison of the heat release rate and the sprinkler activation times for Run 2 (HRR1SHV1DC0): HRR1 with smoke and heat vents and without draft curtains. 35

Figure 12. Sprinkler activation map for Run 2 (HRR1SHV1DC0): HRR1 with smoke and heat vents and without draft curtains. 35

Figure 13. Comparison of the heat release rate and the sprinkler activation times for Run 3 (HRR1SHV1DC1): HRR1 with smoke and heat vents and with draft curtain. 36

Figure 14. Sprinkler activation map for Run 3 (HRR1SHV1DC1): HRR1 with smoke and heat vents

and with draft curtain. 37

Figure 15. Comparison of the net building smoke masses remaining in the building for Runs 1 - 3 (HRR1SHV0DC0, HRR1SHV1DC0, HRR1SHV1DC1). 38

Figure 16. Visibility (in ft) along y = 0 ft at 200 s for HRR1 Runs 1 - 3. The vertical coordinate has been stretched..... 39

Figure 17. Visibility (in ft) along y = 0 ft at 220 s for HRR1 Runs 1 - 3. The vertical coordinate has been stretched..... 40

Figure 18. Visibility (in ft) along y = 0 ft at 240 s for HRR1 Runs 1 - 3. The vertical coordinate has been stretched..... 41

Figure 19. Comparison of the computed heat release rate for Run 4 (HRR2SHV0DC0) with the HRR2 curve..... 42

Figure 20. Comparison of the heat release rate and the sprinkler activation times for Run #4 (HRR2SHV0DC0): HRR2 without smoke and heat vents and without draft curtains.. 43

Figure 21. Sprinkler activation map for Run #4 (HRR2SHV0DC0): HRR2 without smoke and heat vents and without draft curtains. 44

Figure 22. Comparison of the heat release rate and the sprinkler activation times for Run #5 (HRR2SHV1DC0): HRR2 with smoke and heat vents and without draft curtains. 45

Figure 23. Sprinkler activation map for Run #5 (HRR2SHV1DC0): HRR2 with smoke and heat vents and without draft curtains. 45

Figure 24. Comparison of the heat release rate and the sprinkler activation times for Run #6 (HRR2SHV1DC1): HRR2 with smoke and heat vents and with draft curtain. 46

Figure 25. Sprinkler activation map for Run #6 (HRR2SHV1DC1): HRR2 with smoke and heat vents and with draft curtain. 47

Figure 26. Comparison of the net building smoke masses remaining in the building Runs 4 - 6 (HRR2SHV0DC0, HRR2SHV1DC0, HRR2SHV1DC1). 48

Figure 27. Visibility (in ft) along y = 0 ft at 180 s for HRR2 Runs 4 - 6. The vertical coordinate has been stretched..... 49

Figure 28. Visibility (in ft) along y = 0 ft at 270 s for HRR2 Runs 4 - 6. The vertical coordinate has been stretched..... 50

Figure 29. Visibility (in ft) along y = 0 ft at 360 s for HRR2 Runs 4 - 6. The vertical coordinate has been stretched. 51

Figure 30. Comparison of the computed heat release rate for Run 7 (HRR3SHV0DC0) with the HRR3 curve. 52

Figure 31. Comparison of the heat release rate and the sprinkler activation times for Run #7 (HRR3SHV0DC0): HRR3 without smoke and heat vents and without draft curtains. . 53

Figure 32. Sprinkler activation map for Run #7 (HRR3SHV0DC0): HRR3 without smoke and heat vents and without draft curtains. 54

Figure 33. Comparison of the heat release rate and the sprinkler activation times for Run #8 (HRR3SHV1DC0): HRR3 with smoke and heat vents and without draft curtains. 55

Figure 34. Sprinkler activation map for Run #8 (HRR3SHV1DC0): HRR3 with smoke and heat vents and without draft curtains. 55

Figure 35. Comparison of the heat release rate and the sprinkler activation times for Run #9 (HRR3SHV1DC1): HRR3 with smoke and heat vents and with draft curtains. 56

Figure 36. Sprinkler activation map for Run #9 (HRR3SHV1DC1): HRR3 with smoke and heat vents and with draft curtains. 57

Figure 37. Comparison of the net building smoke masses remaining in the building for Runs 7 - 10 (HRR3SHV0DC0, HRR3SHV1DC0, HRR3SHV1DC1, HRR3SHV1DC1CB). 58

Figure 38. Visibility (in ft) along y = 0 ft at 300 s for HRR3 Runs 7 - 9. The vertical coordinate has been stretched. 59

Figure 39. Visibility (in ft) along y = 0 ft at 600 s for HRR3 Runs 7 - 9. The vertical coordinate has been stretched. 60

Figure 40. Visibility (in ft) along y = 0 ft at 900 s for HRR3 Runs 7 - 9. The vertical coordinate has been stretched. 61

Figure 41. Comparison of the heat release rate and the sprinkler activation times for Run #10 (HRR3SHV1DC1CB): HRR3 with smoke and heat vents and with draft curtains and beams at the ceiling. 63

Figure 42. Sprinkler activation map for Run #10 (HRR3SHV1DC1CB): HRR3 with smoke and heat vents and with draft curtains and beams at the ceiling. 63

Figure 43. Visibility (in ft) along y = -20 ft at 35 s for HRR3 Runs 9 and 10. 64

Figure 44. Visibility (in ft) along *y* = -20 ft at 57 s for HRR3 Runs 9 and 10. 64

Figure 45. Visibility (in ft) along *y* = -20 ft at 78 s for HRR3 Runs 9 and 10. 65

Figure 46. Visibility (in ft) along *y* = -20 ft at 90 s for HRR3 Runs 9 and 10. 65

Figure 47. Visibility (in ft) along *y* = -20 ft at 300 s for HRR3 Runs 9 and 10. 66

Figure 48. Visibility (in ft) along *y* = -20 ft at 600 s for HRR3 Runs 9 and 10. 66

Figure 49. Visibility (in ft) along *y* = -20 ft at 900 s for HRR3 Runs 9 and 10. 67

Figure 50. Comparison of the computed heat release rate for Run 11 (HRR4SHV1DC1) with the HRR4 curve. 68

Figure 51. Comparison of the heat release rate and the sprinkler activation times for Run #11 (HRR4SHV0DC0): HRR4 Without Smoke and Heat Vents and Without Draft Curtains. 69

Figure 52. Sprinkler activation map for Run #11 (HRR4SHV0DC0): HRR4 without smoke and heat vents and without draft curtains. 69

Figure 53. Comparison of the heat release rate and the sprinkler activation times for Run #12 (HRR4SHV1DC1): HRR4 with smoke and heat vents and with draft curtain. 70

Figure 54. Sprinkler activation map for Run #12 (HRR4SHV1DC1): HRR4 with smoke and heat vents and with draft curtain. 71

Figure 55. Comparison of the building net smoke masses for Runs 11 - 12 (HRR4SHV0DC0, HRR4SHV1DC1). 72

Figure 56. Visibility (in ft) along *y* = 0 ft at 300 s. The vertical coordinate has been stretched. ... 73

Figure 57. Visibility (in ft) along *y* = 0 ft at 600 s. The vertical coordinate has been stretched. ... 73

Figure 58. Visibility (in ft) along *y* = 0 ft at 900 s. The vertical coordinate has been stretched. ... 74

Figure 59. Visibility (in ft) along *y* = 0 ft at 1200 s. The vertical coordinate has been stretched. . 74

Figure 60. Visibility (in ft) along *y* = 0 ft at 1500 s. The vertical coordinate has been stretched. . 75

Figure 61. Visibility (in ft) along *y* = 0 ft at 1800 s. The vertical coordinate has been stretched. . 75

Figure 62. Visibility (in ft) along *y* = 0 ft at 2100 s. The vertical coordinate has been stretched. . 76

Figure 63. Visibility (in ft) along *y* = 0 ft at 2400 s. The vertical coordinate has been stretched. . 76

Figure 64. View of the computational domain for Run 13 (HRR3SHV1DC1R): burning racks centered on row farthest away from the draft curtain. 77

Figure 65. Comparison of the heat release rate and the sprinkler activation times for Run 13 (HRR3SHV1DC1R): burning racks centered on row farthest away from the draft curtain. 78

Figure 66. Sprinkler activation map for Run 13 (HRR3SHV1DC1R): burning racks centered on row farthest away from the draft curtain. 79

Figure 67. Visibility (in ft) along $y = 0$ ft for Run 13 (HRR3SHV1DC1R): burning racks centered on row farthest away from the draft curtain. The vertical coordinate has been stretched.. 80

Figure 68. View of the computational domain for Run 14 (HRR3SHV1DC1RC): burning racks located on the corner farthest away from the draft curtain. 81

Figure 69. Comparison of the heat release rate and the sprinkler activation times for Run 14 (HRR3SHV1DC1RC): burning racks located on corner farthest away from the draft curtain. 81

Figure 70. Sprinkler activation map for Run 14 (HRR3SHV1DC1RC): burning racks located on corner farthest away from the draft curtain. 82

Figure 71. Visibility (in ft) along $y = 0$ ft for Run 14 (HRR3SHV1DC1RC): burning racks located on corner farthest away from the draft curtain. The vertical coordinate has been stretched.83

Figure 72. View of the computational domain for Run 15 (HRR3SHV1DC0FC): burning racks located on corner nearest to the draft curtain location with smoke and heat vents and without draft curtains. 84

Figure 73. Comparison of the heat release rate and the sprinkler activation times for Run 15 (HRR3SHV1DC0FC): burning racks located on corner nearest to the draft curtain location with smoke and heat vents and without draft curtains. 85

Figure 74. Sprinkler activation map for Run 15 (HRR3SHV1DC0FC): burning racks located on corner nearest to the draft curtain location with smoke and heat vents and without draft curtains. 85

Figure 75. View of the computational domain for Run 16 (HRR3SHV1DC1FC): burning racks located on corner nearest to the draft curtain location with smoke and heat vents and with draft curtains. 86

Figure 76. Comparison of the heat release rate and the sprinkler activation times for Run 16 (HRR3SHV1DC1FC): burning racks located on corner nearest to the draft curtain location

with smoke and heat vents and with draft curtains. 86

Figure 77. Sprinkler activation map for Run 16 (HRR3SHV1DC1FC): burning racks located on corner nearest to the draft curtain location with smoke and heat vents and with draft curtains. 87

Figure 78. Visibility (in ft) along y = 0 ft at 300 s for HRR3 Runs 15 and 16. The burning racks are located on the corner nearest to the draft curtain location. The vertical coordinate has been stretched. 88

Figure 79. Visibility (in ft) along y = 0 ft at 600 s for HRR3 Runs 15 and 16. The burning racks are located on the corner nearest to the draft curtain location. The vertical coordinate has been stretched. 88

Figure 80. Visibility (in ft) along y = 0 ft at 900 s for HRR3 Runs 15 and 16. The burning racks are located on the corner nearest to the draft curtain location. The vertical coordinate has been stretched. 89

Figure 81. Comparison of the net building smoke masses for Runs 13 - 16 (HRR3SHV1DC1R, HRR3SHV1DC1RC, HRR3SHV1DC0FC, HRR3SHV1DC1FC)..... 90

List of Table Captions

Caption **Page**

Table 1: Summary of FDS input parameters used in this study..... 15

Table 2: Thermal properties, as input, of the thermally thick surfaces used in the FDS modeling. 17

Table 3: Sprinkler activation results for the plastic commodity test series as reported in [McGrattan, Hamins, & Stroup, 1998]. The plus sign was used by the authors to indicate that the sprinkler activations went to the edge of the 14,400 sq. ft. facility. 21

Table 4: Summary of the heat release rate histories. All had the same t^2 growth rate of 1.78 kW/s^2. 22

Table 5: Distinguishing features of the simulations used in this study. The results for sprinkler performance are also included. 30

Table 6: Sprinkler activation results for the heptane spray burner test series II as reported in [McGrattan, Hamins, & Stroup, 1998]. 31

EXECUTIVE SUMMARY

The objective of this study was to evaluate the performance of gang operated smoke and heat vent systems in sprinklered facilities. The gang operation concept involves opening all the vents within the coverage area of the sprinkler system in which the fire originates one minute after the first sprinkler has operated.

A numerical study was undertaken to explore the performance of gang operated smoke and heat vents, working with and without draft curtains, in an 7,430 m^2 (80,000 sq. ft.) sprinklered warehouse. A range of fire growth histories were employed in the study to span the range of actual sprinkler performance. Simulations were done with and without draft curtains and the location of the fire was varied. Modeling results of sprinkler operations compared favorably with testing available in the literature.

Comparison of sprinkler operations between vented and unvented cases clearly shows that the operation of sprinklers was not affected by smoke and heat vents or by smoke and heat vents with draft curtains. The time to first sprinkler operation, the number of sprinkler operations and the pattern of operation were not impacted by the venting system. The use of a one minute delay in vent operation allowed all sprinklers capable of applying water to the fire to operate before the vents operated, thus assuring that the sprinkler system performance would be unimpeded by the venting.

The use of ganged smoke and heat vents markedly reduced the smoke logging of the building. The visibility in the warehouse was measurably and qualitatively enhanced. The total quantity of smoke mass remaining in the building was found to be an effective metric for smoke and heat vent performance. Typically, venting reduced the total smoke load in the facility by an order of magnitude and drastically reduced the total exposure of goods to smoke.

The impact of smoke and heat venting upon the visibility and general environment for firefighting was significantly enhanced. For challenging fires without smoke and heat venting, loss of visibility was nearly complete. With smoke and heat venting, excellent visibility was maintained throughout the facility including in the area of actual sprinkler operation.

While excellent smoke and heat vent performance was realized even without draft curtains, the inclusion of draft curtains delineating sprinkler coverage areas enhanced smoke extraction and limited

lateral movement of smoke to areas outside the sprinkler coverage area where the fire occurred. Lateral smoke movement was shown to have negative impacts upon goods stored high in the racks and upon every object from the top of the racks to the ceiling. For fires with sprinkler operations adjacent to draft curtains, smoke drag down allowed smoke to move under the draft curtain. While this allowed some smoke exposure for goods high in the racks in the adjacent zone, overall performance remained quite satisfactory. The modeling results indicate that draft curtains offer value to owners and their insurers by limiting smoke damage to the building and contents outside the coverage area of the sprinkler system where the fire occurred.

While only limited data for smoke production from controlled fires is available in the literature, the modeling results show that smoke and heat venting is very effective in removing smoke even for heat release rates associated with controlled fires. This facilitates fire department operations to extinguish the controlled fire.

This investigation has shown that ganged operation of smoke and heat vents is highly effective in removing heat and smoke from the building. The action of the smoke and heat vent system markedly improved the visibility throughout the building and significantly reduced the exposure of the building and contents to smoke. Draft curtains, although not vital to the performance of the smoke and heat vents, did limit lateral spread of smoke to other zones and enhanced the extraction of smoke from the building. The operation of the smoke and heat vent system had no effect on the operation of sprinklers and as such maintained the operational effectiveness of the sprinkler system while improving the conditions within the building in support of fire department operations.

Analysis of the Performance of Ganged Operation of Smoke and Heat Vents with Sprinklers and Draft Curtains

1.0 Introduction

Smoke and heat vents, working in conjunction with draft curtains, have long been used as an effective fire protection measure. They can typically be found installed in industrial buildings, warehouses, stores, and malls. Their significance is recognized throughout the professional fire protection literature. The National Fire Protection Association (NFPA) has a standard dealing with smoke and heat vents [NFPA 204, 2007]. NFPA 92A [2006] and NFPA 92B [2005] can also be consulted for further smoke management practices. The *NFPA Fire Protection Handbook* contains a chapter entitled "Venting Practices" [Heskestad, 2003] which provides introductory material and design guidelines. The Society of Fire Protection Engineers' (SPFE's) handbook also contains a chapter [Cooper, 2002] which covers more of the physics behind the design criteria.

Current US design of smoke and heat vents typically utilizes thermal activation of individual vents. In Europe, it is typical to have smoke and heat vents operate in a ganged fashion. Ganged operation can provide more efficient venting in sprinklered facilities where the activation of individual vents is limited by the thermal management provided by the sprinklers. To eliminate any potential effect of venting upon the operation of sprinklers that provide water to the burning area, vent operation one minute after the first sprinkler operates will allow the sprinklers to operate without potential interference, yet provide effective venting of smoke and heat. For ganged operation based upon water flow, vents located within the area covered by the sprinkler system in which a sprinkler activates will open one minute after sprinkler water flow is detected.

In this investigation, the effectiveness of smoke and heat venting with ganged operation of vents was evaluated using computational fluid dynamics (CFD). The modeled building was an 7,430 m^2 (80,000 sq. ft.) warehouse that was 8.23 m (27 feet)† tall. The space was divided into two sprinkler systems each having a coverage area of 3,720 m^2 (40,000 ft^2). Thirty industry standard 2.44 m×1.22 m (8′×4′) vents were placed in each coverage area in a manner such that they were not

† This is the maximum height used in the tests reported in [McGrattan, Hamins, & Stroup, 1998].

coincident with sprinklers and were not obstructed in any way. Ganged operation occurred over the entire sprinkler system coverage area for a single sprinkler system. It was initiated by the activation of the sprinkler system with a one minute delay from the detection of flowing water. Some scenarios included a 6′ deep draft curtain that divided the two protection areas. No merchandise was stored underneath this draft curtain.

CFD was used to investigate the performance of the design. The employed model was a later version of that used in [McGrattan, Hamins, & Stroup, 1998] as well as in [Trelles & Beyler, 1999a; Trelles & Beyler, 1999b; Trelles & Beyler, 1999c; Beyler, 2006]. The goal is to follow [McGrattan, Hamins, & Stroup, 1998] whenever possible. Some example exceptions include circumstances in which [McGrattan, Hamins, & Stroup, 1998] did not obtain good results and the employment of a full warehouse.

2.0 Computational Fluid Dynamics

The Fire Dynamics Simulator, version 4 (FDS4), was used to perform the field calculations. FDS4 is a three-dimensional large eddy simulation CFD program developed at the National Institute of Standards and Technology's (NIST's) Building and Fire Research Laboratory (BFRL) [McGrattan & Forney, 2004; McGrattan, 2005]. FDS4 is a multidimensional, multiphysics simulation that solves the low Mach number equations of expandable flow [Rehm & Baum, 1978]. FDS was specifically written to address fire scenarios. It has over a twenty year development history. Some of its antecedents include the Industrial Fire Simulator (IFS) and LES3D. The current version of FDS (4.0.7) contains updated source code from these previous projects. FDS can handle isothermal or thermally variable flows. It can directly simulate the effects of turbulence or it can perform large eddy simulations of turbulence. It can also handle axisymmetric cylindrical, two-dimensional Cartesian, and three-dimensional Cartesian coordinates. FDS4 uses Lagrangian droplet transport to simulate the delivery of water from suppression systems. The droplets and the fluid mechanics are coupled. The flow of air and gas components affect the drag on the droplets. The force that the droplets exert on the surrounding gas shows up as a body force in the Eulerian momentum equations. This coupling allows the model to simulate sprinkler-smoke layer interaction. Some validation studies for FDS4 and its predecessors are given in [Baum, McGrattan, & Rehm, R.G., 1994; Baum, McGrattan, & Rehm, 1996; Baum, McGrattan, & Rehm, 1997; Floyd & Lattimer, 2004; McGrattan, 2005; McGrattan, Baum, &

Rehm, 1996; McGrattan, Baum, Walton, & Trelles, 1997; McGrattan, Hamins, & Stroup, 1998; Najafi, Salley, Joglar, and Dreisbach, 2006; Trelles, Mawhinney, & DiNenno, 2004].

Table 1: Summary of FDS input parameters used in this study

Category	Parameter	Value
CFD Domain	Facility	7,430 m^2 (80,000 ft^2) warehouse
	Simulation dimensions	122 m×61.0 m×8.23 m (400′×200′×27′)
Numerical	Grid dimensions	400×200×27 cells
	Cell size	30.5 cm×30.5 cm×30.5 cm (12″×12″×12″)
	Exterior boundary condition	Insulated
Fuel	Type	Std. plastic commodity
	Heat release rate per unit area $\dot{Q}''$	500 kW/m^2 (215 BTU/s/lbm)
	Soot yield y_s	0.10
	Heat of combustion ΔH_c	27 MJ/kg (11,600 BTU/lbm)
	Visibility contrast coefficient c	3
	Specific extinction coefficient K_s	8710 m^2/kg (42,500 ft^2/lbm)
Leakage	Walls	2.0 m^2 (21.5 ft^2)
Environment	Indoor temperature	15.6 °C (60 °F)
	Outdoor temperature	15.6 °C (60 °F)
Sprinkler	Model	K-11
	Pressure	1.3 bar (18.9 psig)
	K-factor	166 L/min/$bar^{1/2}$ (11.5 gal/min/$psig^{1/2}$)
	Volumetric flow rate	189 L/min (49.9 gal/min)
	Spray angles	10° - 80°
	Initial droplet velocity	30 m/s (67 mph)
	Mean droplet diameter d_m	0.9 mm (0.0354″)
	Rosin-Rammler exponent γ	2.43
	Log-normal standard deviation σ	0.58
	RTI	148 $(m \cdot s)^{1/2}$ (268 $(ft \cdot s)^{1/2}$)
	Activation temperature	74 °C (165 °F)
	Water temperature	15.6 °C (60 °F)
S & H Vents	Location	Ceiling, array centered on each design area
	Area	2.44 m×1.22 m (8′×4′)
	Configuration	5×6 per design area
	Number of design areas	2
	Open time	127 s
Inlet Vents	Location	All walls
	Area	2.74 m×3.05 m (9′×10′)
	Configuration	7 on long side, 3 on short side
	Spacing	12.8 m on long side, 13.5 m on short side (42′ on long side, 44′ on short side)

2.1 Computational Domain

The details of the computational domain are summarized in Table 1 and in Figures 1 and 2.

The dimensions of the computational domain were 123 m (400 ft) in the x-direction, 61.0 m (200 ft) in the y-direction, and 8.23 m (27 ft) in the z-direction. There were 400 cells in the x-direction, 200 in the y-direction, and 27 in the z-direction. Thus the resolution was 30.5 cm (12 in) in the x-direction, y-direction, and z-direction. The total number of cells was 2,160,000.

2.2 Initial and Boundary Conditions

The indoor and outdoor temperatures were set to 60 °F. Internal warehouse conditions were calm with the exception of the random disturbances used by FDS to initialize each run. The thermal boundary conditions that were used are given in Table 2. FDS allows either the triplet (density, ρ, specific heat, c, and thermal conductivity, k) or the pair (thermal diffusivity, α, and k) to be input. Table 2 reflects the chosen input option. The outer walls were given the thermal properties of fiberglass insulation because in a composite steel-insulation wall, the insulation controls the heat transfer.

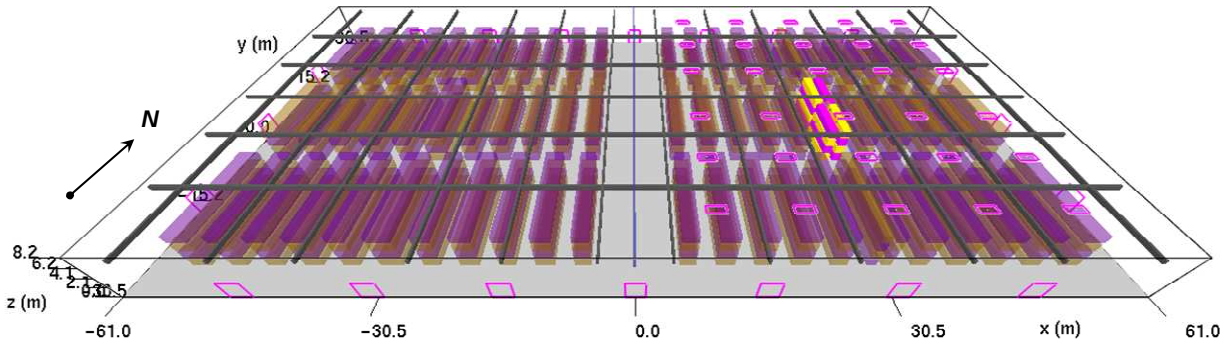

Figure 1. View of a computational domain with smoke and heat vents and a curtain.

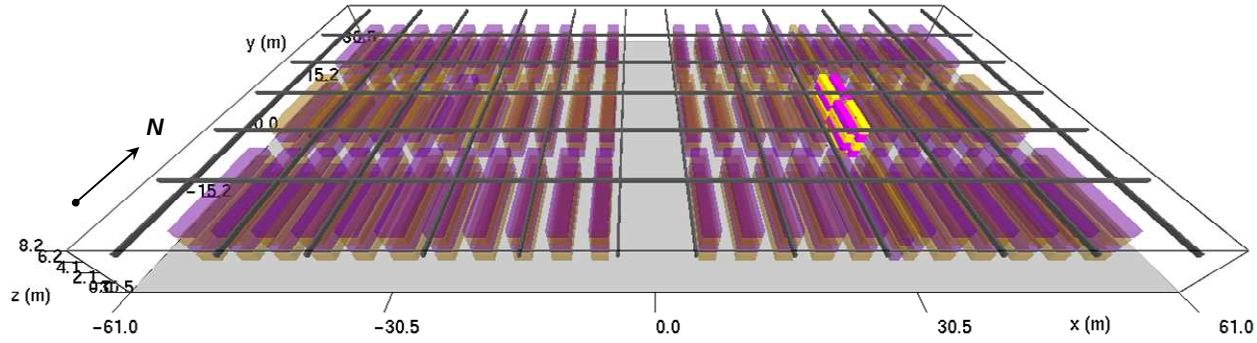

Figure 2. View of a computational domain without vents or curtains.

Table 2: Thermal properties, as input, of the thermally thick surfaces used in the FDS modeling.

Surface Name	Thermal Conductivity k [W/(m·K)]	Density ρ [kg/m^3]	Specific Heat c [J/(kg·K)]	Thermal Diffusivity [m^2/s]	Reference
Floor (concrete)	1.0	2,100	880	▬	[Quintiere, 1998]
Ceiling (Armstrong Ceramagard)	0.064	▬	▬	2.6×10^{-7}	[McGrattan, Hamins, & Stroup, 1998]
FibGlasInsul (glass wool)	0.038	24	700	▬	[Holman, 1986]
STEEL	40	7,800	460	▬	[Quintiere, 1998]
Commodity (cardboard)	0.05	400	1,300	▬	[Holman, 1986] [Lienhard IV & Lienhard V, 2006] [Yu, Lee, & Kung, 1994]

2.3 Growth Rate in Four-Tier Rack-Mounted Plastic Commodities

Commodities are typically stored in cardboard boxes. Pallet loads are vertically arranged either in tiers or in piles (some researchers use the term "stacks"). Rack mounting is achieved with the aid of a warehouse's rows of storage structures. Piling is realized by stacking one pallet load on top of another. In either arrangement, when multiple pallet loads are grouped together, the vertical spaces in between loads constitute the flue spaces in the case of a fire. Vertical spread is greatly assisted by the presence of these flues. Horizontal spread is controlled by the packaging (typically cardboard). The burn rate that occurs after the growth period is determined by the materials within in the boxes. The initial flame spread is vertical and quite rapid. Once the fire has burned to the top of the flue space, the remainder of the growth period is governed by lateral flame spread in the flues. (See Figure 3.) Growth essentially ends when the flames have involved all the contiguous pallet loads. Further information can be obtained from Yao [1997], Zalosh [2003], and Golinveaux & Hankins [2003].

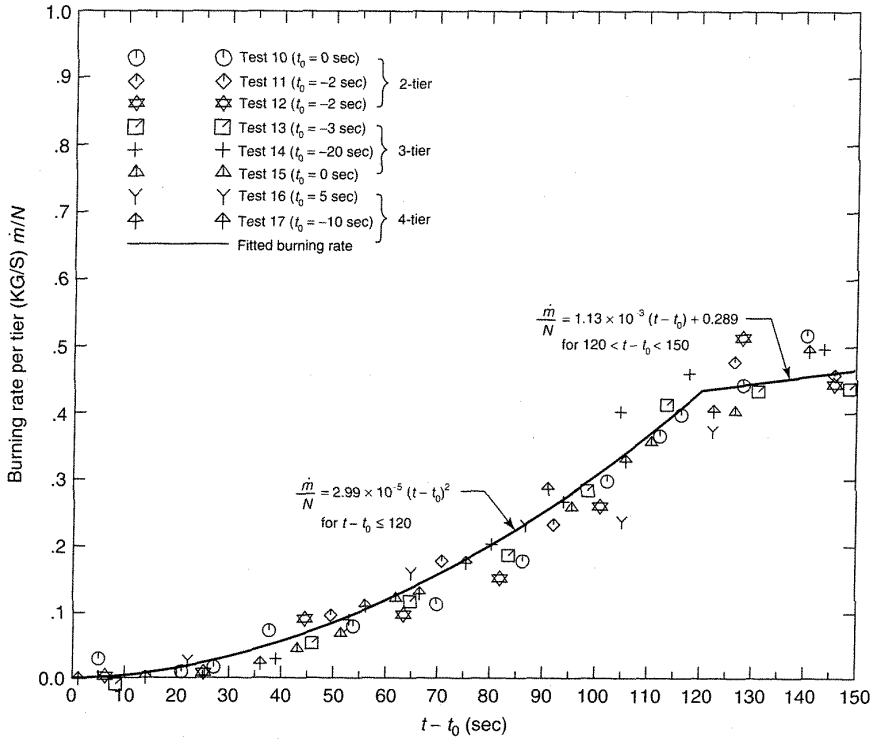

Figure 3. Burning rate of the standard plastic commodity – two, three, and four tiers high. Figure from [Zalosh, 2003], based on the work of [Kung, Spaulding, & You, 1984].

Pioneering work in the field of commodity fire hazards was performed by the Factory Mutual Research Corporation (FMRC). The standard plastic commodity was developed by FMRC. It consists of a set of cardboard boxes filled with a total of 1000 polystyrene cups contained in eight partitioned cartons. A collection of these boxes is mounted on a pallet. This constitutes the standard plastic commodity. Each pallet load has the overall dimensions of 1.07 m (3.51 ft) in the horizontal directions and 1.05 m (3.44 ft) in the vertical, yielding a volume of 1.2 m^3 (42.5 ft^3) [Lee, 1987].

The heat of combustion, ΔH_C, for the plastic commodity is 27 MJ/kg (11,600 BTU/lbm) [Lee, 1987; Spaulding, 1988]. Fire growth data for fuels in storage arrays was determined from the experimental results reported in Kung et al. [1984]. Measurements of mass burning rates obtained by Kung et al. [1984] are shown in Figure 3 and indicate that the mass burning rates for the standard plastic commodity is directly proportional to the number of rack storage tiers. The curve fit burning rate in Figure 3 (as developed by [Kung et al., 1984]) provides a growth rate expression for the standard plastic commodity in a four-tier arrangement that follows the widely used t^2-fire form:

$$\dot{Q} = 3.23 t^2 \qquad \text{for} \quad t \le 120 \text{ s}, \quad t \text{ in s}, \quad \dot{Q} \text{ in kW}, \tag{1}$$

where $\dot{Q}$ is the heat release rate (kW) and t in the time (s). Although the cumulative heat release rate (HRR) depends on the number of tiers, the HRR per unit combustible area does not. For the standard plastic commodity based upon the prior Factory Mutual references,

$$\dot{Q}'' = 498 \text{ kW/m}^2 = 214 \text{ BTU/s/ft}^2. \quad (2)$$

This certainly is not the heat release rate per unit area at the surface even though for the purpose of calculations it is used as that. At the surface there is only volitalization, i.e., no combustion. The actual heat comes from the flame surface that is off the body of the fuel. This surface is correspondingly larger than the fuel surface area. Therefore the heat flux per area coming off of the flame surface would be lower than that given in Eq. (2). However, since the flame area is non-standard, being subject to great variability due to influences such as available oxygen and the magnitude of crosswinds, it is of greater utility to define $\dot{Q}''$ on the fuel area that can burn.

Using the early FMRC data presents several challenges. Many of the technical reports are not publicly available. Although the FMRC authors did find the opportunity to publish some of their results, they rarely published heat release rate data. Equation (1) suffers from the fact that it was derived from data published in various reports and articles. Serendipitously, as part of the NFPA Research Foundation study, FMRC heat release rate data was included in McGrattan et al [1998]. Figure 4 shows freeburn data for a four-tier standard rack. Keeping in mind that Figure 4 shows the convective heat release rate, it can be determine that, approximately,

$$\dot{Q} \approx 1.78 t^2 \qquad t \text{ in s}, \qquad \dot{Q} \text{ in kW}. \quad (3)$$

The heat release rate per unit area used by McGrattan et al [1998],

$$\dot{Q}'' = 500 \text{ kW/m}^2 = 215 \text{ BTU/s/ft}^2, \quad (4)$$

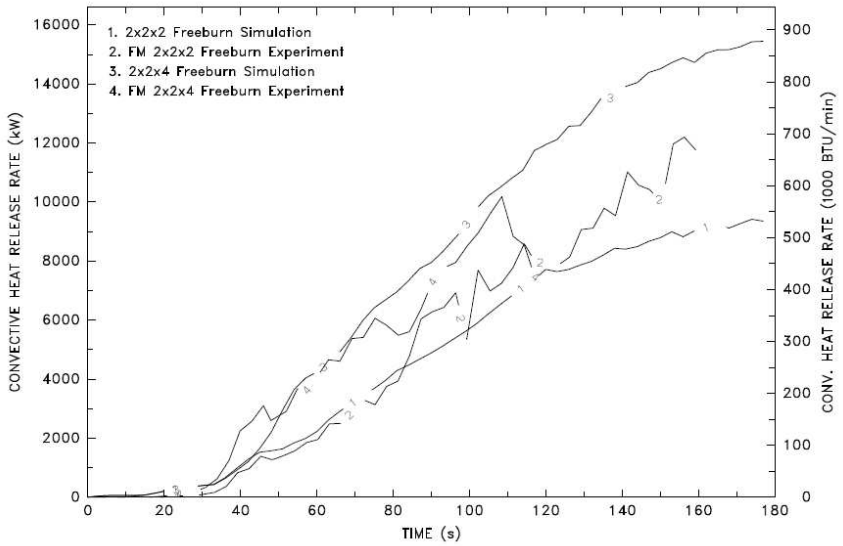

Figure 4. Plastic commodity convective heat release rates from FMRC experiments and from IFS simulations (Figure 47 of [McGrattan, Hamins, & Stroup, 1998]).

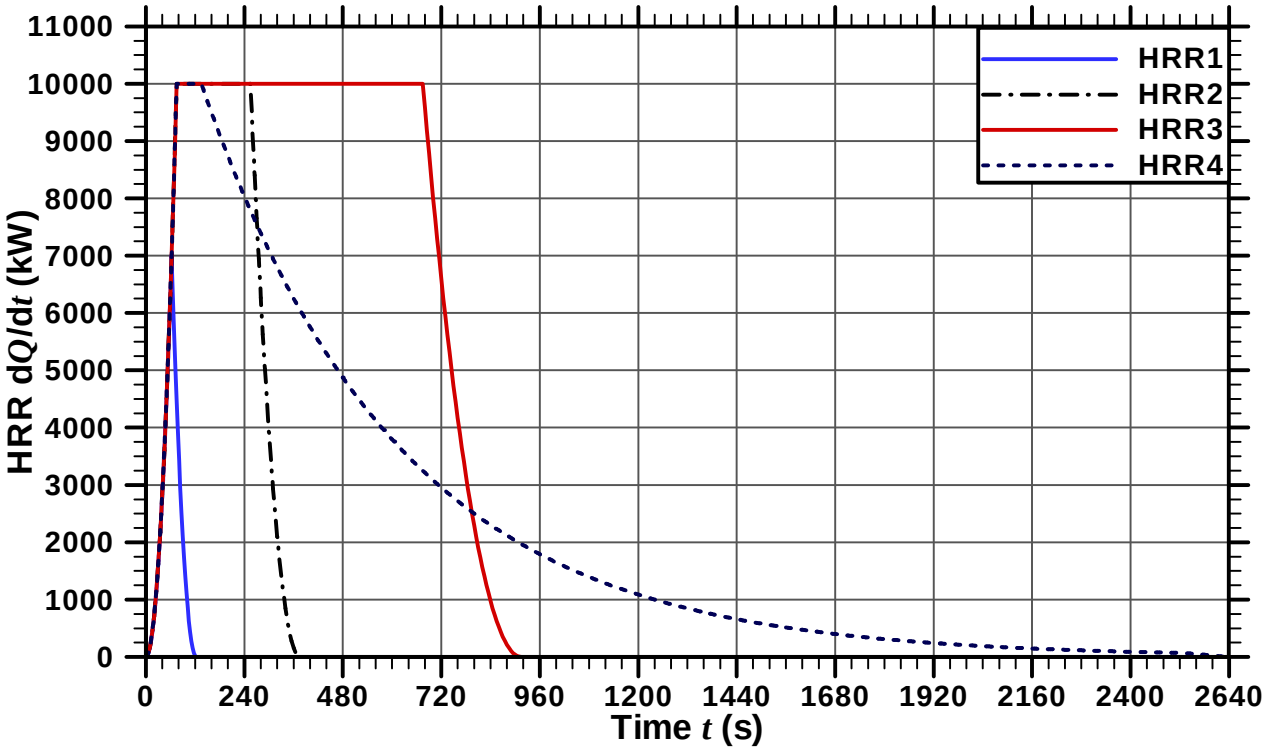

Figure 5. The four heat release rate curves used in this study differed in their maximum attained rates and in the duration of their steady burn and decay periods.

is very close to that in Eq. (2). For these reasons it was decided to base the plastic commodity fire properties used in this study on Eqs. (3 and 4).

Table 3: Sprinkler activation results for the plastic commodity test series as reported in [McGrattan, Hamins, & Stroup, 1998]. The plus sign was used by the authors to indicate that the sprinkler activations went to the edge of the 14,400 sq. ft. facility.

Run #	Flue Position	1st Sprink Act Time	# of Active Sprinklers
P-1	D	76 s	20
P-2	A	100 s	23+
P-3	B	67 s	19+
P-4	D	93 s	5
P-5	D	74 s	7

2.4 Heat Release Rate

In their simulations, McGrattan, Hamins, & Stroup [1998] used the then newly developed IFS flame spread and suppression algorithms to predict the heat release rate. Although the HRR predictions were reasonable, the comparisons with the damage patterns from the test series were not. Hence it was decided to use a prescribed fire approach in this study because of its repeatability. A series of four fuel package specifications were thus employed. Figure 5 compares the heat release rate histories of these fires. Each had the same t^2-fire growth rate of 1.78 kW/m^2 (0.157 BTU/s/ft^2) used for the heptane tests in McGrattan, Hamins, & Stroup [1998] (which was also consistent with the free burn rack testing data found therein). The four burn rate histories differed in their maxima, in the time required to reach their peak HRRs, in the duration of their steady burn periods, and in their decays. These curves were based upon the commodity test results developed by McGrattan, Hamins, and Stroup [1998] and span the normal range of sprinklers operated during a fire from four to the number of sprinklers in the design area. (See Table 3.) The curves do not include the ongoing smoke production after the decay period has ended. These four heat release rate histories are summarized in Table 4. The validation of the model (presented Section 3.1) was facilitated by the fact that the growth rate was identical to that found in the tests reported in [McGrattan, Hamins, & Stroup, 1998].

Fire source representation HRR1 is a fire that was quickly controlled by the sprinklers and has no steady burn period. For HRR2, the fire grows to 10 MW and remains at that heat release rate until decay in heat release rate began at 255 s. The decay period for HRR2 is longer than that of HRR1, reflecting that it is more difficult to control a 10 MW (9,480 BTU/s) fire than a 7 MW (6,640 BTU/s) fire. HRR3 has the same growth to 10 MW (9,480 BTU/s) as HRR2 and has correspondingly longer

steady burn and decay periods than does HRR2. HRR3 represents the most severe fire employed in this study. Sprinkler response to HRR3 within the wide performance range of the sprinklers reported in the McGrattan, Hamins, & Stroup [1998] commodity tests. (See Table 3.) HRR4 was used to investigate the effect that cooler smoke associated with a longer decay period would have on smoke and heat vent performance. This fuel package specification was based upon commodity classification test results and the recognition that control-mode sprinklers are not designed to extinguish fire. In reality combustion could continue up to the point where firefighters completely extinguish the reaction by manual action.

Table 4: Summary of the heat release rate histories. All had the same t^2 growth rate of 1.78 kW/s^2.

History #	Peak HRR [MW]	Growth Period [s]	Steady [s]		Decay [s]	
			Period	Time	Period	Time
1	7	62.7	0	62.7	60	122.7
2	10	75	180	255	120	375
3	10	75	600	675	240	915
4	10	75	60	135	2500	2635

An algorithm was devised in order to realize these fire specifications. This algorithm was coded into a FORTRAN95 program in order to allow calculation on a digital computer. The resulting executable required that computational cells in the rack flue space become involved according to an idealized representation of the fire spread associated with standard rack fire tests. The methodology revolved around igniting flue cells in a sequence that matched the desired HRR curve in Figure 5 to within a given tolerance. Each involved flue cell had a fixed heat release rate per unit area of 500 kW/m^2 (215 BTU/s/lbm). The overall tolerance was set to half the contribution of a flue cell. The individual HRR profile for a face was a trapezoid including a brief growth period to 500 kW/m^2 (215 BTU/s/lbm), a short decay period, and an interim steady burn period of variable duration. Refer to Figure 6. The ramp-up and ramp-down times were specified. The duration of steady contribution by the cell was determined from the specified overall HRR curve but could be no longer than the time span of the HRR curve. The inputs were different for the three stages of the HRR curve.

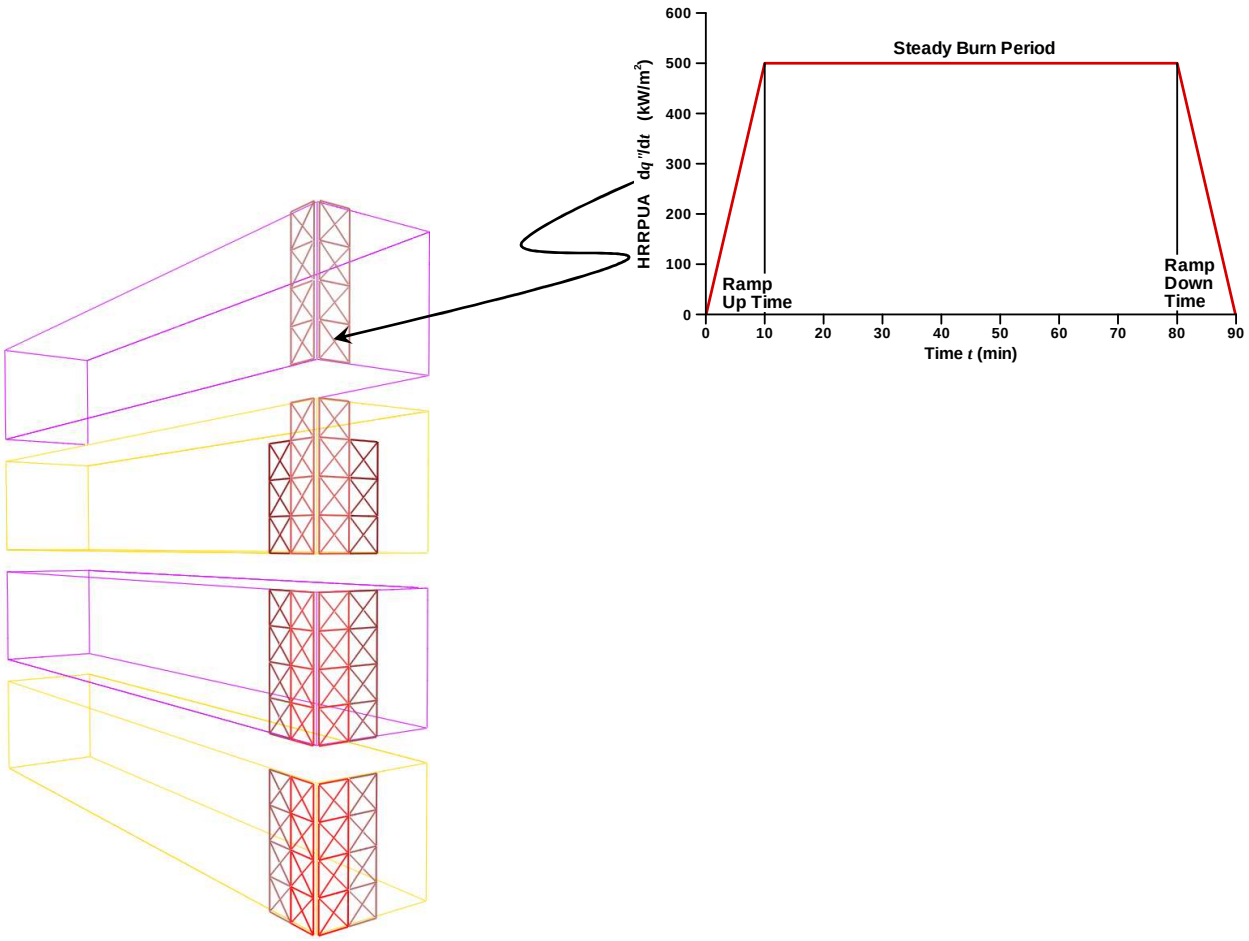

Figure 6. Example of fire growth methodology for one quarter of the commodity racks that define the flue. The commodities are shown in outline format. Cells that contribute to the heat release rate are marked with an ×. Each cell has a heat release rate per unit area similar to the one shown above. The length of the steady burn period varies from cell to cell. The durations of the ramps vary with heat release rate number.

The "ignition sequence" started on the bottom corner cells within the flue. Ignition proceeded clockwise on a corner-cell-by-corner-cell basis. Once the eight cells in the lowest tier of the flue corners were involved, the process would move up to the next sequence of cells. (See Figure 6.) Once the top of a tier was achieved, the sequence would move to the next tier. This progression would then be repeated until the top of the highest tier was reached. The sequence would then revert to the bottom level of cells on the bottom tier. Cells on each face would become involved. Once a tier was exhausted the process would move up to the next tier. The overall heat release rate is the sum of all the individual cell contributions. When a cell became involved, its face was set to follow the individual HRR trapezoid. When the overall heat release rate began to decay, the burnout time for

blocks would be set again so as best to match the curve. The "turn off" sequence went in the same order as the "turn on" sequence.

The fire source resulting from the burning commodities rack could be moved to various locations in the warehouse. Most computer simulations had the fire source centered on the east roof vent zone. The center of the rack fire source coincides with the center of the four nearest sprinklers and the four nearest vents. This level of symmetry was not employed in other fire source locations.

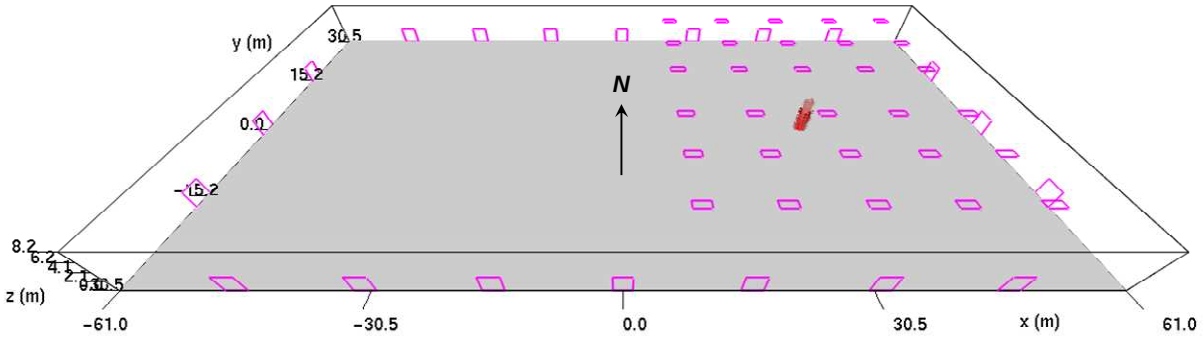

Figure 7. Vents used in simulations with smoke and heat vents.

2.5 Configuration for Burning Racks

Whenever possible, the rack specifications given by You and Kung [1984] for standard rack-mounted commodities were used as the bases for the burning racks. The vertical spacing between pallet loads were used without alteration. The depth in the x-direction was the same but the y-direction was elongated to about half the central rack array length. (According to the standard rack configuration, the extent in the y-direction should be one pallet load. This, however, leads to many obstacles in the input file which otherwise do not add to the analysis. Hence the stretching in the y-direction as Figure 6 shows.)

For the standard arrangement, pallet loads are positioned so that 15.2 cm (6″) flues result. As was mentioned earlier, this small gap allows good radiative feedback between pallet loads, resulting in a rapid growth rate. However, due to resolution limitations, the burning rack flue space was set to 0.610 m (2′), which means two cells separating each pallet load in the x- and y-directions. The reason is that two cells by two cells allow more dynamic flue flows than would be the case with one cell flues. And, because of the flame spread methodology presented above, the desired growth rate is ensured in spite of the larger flues.

The remaining rack-mounted commodities in the warehouse were similar to the burning racks except that, due to resolution limitations, no flues were modeled (i.e. the double row racks were modeled as a single solid object). Similarly, geometric details such as the particulars of the metal rack structure were not modeled.

2.6 Smoke and Heat Vents

Thirty industry standard 2.44 m×1.22 m (8′×4′) smoke and heat vents were used per each sprinkler system coverage area. These vents were situated on the ceiling in such a fashion that they did not interfere with sprinklers or support beams. (See Figures 1 and 7.) The smoke and heat vent areas were closed until 127 s, when they became "OPEN" vents. The opening time was about one minute after the first sprinkler activated.

2.7 Makeup Air

The normal inlet vent requirement for makeup air area is twice that of the roof vents in order to avoid inlet flow restriction. Garage door style inlet vents were used for makeup air in the simulations that included smoke and heat vents. The inlets were designed to be adequate and to minimally impact the simulation results. These were placed symmetrically along the outer walls of the warehouse (see Figures 1 and 7) according to the specification given in Table 1. Leaks were applied to the outer walls based on the data for medium leakage construction given in Klote & Milke [2002]. See Table 1 for the details. For simulations without smoke and heat vents, leaks were the only openings to the outside. (See Figure 2.)

2.8 Sprinklers

K-ll sprinklers were used in the vicinity of the burning racks. The data file that comes with FDS4 was accepted for the characteristics of K-ll sprinklers. These properties can be found in Table 1. Although the whole warehouse would be sprinklered, only the sprinklers near the burning racks that might operate were included in the simulations in order to improve run time performance. The sprinkler spacing was 3 m×3 m (10′×10′). The distance between the ceiling and the center of the spray was 0.0762 m (3″). This is roughly the distance from the ceiling to the sprinkler deflector.

FDS4 has two ways to account for radiative transport. One technique uses the finite volume method to approximate the solution of the equation of transfer. This feature was turned off for the

following reasons. The main concern of this investigation is the activation of sprinklers. Sprinkler activation typically occurs after the ceiling jet engulfs a sprinkler head. Because of the smoke, radiation transfer within the upper layer is not a contributing factor. It is possible to have heat from the upper layer reach a sprinkler outside of the ceiling jet by means of radiative transfer. As is usually the case, the higher the temperature difference, the more intense the radiative heat transfer. However, activating sprinklers will cool the ceiling jet. The ten foot sprinkler spacing is standard because it has been found not to lead to activations ahead of the ceiling jet. If this were not the case then a runaway activation sequence could occur that could exceed the sprinkler design area. Hence, based on the cooling effects of the sprinkler sprays and the spacing of the heads, it is not expected that radiative heat transfer will be a contributing factor in sprinkler activation. Furthermore, because the heat release rate is specified (i.e., not driven by flame spread) and because the heating of targets was not part of the scope of the present investigation (again, the cooling of the sprinklers minimizes this effect), there was no motivation to perform radiative heat transfer calculations that would extend the overall run time of each simulation. Therefore radiation effects were taken into account by using FDS4's constant loss feature. The specified radiative fraction was 35%.

2.9 Draft Curtain

Certain simulations evaluated the performance of draft curtains. For these scenarios, a 1.82 m (6′)-deep draft curtain was placed down the center of the domain at $x = 0$. In other words, it separated the two 3,720 m^2 (40,000 sq. ft.) sprinkler design areas. (See Figure 1.) The draft curtain was given the thermal properties of steel and could transmit heat from one zone to the other.

2.10 Structural Elements

Structural members near the ceiling can have an impact ceiling flows. Therefore some information is provided on the assumed structural makeup of the warehouse in question. A variety of construction methods can be used for warehouses. Currently open web steel joists and joist-girders (mini-trusses) are widely used. The main concern for the present investigation is in regards to the

impact that ceiling structural elements and other forms of equipment situated near the ceiling would have on the evolving ceiling jet. The structural elements employed in the simulations conform to the following criteria

1. Standards consistent with the 2000 edition of the International Build Code (IBC) (as well as 1980's-90's editions of the IBC),
2. moderate snow design load of no more than 958 N/m^2 (20 lbf/ft^2),
3. dead weight of no more than 479 N/m^2 (10 lbf/ft^2),
4. low or non-seismic area,
5. regular wind design (non-hurricane area).

The design meeting these criteria has

1. about 10.7 m×12.2 m (35 ft×40 ft) bays,
2. 61 cm (24 inch)-deep joists, spanning 12.2 m (40 ft), 2.13 m (7 ft) OC, framing into nominal 76.2 cm (30 inch) deep joist girders for 10.7 m (35 ft) spans,
3. 8.23 m (27 ft) roof height, with 3.81 cm (1 ½ inch) deck,
4. about 22.9 cm (9 inch)-30.5 cm (12 inch) diameter, round pipe columns at corners of each roof bay (at 10.7 m (35 ft) and 12.2 m (40 ft) OC in the 2 directions).

Due to resolution limitations, the structural elements of the rack systems were not included in the simulations. The columns were excluded for the same reason. Support beams near or on the ceiling conform to the specification given above. The fact that the beams could act as small draft curtains motivated moving them off the ceiling by two feet. The connection to the ceiling would be by purlins. (See Figures 1 and 2.) One of the simulations (Run 10) was used to investigate the impact that beams in contact with the ceiling have on the smoke spread.

2.11 Visibility

The light extinction coefficient, K (m^{-1}), such as can be found in the familiar Beer's law of radiation attenuation [Holman, 1986],

$$I_\lambda = I_{\lambda 0}\, \mathrm{e}^{-KL}, \tag{5}$$

where I_λ is the beam intensity (W/m^2) and L is the length (in m) through which the beam has been attenuated from $I_{\lambda 0}$ to I_λ, can be derived from the smoke density, ρ_s (kg/m^3), by means of the specific extinction coefficient, K_m:

$$K = K_m \rho_s. \tag{6}$$

For flaming combustion, Mulholland & Croarkin [2000] report K_m = 8710 m^2/kg ± 1230 m^2/kg = 42,500 ft^2/lbm ± 6000 ft^2/lbm at the best current estimate of the optical properties of smokes. Their specific extinction coefficient is used in this work.

The contrast, c_c, is a dimensionless factor that quantifies the difference between background and object luminance. It has the value of

$$c_c = \begin{cases} 3 & \text{for a light} - \text{reflecting sign} \\ 8 & \text{for a light} - \text{emitting sign} \end{cases}. \tag{7}$$

The visibility, S (m), can be related to smoke density via the extinction coefficient and the contrast using the formula [Jin, 2002; Mulholland, 2002]

$$S = \frac{c_c}{K} = \frac{c_c}{K_m \rho_s}. \tag{8}$$

Two crucial factors that determine the visibility are the smoke yield, y_s, and the heat of combustion, ΔH_C, of the fuel. The heat output from the fire, $\dot{Q}$, can be determined from ΔH_C and the fuel consumption rate, $\dot{m}_F$,

$$\dot{Q} = \dot{m}_F \, \Delta H_C. \tag{9}$$

The fuel consumption rate and the smoke production rate, $\dot{m}_s$, are related via the smoke yield as follows

$$\dot{m}_s = y_s \dot{m}_F. \tag{10}$$

Making this substitution into the previous equation results in

$$\dot{m}_s = \frac{y_s \dot{Q}}{\Delta H_C}. \tag{11}$$

The smoke production rate can be related to the smoke density via the definition of density, $\rho_s = \mathrm{d}\, m_s / \mathrm{d}\, V_s$, and the chain rule for differentiation. The result is

$$\rho_s \dot{V}_s = \frac{y_s \dot{Q}}{\Delta H_C}. \tag{12}$$

The quantity $\dot{V}_s$ represents the volumetric production rate of smoke. Substituting this relation in Eq. (8) yields

$$S = \frac{c_c}{K_m} \frac{\dot{V}_s}{\dot{Q}} \frac{\Delta H_C}{y_s}. \tag{13}$$

In other words, the visibility is directly proportional to the heat of combustion and inversely proportional to the soot yield [Zalosh, 2003, pg. 6]. I.e.,

$$S \propto \frac{\Delta H_C}{y_s}. \tag{14}$$

Given the same heat release rate, the visibility is poorer for fuels that have low heats of combustion or high smoke yields. Visibility scales based on the ratio of heat of combustion to smoke yield.

FDS automatically calculates S as an output field according to the procedure detailed above. As Table 1 shows, the inputs that affect visibility were conservatively set to c_c = 3 and K_m = 8710 m^2/kg (42,500 ft^2/lbm) with y_s = 0.1 [Tewarson, 2002] and ΔH_C = 27 MJ/kg (11,600 BTU/lbm) [Lee, 1987; Spaulding, 1988].

2.12 Simulation Matrix

A résumé of the simulations that have been performed is given in Table 5. The simulation scenario matrix consisted of heat release rate number, location of the burning racks, support beam configuration, and the presence of vents and draft curtains. A code was also developed which is more mnemonic than plain run number. It is shown in Table 5. The FDS simulations were run on a cluster of Linux computers comprised of Pentium IV single processors with 4 GB of memory each and multicore processors with access to 8 GB of memory.

Table 5: Distinguishing features of the simulations used in this study. The results for sprinkler performance are also included.

Run #	Code	HRR #	Location of Burning Racks	Support Beam Configuration	S&H Vents?	Draft Curtain?	1st Sprink Act Time	Total #
1	HRR1SHV0DC0	1	Center	Offset from ceiling	No	No	69.9 s	5
2	HRR1SHV1DC0	1	Center	Offset from ceiling	Yes	No	70.2 s	6
3	HRR1SHV1DC1	1	Center	Offset from ceiling	Yes	Yes	70.1 s	6
4	HRR2SHV0DC0	2	Center	Offset from ceiling	No	No	71.2 s	19
5	HRR2SHV1DC0	2	Center	Offset from ceiling	Yes	No	71.4 s	18
6	HRR2SHV1DC1	2	Center	Offset from ceiling	Yes	Yes	71.6 s	20
7	HRR3SHV0DC0	3	Center	Offset from ceiling	No	No	70.3 s	21
8	HRR3SHV1DC0	3	Center	Offset from ceiling	Yes	No	70.4 s	19
9	HRR3SHV1DC1	3	Center	Offset from ceiling	Yes	Yes	70.2 s	20
10	HRR3SHV1DC1CB	3	Center	In contact w/ ceiling	Yes	Yes	64.6 s	20
11	HRR4SHV0DC0	4	Center	Offset from ceiling	No	No	70.5 s	18
12	HRR4SHV1DC1	4	Center	Offset from ceiling	Yes	Yes	70.0 s	17
13	HRR3SHV1DC1R	3	Rear Center	Offset from ceiling	Yes	Yes	68.7 s	19
14	HRR3SHV1DC1RC	3	Rear Corner	Offset from ceiling	Yes	Yes	63.4 s	22
15	HRR3SHV1DC0FC	3	Front Corner	Offset from ceiling	Yes	No	65.9 s	20
16	HRR3SHV1DC1FC	3	Front Corner	Offset from ceiling	Yes	Yes	65.4 s	21

3.0 Results

Sprinkler activation data and smoke mass and visibility were used as the performance metrics. Smoke mass and visibility were used to assess the performance of smoke and heat vents. For convenience, the time of the first activation and the final number of active sprinklers are summarized in Table 5.

3.1 Validations

As was indicated above, the reason for choosing the t^2 growth rate of 1.78 kW/s^2 (0.157 BTU/s/ft^2) was to facilitate comparisons with the results of the tests reported in [McGrattan, Hamins, & Stroup, 1998]. For Runs 1 – 12, the center of the burning racks coincided with the center of the four nearest sprinklers. However, only Runs 4 – 12 went up to 10 MW (9,480 BTU/s). The average of the first sprinkler activation times reported in Table 5 for these runs is 70.0 s. The sprinkler performance results for the heptane tests from [McGrattan, Hamins, & Stroup, 1998] are reported in Table 6. Only burner positions E and F correspond to the burner being centered on four sprinklers. The average of the first sprinkler activation times reported in Table 5 for these two cases is 70.5 s. The

difference between these tests and the current study is 0.7%. For Runs 4 – 12, an average of 19 sprinklers[‡] operated. From Table 6, an average of 21 sprinklers operated with the heptane burner tests II-9 and II-10. The difference is 9.5%.

The remaining positions in Table 6 are for the spray burner centered on two sprinklers. Although this is not exactly the case with Runs 13 – 16, a comparison will be made just the same. From Table 5, the averages are 65.9 s for the first activation and 21 sprinklers overall. From Table 6, the averages are 67 s for the first activation and 22 sprinklers overall. The differences are 1.6% and 5%, respectively.

Table 6: Sprinkler activation results for the heptane spray burner test series II as reported in [McGrattan, Hamins, & Stroup, 1998].

Run #	Burner Position	1st Sprink Act Time	# of Active Sprinklers
II-1	D	75 s	27
II-2	D	65 s	28
II-3	A	68 s	12
II-4	B	63 s	16
II-5	D	70 s	28
II-6	D	70 s	27
II-7	A	69 s	18
II-8	B	70 s	13
II-9	E	67 s	23
II-10	F	74 s	19
II-11	C	62 s	23
II-12	C	58 s	23

For a variety of reasons, comparisons with the commodity tests in [McGrattan, Hamins, & Stroup, 1998] are not appropriate. For example, in the current set of simulations, the heat release rate is well defined. It was not measured for the commodity tests in [McGrattan, Hamins, & Stroup, 1998]. Without this information, it is difficult to determine which experiments best correspond with the sixteen simulations available in this report. Some of the NFPARF tests, such as P-3, are not applicable at all because fuel was placed directly underneath the draft curtain. Nonetheless, the averages of the

‡ The noninteger average was 19.1 sprinklers.

first sprinkler activations will be compared. For tests P-1 – P-5 of [McGrattan, Hamins, & Stroup, 1998], the average is 70.6 s. For Runs 1 – 9, the average is 71 s. The difference is 14%. The comparisons presented in the section are of suitably low percent differences to conclude that the validation exercise is a success.

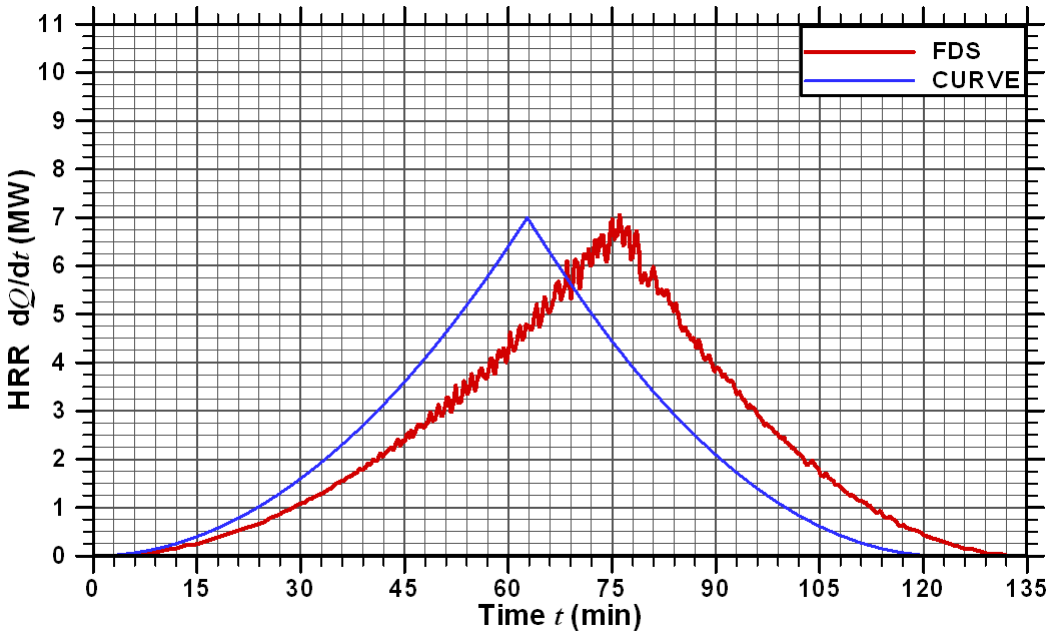

Figure 8. Comparison of the computed heat release rate for Run 1 (HRR1SHV0DC0) with the HRR1 curve.

3.2 HRR1 Fire Source

This series of simulations used the HRR1 fire source. Figure 8 shows the output heat release rate for Run 1 that was generated according to the algorithm detailed in Section 2.4 alongside the HRR1 curve. Comparison establishes that the two curves match well. The HRRs for Runs 2 and 3 are very similar and will therefore not be shown by themselves. They will, however, be compared with the sprinkler activation histories presented below.

3.2.1 Run #1 (HRR1SHV0DC0): HRR1 without Smoke and Heat Vents and without Draft Curtains

A comparison of the cumulative number of operating sprinklers with the associated output heat release rate is given in Figure 9. Because sprinkler activations are discrete events, they are represented as spikes. Each successive activation is drawn as an impulse that, based on the right-hand axis, is as tall as the total number of active sprinklers at that time. Figure 9 shows that in the time span of less

than six seconds four sprinklers activated.

Figure 10 shows the sprinkler activation map. It is a plan view representation of the computational domain with obstacles and sprinkler locations projected onto the floor of the facility. Because projection can overlap objects that in reality are separated in the missing dimension, obstacles are rendered in monochrome. The locations of unopened sprinklers are denoted by the sprinkler head symbol ( ). If the sprinkler did open then a box appears in its location with the sprinkler activation time written inside the box. This and all of the following sprinkler maps are zoomed into the area of the burning racks in order to render the activation time boxes legible. The coordinates are shown in English units to facilitate comparison with older building code standards. Figure 10 shows that the active sprinklers were the five closest to the center of the burning racks.

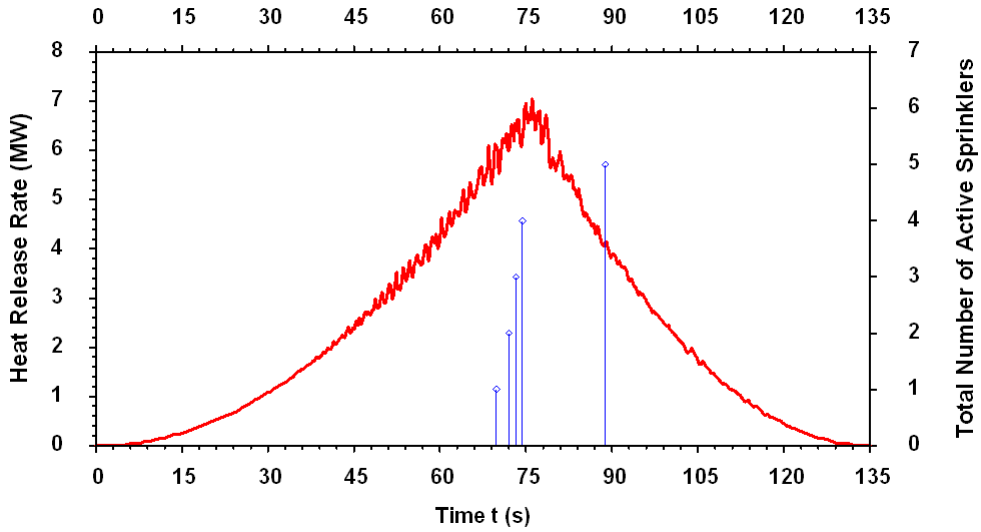

Figure 9. Comparison of the heat release rate and the sprinkler activation times for Run 1 (HRR1SHV0DC0): HRR1 without smoke and heat vents and without draft curtains.

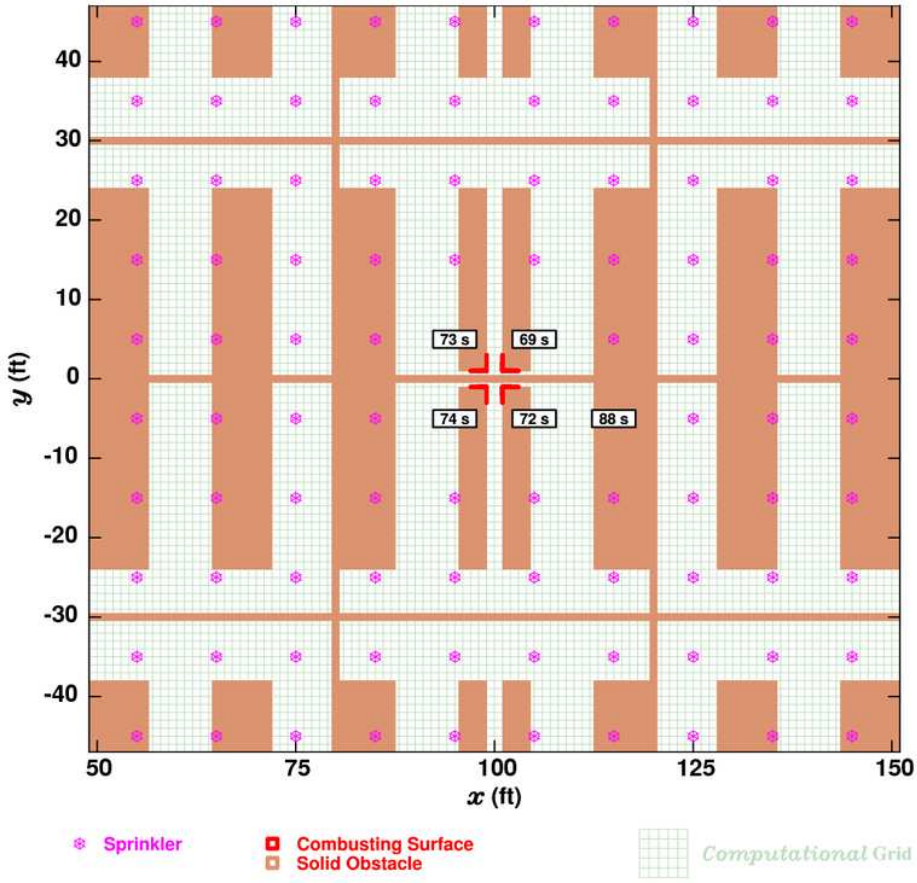

Figure 10. Sprinkler activation map for Run 1 (HRR1SHV0DC0): HRR1 without smoke and heat vents and without draft curtains.

3.2.2 Run #2 (HRR1SHV1DC0): HRR1 with Smoke and Heat Vents and without Draft Curtains

For Run 2, the cumulative activation plot (Figure 11) and sprinkler activation map (Figure 12) are very similar to those of Run 1. This is because the HRR started to decline at about the same time that the fourth sprinkler activated and because the vents opened essentially when the fire was in the decay phase. Because the fifth and sixth sprinklers that activated were separated by 9 m (30 ft), the later response of the fifth sprinkler (when compared with Run 1) allowed the sixth to go off as well because of the transport time required to have the cooling sensed at the other location.

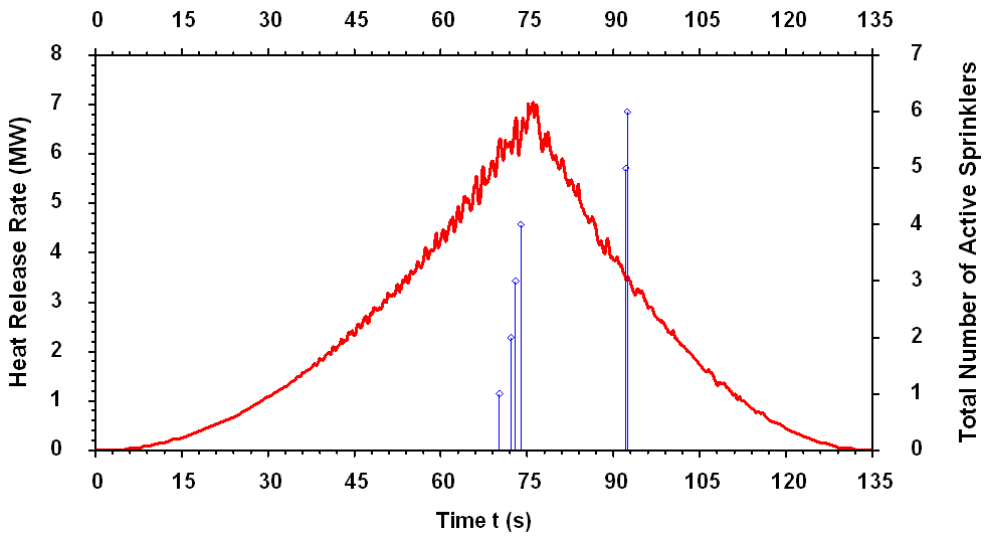

Figure 11. Comparison of the heat release rate and the sprinkler activation times for Run 2 (HRR1SHV1DC0): HRR1 with smoke and heat vents and without draft curtains.

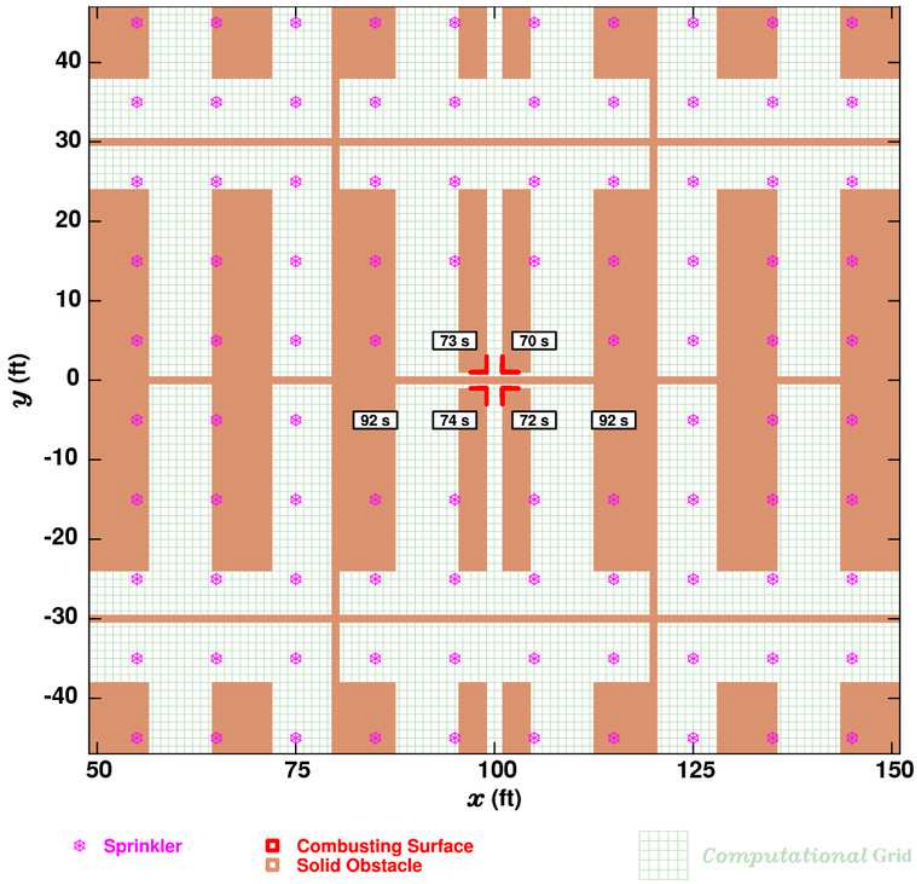

Figure 12. Sprinkler activation map for Run 2 (HRR1SHV1DC0): HRR1 with smoke and heat vents and without draft curtains.

3.2.3 Run #3 (HRR1SHV1DC1): HRR1 with Smoke and Heat Vents and with Draft Curtain

For Run 3, the cumulative activation plot (Figure 13) and sprinkler activation map (Figure 14) are very similar to Runs 2. Although the reasons are the same, they can be augmented by the facts that the ceiling jet reflected by the curtain was being driven by a dying fire and that the ceiling jet gases had already been cooled by the active sprinklers.

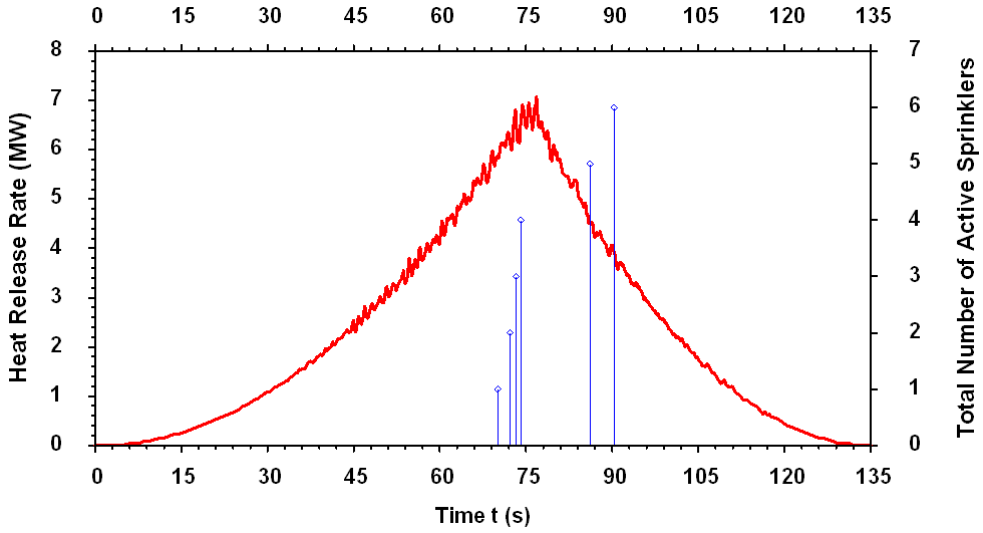

Figure 13. Comparison of the heat release rate and the sprinkler activation times for Run 3 (HRR1SHV1DC1): HRR1 with smoke and heat vents and with draft curtain.

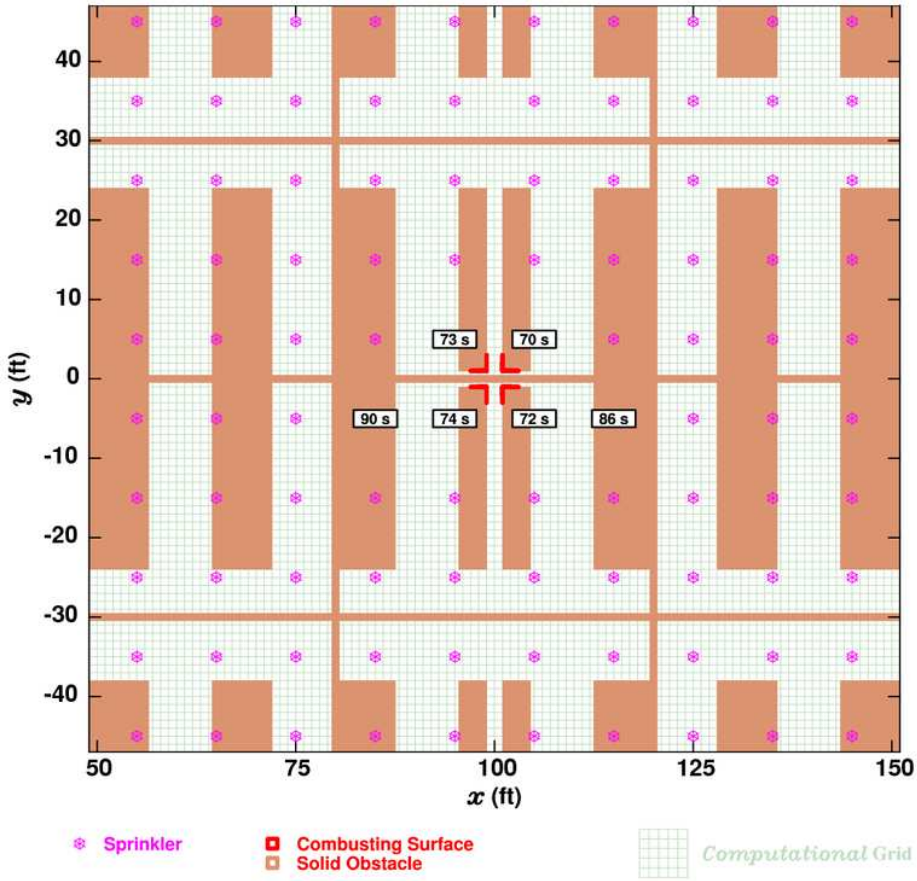

Figure 14. Sprinkler activation map for Run 3 (HRR1SHV1DC1): HRR1 with smoke and heat vents and with draft curtain.

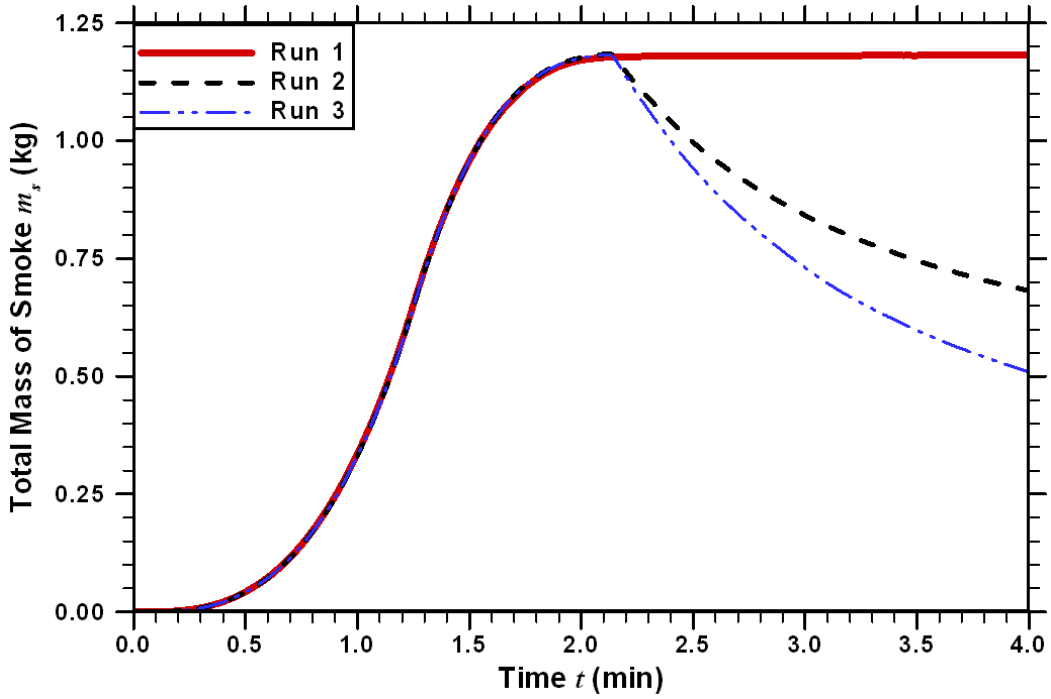

Figure 15. Comparison of the net building smoke masses remaining in the building for Runs 1 - 3 (HRR1SHV0DC0, HRR1SHV1DC0, HRR1SHV1DC1).

The total mass of smoke contained in the warehouse is compared in Figure 15 for Runs 1 – 3. Even though the smoke output from HRR1 was relatively low, Figure 15 shows that smoke and heat vents reduced the smoke mass by 43% in about 1.9 min. With the addition of a draft curtain, the performance of the vents improved such that 57% of what would be the total smoke was removed in the same 1.9 min time period.

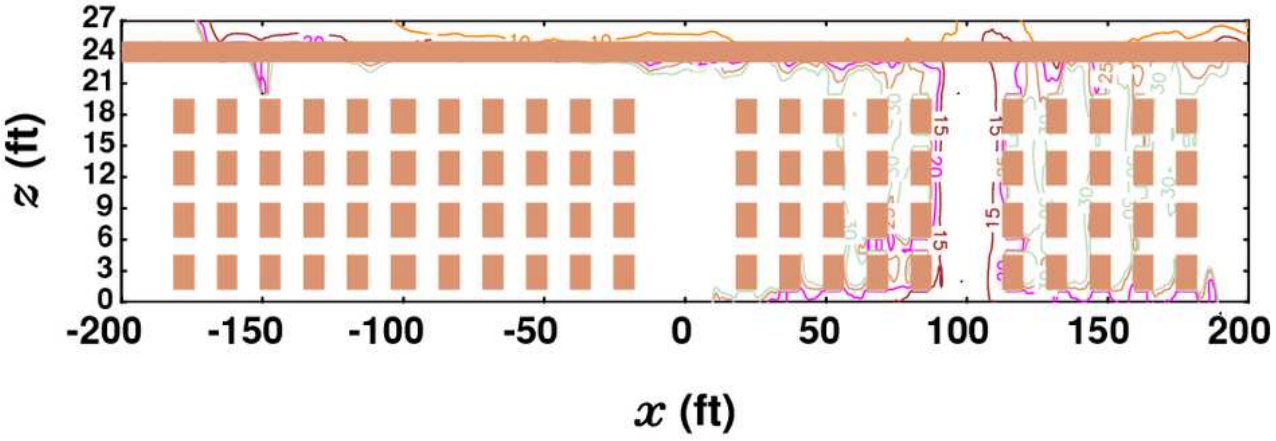

a) Run 1 (HRR1SHV0DC0): without smoke and heat vents and without draft curtains

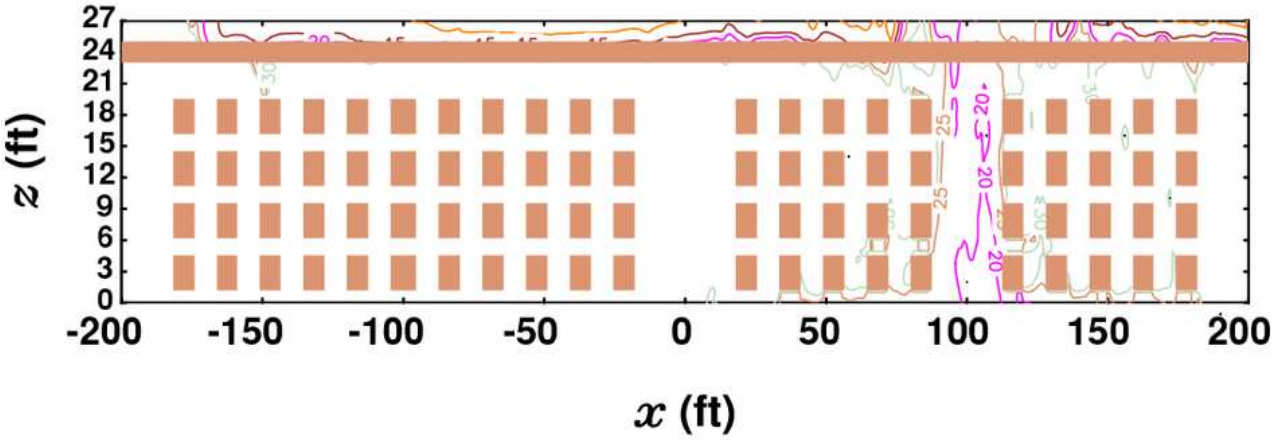

b) Run 2 (HRR1SHV1DC0): with smoke and heat vents and without draft curtains

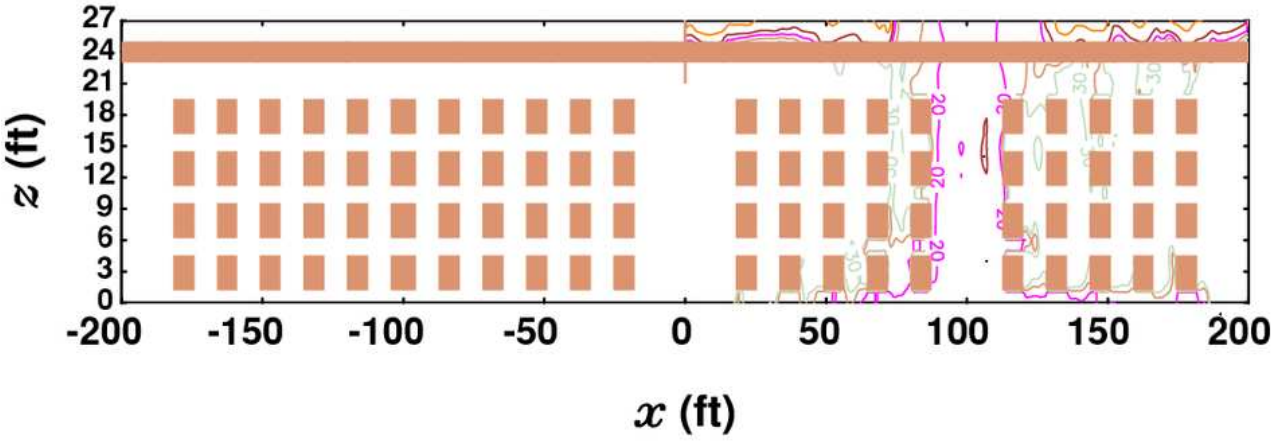

c) Run 3 (HRR1SHV1DC1): with smoke and heat vents and with draft curtain

Figure 16. Visibility (in ft) along *y* = 0 ft at 200 s for HRR1 Runs 1 - 3. The vertical coordinate has been stretched.

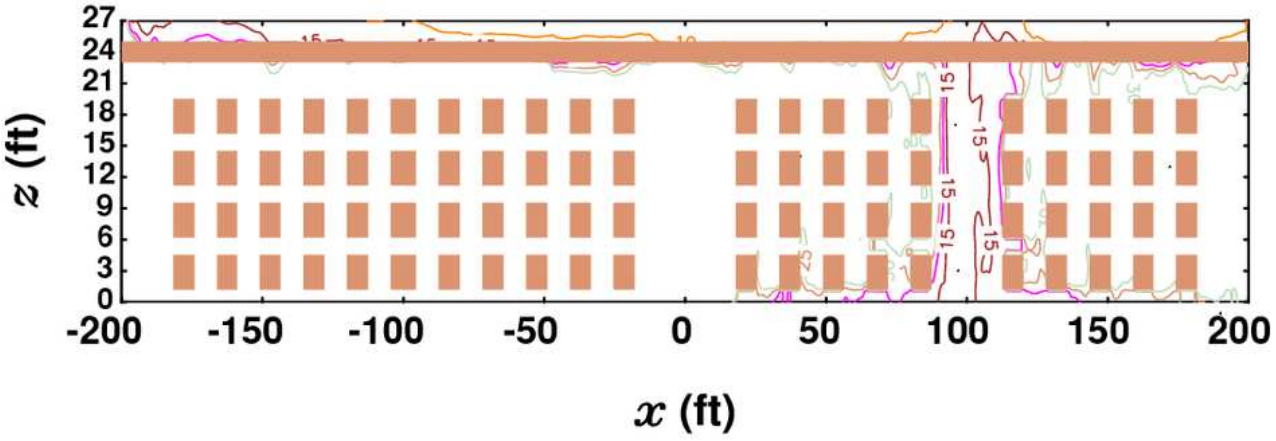

a) Run 1 (HRR1SHV0DC0): without smoke and heat vents and without draft curtains

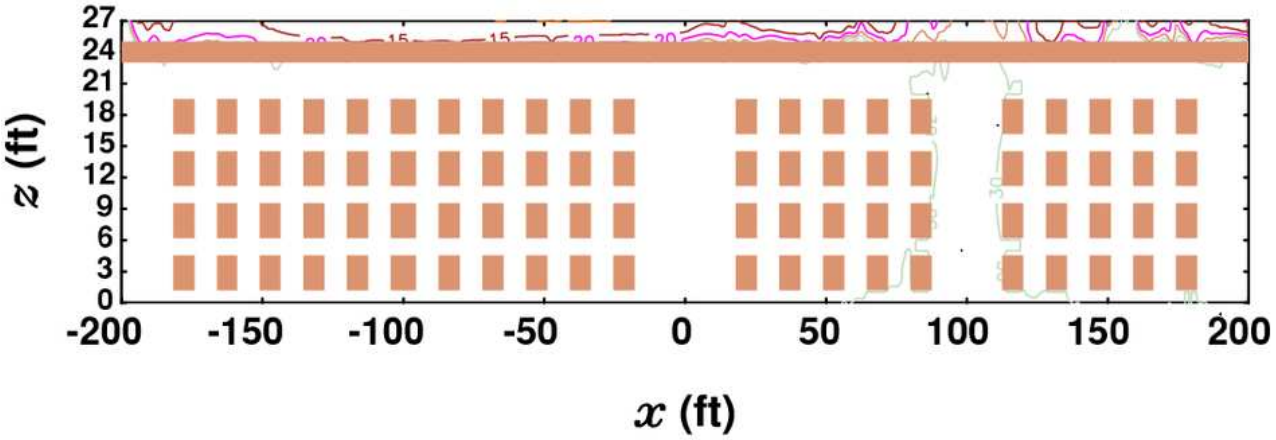

b) Run 2 (HRR1SHV1DC0): with smoke and heat vents and without draft curtains

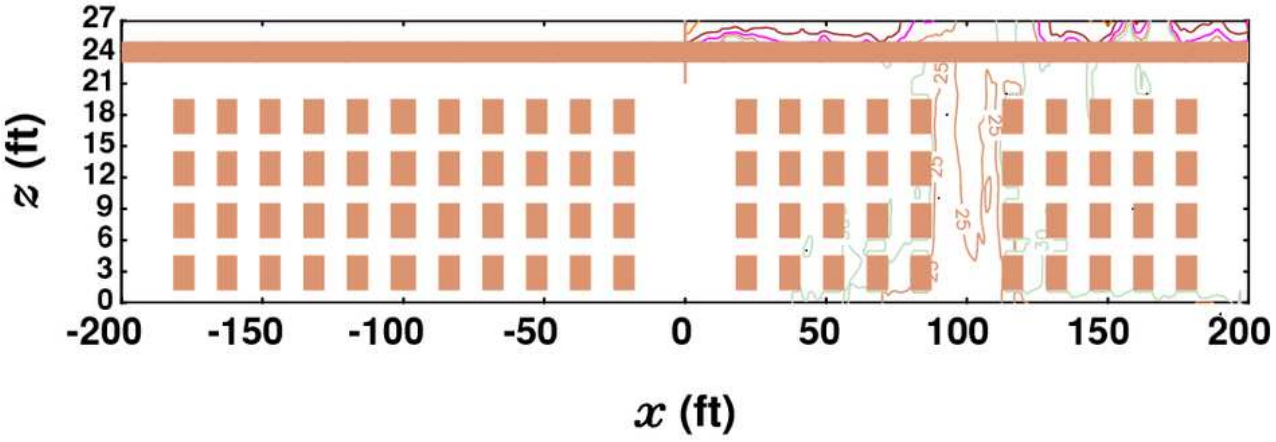

c) Run 3 (HRR1SHV1DC1): HRR1 with smoke and heat vents and with draft curtain

Figure 17. Visibility (in ft) along *y* = 0 ft at 220 s for HRR1 Runs 1 - 3. The vertical coordinate has been stretched.

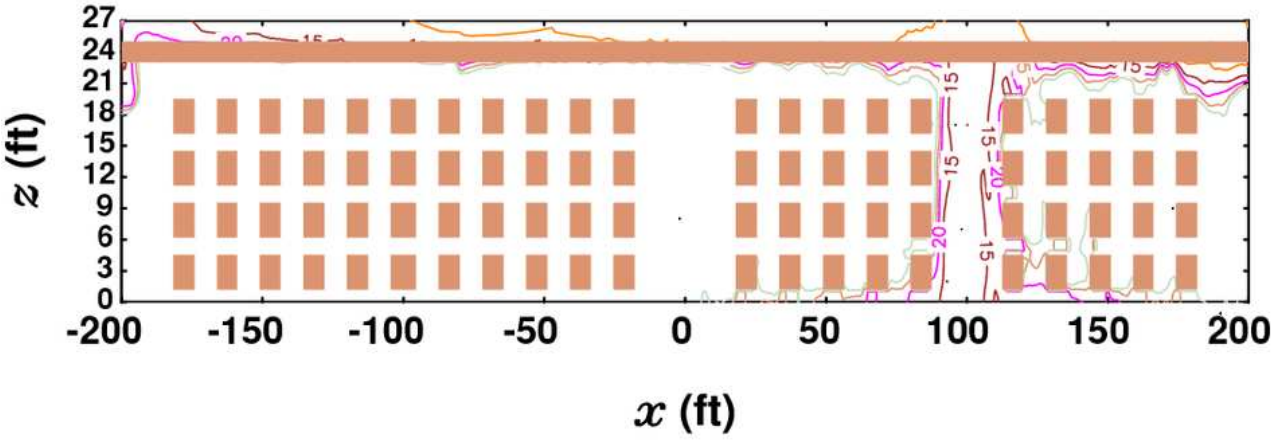

a) Run 1 (HRR1SHV0DC0): without smoke and heat vents and without draft curtains

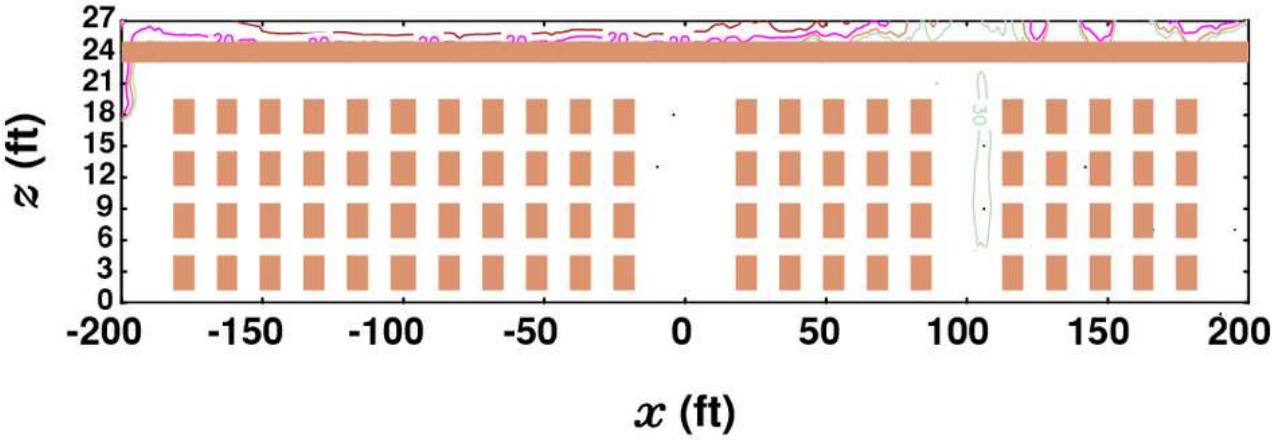

b) Run 2 (HRR1SHV1DC0): with smoke and heat vents and without draft curtains

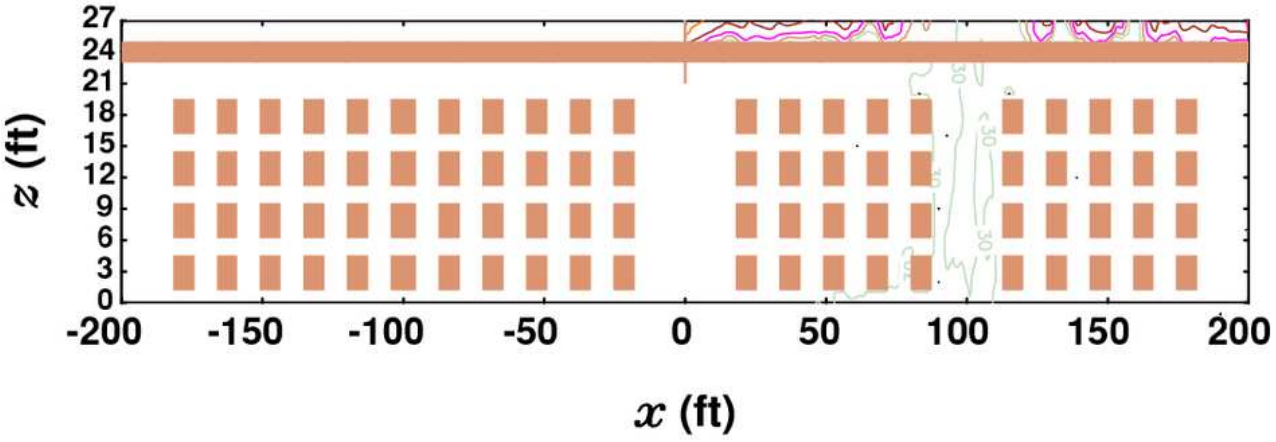

c) Run 3 (HRR1SHV1DC1): with smoke and heat vents and with draft curtain

Figure 18. Visibility (in ft) along *y* = 0 ft at 240 s for HRR1 Runs 1 - 3. The vertical coordinate has been stretched.

Contours of the visibility along the center of the building ($y = 0$) are shown in Figures 16 – 18. Because the whole length of the warehouse has been shown, this and most of the other contour plots

are stretched in the vertical direction. This overall improves the view but has the drawback that certain features can appear elongated. Again, for legacy building code reasons, the dimensions and the visibility are presented in English units.

HRR1 is so relatively small and short-lived of a fire that it has little impact on the warehouse with the exception of the flue spaces and the ceiling region. The real story of vent and draft curtain performance was told in Figure 15. However, from the contours of visibility the following can be ascertained. Run 1 had persistent pockets of reduced visibility near the floor. By 240 s, Run 2 had stratified smoke throughout the whole of the warehouse ceiling. The draft curtain in Run 3 kept the smoke from entering the west portion of the warehouse. Thus for HRR1 the upper layer never drops to the tops of the commodities, let alone to the 1.83 m (6′) level that is of concern for occupants.

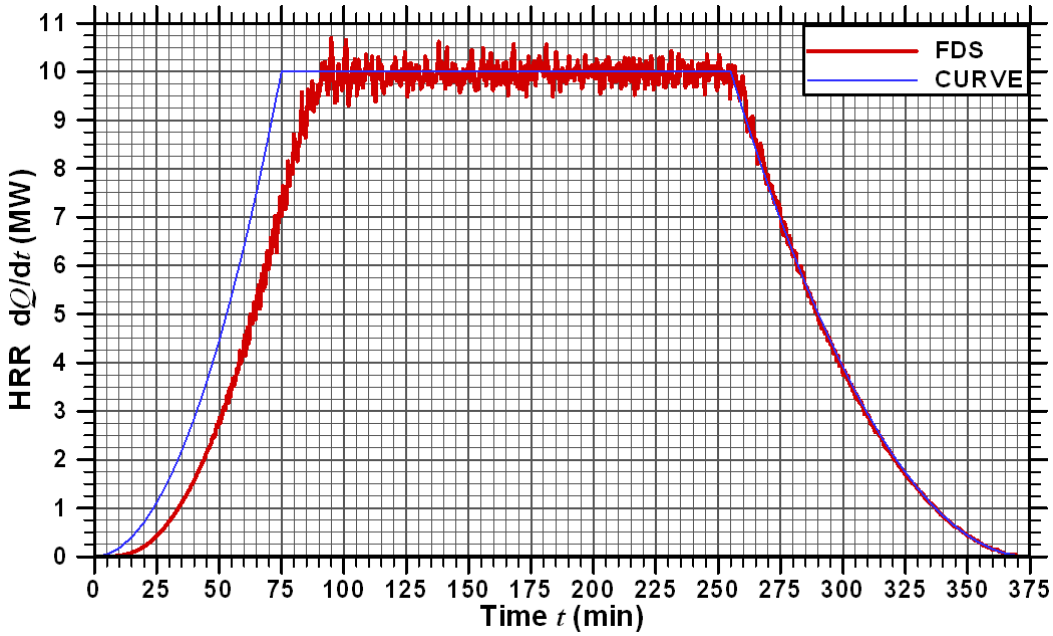

Figure 19. Comparison of the computed heat release rate for Run 4 (HRR2SHV0DC0) with the HRR2 curve.

3.3 HRR2 Fire Source

The next three simulations deal with HRR2, a medium impact fire that was controlled at 10 MW for 180 s before decay occurred. The fire originated from the center racks on the east side of the warehouse (Figures 1 and 2). The simulations differ in the presence of vents and/or draft curtains. Figure 19 shows the HRR computed by Run 4. The output HRR for Runs 5 and 6 are very similar. Comparison reveals good agreement with the target profile.

3.3.1 Run #4 (HRR2SHV0DC0): HRR2 without Smoke and Heat Vents and without Draft Curtains

In the case of Run 4, Figure 19 compares the cumulative number of active sprinklers with the heat release rate. Most of the sprinkler activations occurred within one minute of the first sprinkler operating. Only three sprinklers operated after 135 s. The total number of operating sprinklers was 19. The corresponding sprinkler activation map in Figure 21 shows that the sprinklers opened in a ring-like fashion around the center of the racks.

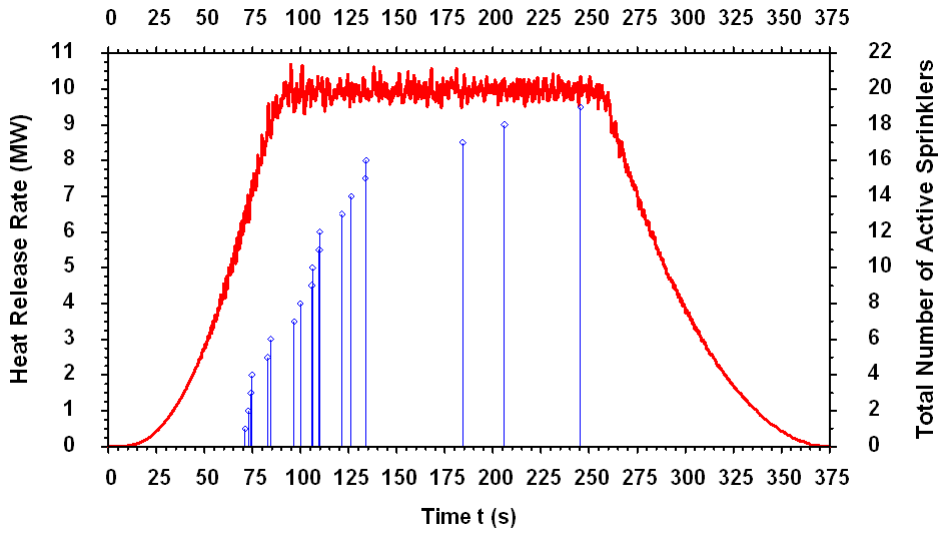

Figure 20. Comparison of the heat release rate and the sprinkler activation times for Run #4 (HRR2SHV0DC0): HRR2 without smoke and heat vents and without draft curtains.

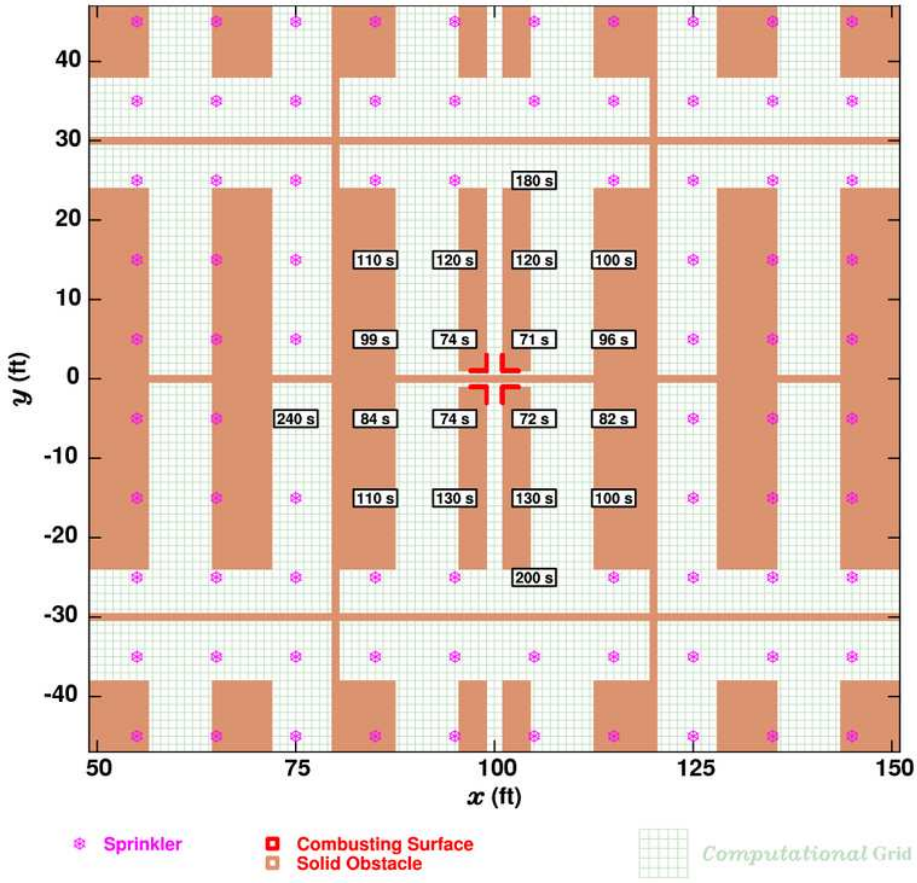

Figure 21. Sprinkler activation map for Run #4 (HRR2SHV0DC0): HRR2 without smoke and heat vents and without draft curtains.

3.3.2 Run #5 (HRR2SHV1DC0): HRR2 with Smoke and Heat Vents and without Draft Curtains

With smoke and heat vents installed, Figure 22 shows that eighteen sprinklers operated as compared to the 19 sprinklers that operated in Run #4 (i.e. no dramatic change). As before, most sprinklers operated before 135 s. The final two sprinkler operations lagged their unvented counterparts in Figure 20 by no more than 40 s. The sprinkler activation map in Figure 23 shows that the ring-by-ring activation pattern was not affected by the presence of the vents.

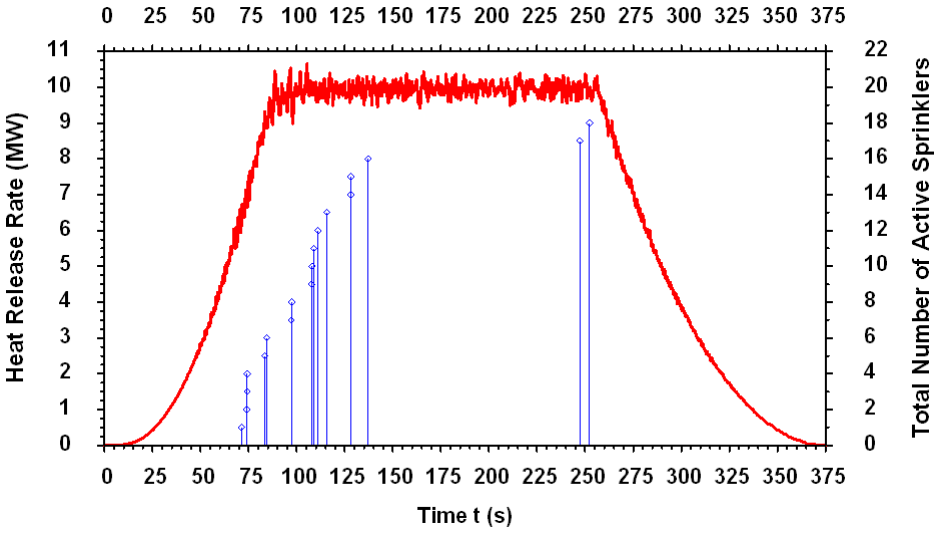

Figure 22. Comparison of the heat release rate and the sprinkler activation times for Run #5 (HRR2SHV1DC0): HRR2 with smoke and heat vents and without draft curtains.

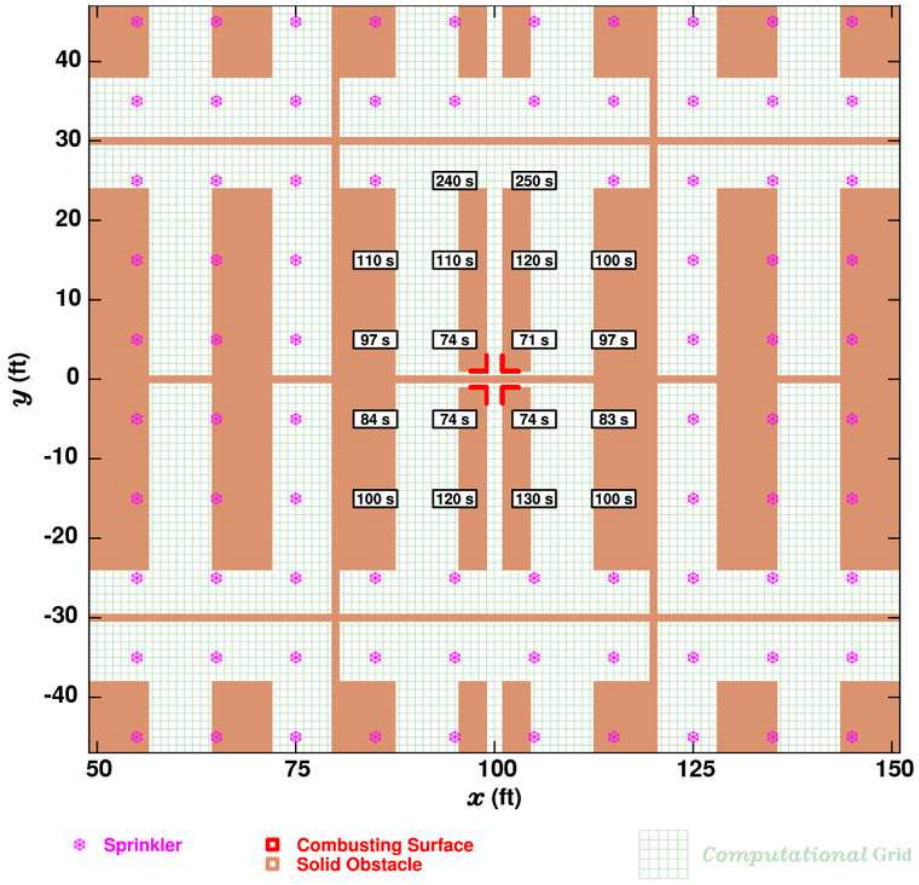

Figure 23. Sprinkler activation map for Run #5 (HRR2SHV1DC0): HRR2 with smoke and heat vents and without draft curtains.

3.3.3 Run #6 (HRR2SHV1DC1): HRR2 with Smoke and Heat Vents and with Draft Curtain

When a draft curtain is added to the warehouse with vents, Figure 24 shows that twenty sprinklers activated. The sprinkler activation map in Figure 25 shows no adverse impact by the draft curtain on the expected activation pattern.

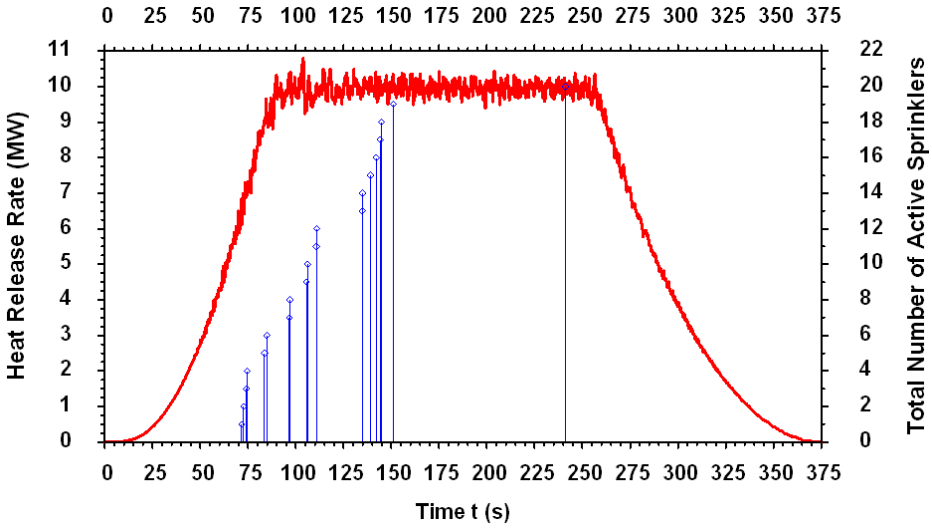

Figure 24. Comparison of the heat release rate and the sprinkler activation times for Run #6 (HRR2SHV1DC1): HRR2 with smoke and heat vents and with draft curtain.

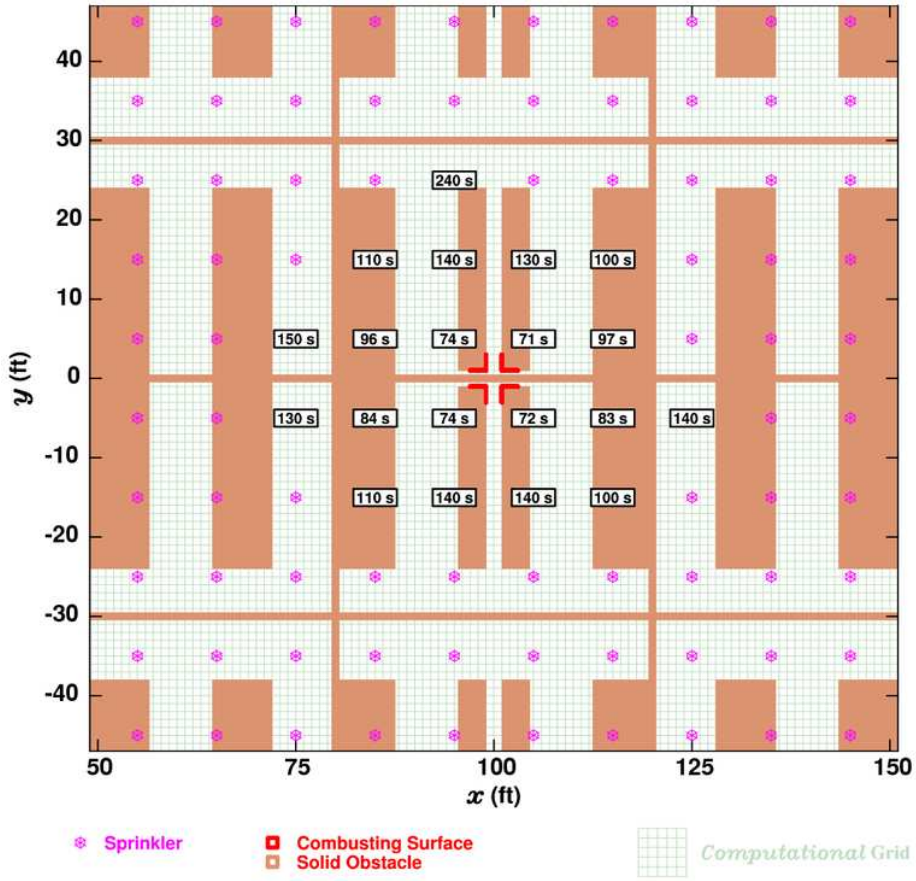

Figure 25. Sprinkler activation map for Run #6 (HRR2SHV1DC1): HRR2 with smoke and heat vents and with draft curtain.

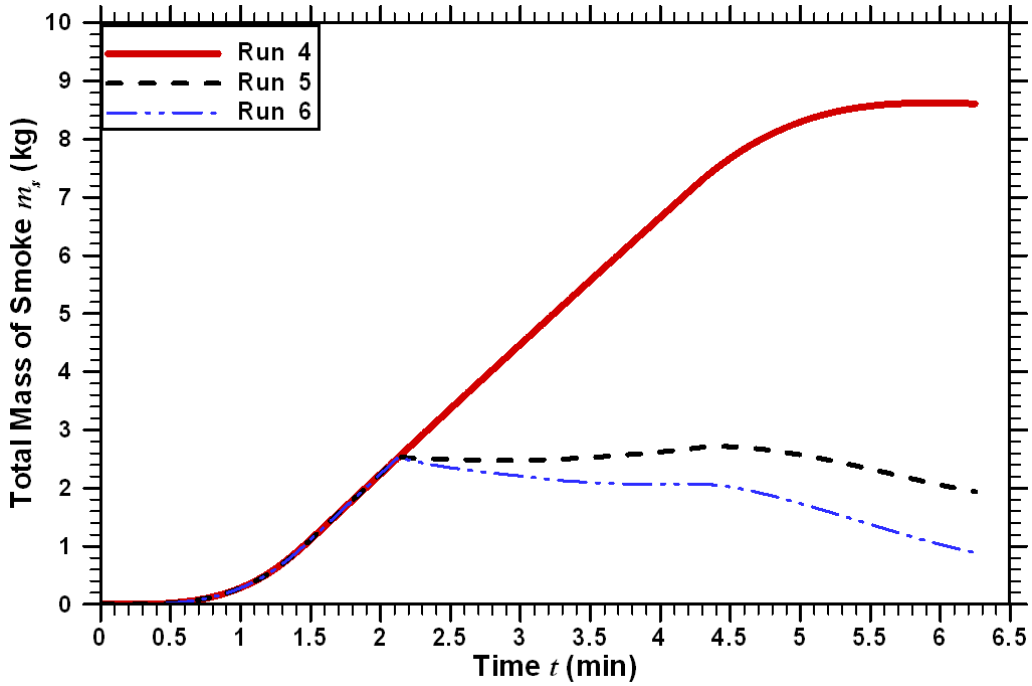

Figure 26. Comparison of the net building smoke masses remaining in the building Runs 4 - 6 (HRR2SHV0DC0, HRR2SHV1DC0, HRR2SHV1DC1).

Figure 26 compares the net smoke masses for Runs 4 – 6. The trend evident in Figure 15 is repeated. Run 4 indicates that the net smoke mass from HRR2 was about 8.5 kg. Run 5, which had smoke and heat vents, maintained the smoke mass essentially constant at about 2.2 kg until the decay period began, during which the smoke mass in the warehouse dropped. When the draft curtain was also included (Run 6), the performance improved, resulting in reduction of the smoke mass during the steady burn period. The differences by the end of the runs are striking: at least 4.25 times more smoke when comparing Run 4 to Run 5 and about 8.5 times for Runs 4 to 6.

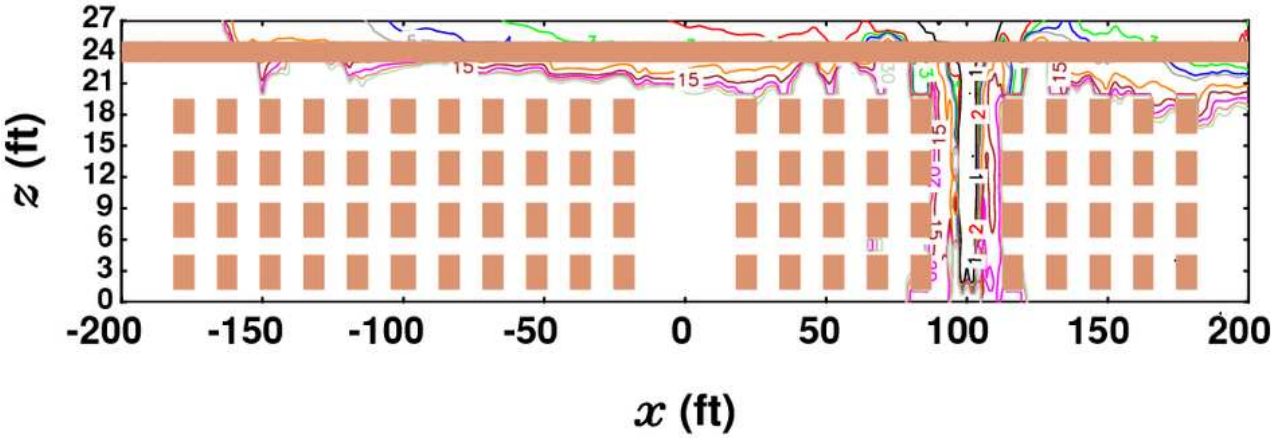

a) Run #4 (HRR2SHV0DC0): Without Smoke and Heat Vents and Without Draft Curtains

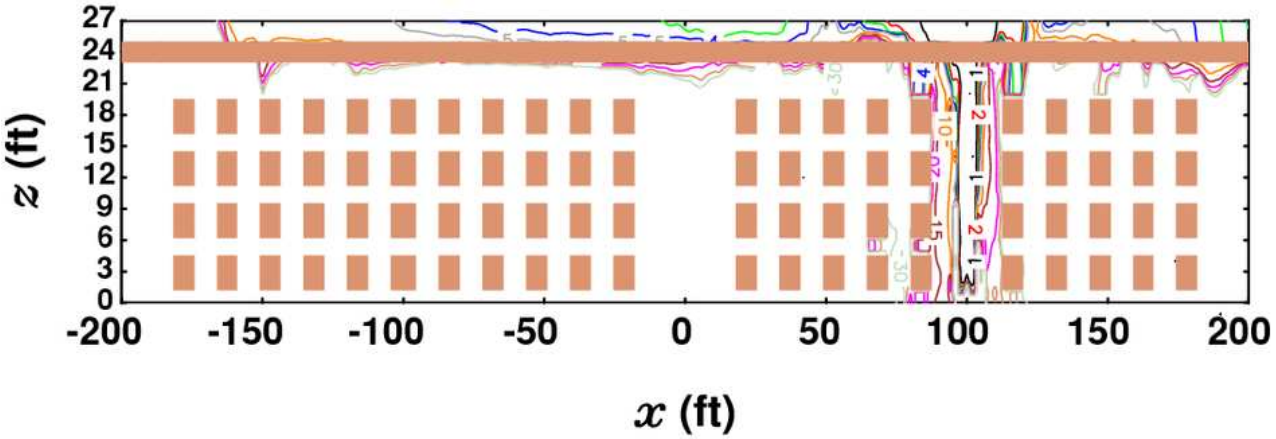

b) Run #5 (HRR2SHV1DC0): With Smoke and Heat Vents and Without Draft Curtains

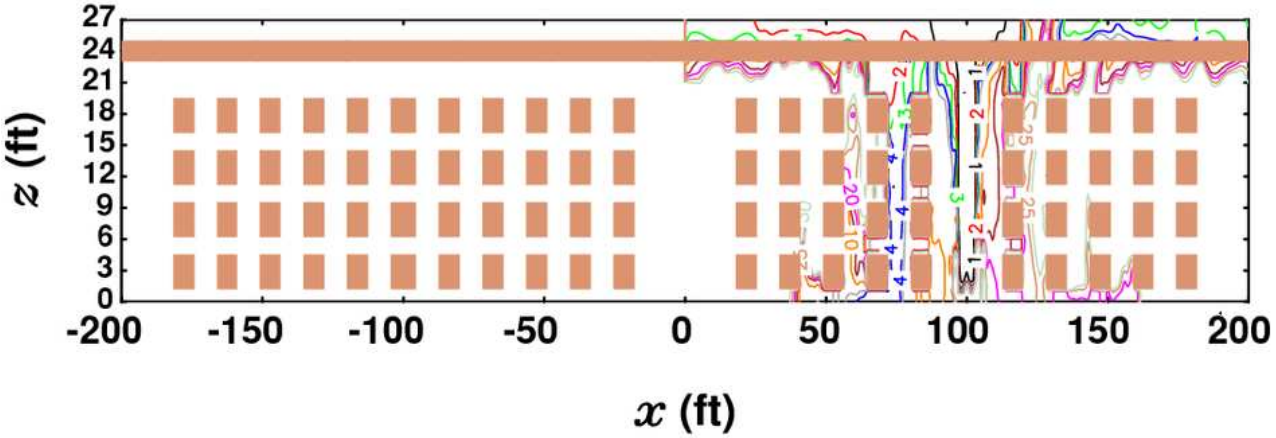

c) Run #6 (HRR2SHV1DC1): With Smoke and Heat Vents and With Draft Curtain

Figure 27. Visibility (in ft) along *y* = 0 ft at 180 s for HRR2 Runs 4 - 6. The vertical coordinate has been stretched.

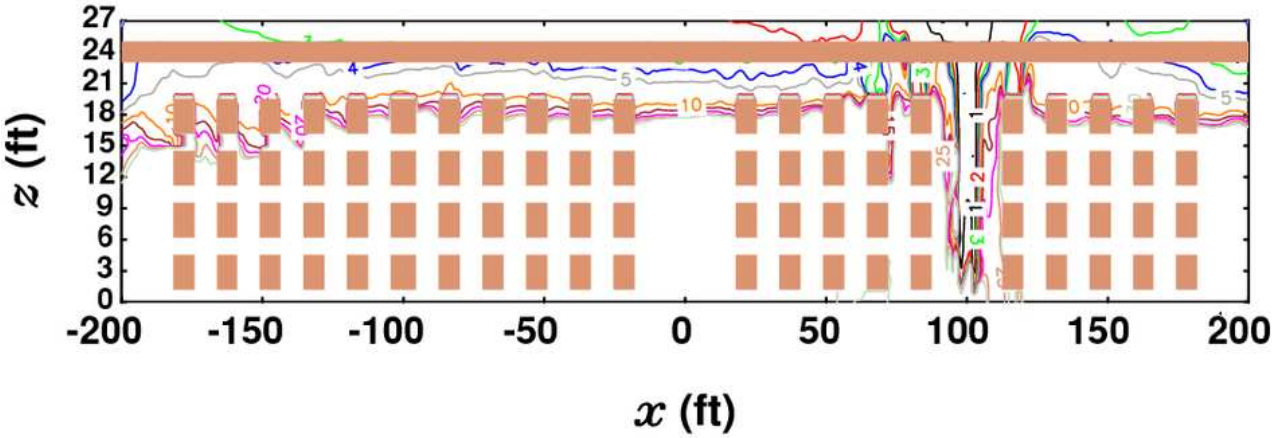

a) Run #4 (HRR2SHV0DC0): Without Smoke and Heat Vents and Without Draft Curtains

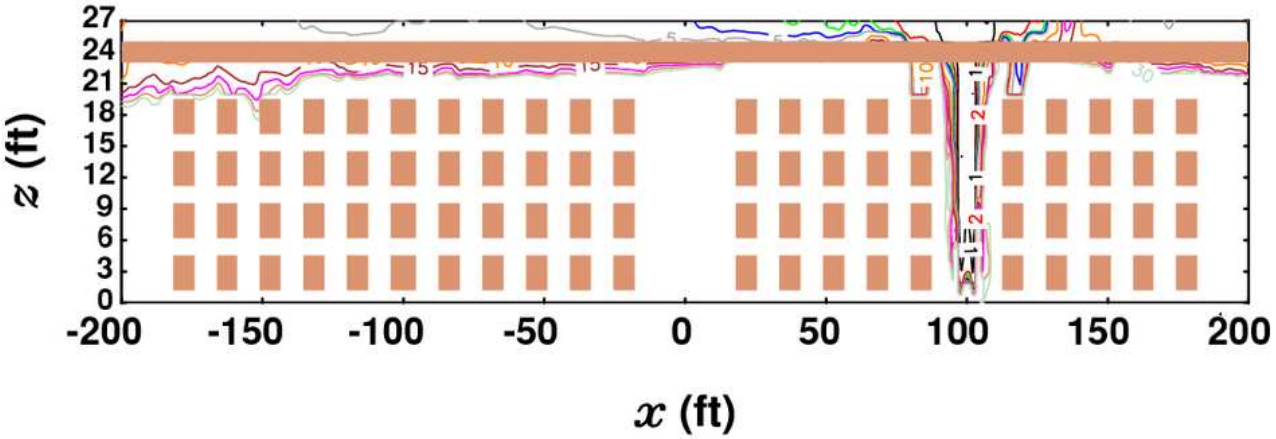

b) Run #5 (HRR2SHV1DC0): With Smoke and Heat Vents and Without Draft Curtains

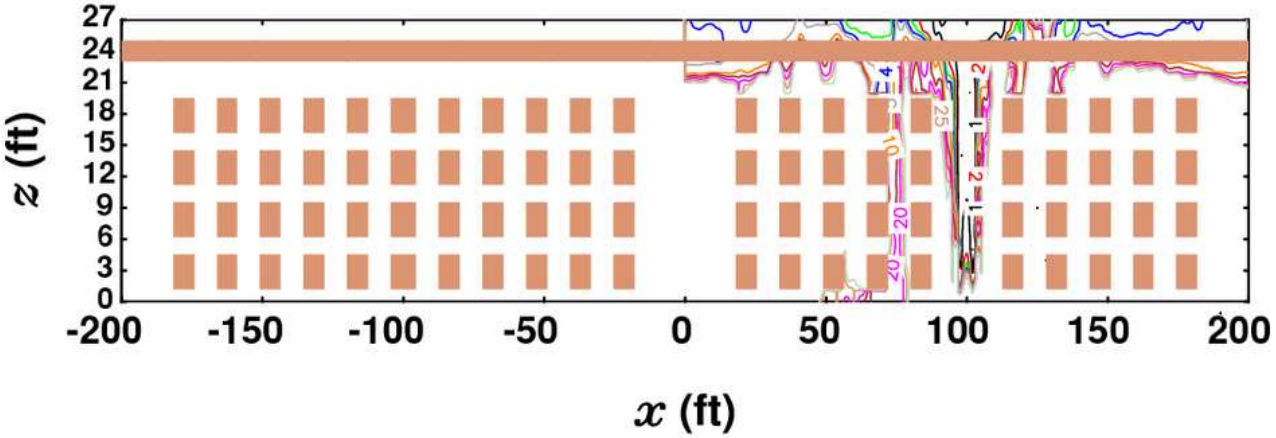

c) Run #6 (HRR2SHV1DC1): With Smoke and Heat Vents and With Draft Curtain

Figure 28. Visibility (in ft) along *y* = 0 ft at 270 s for HRR2 Runs 4 - 6. The vertical coordinate has been stretched.

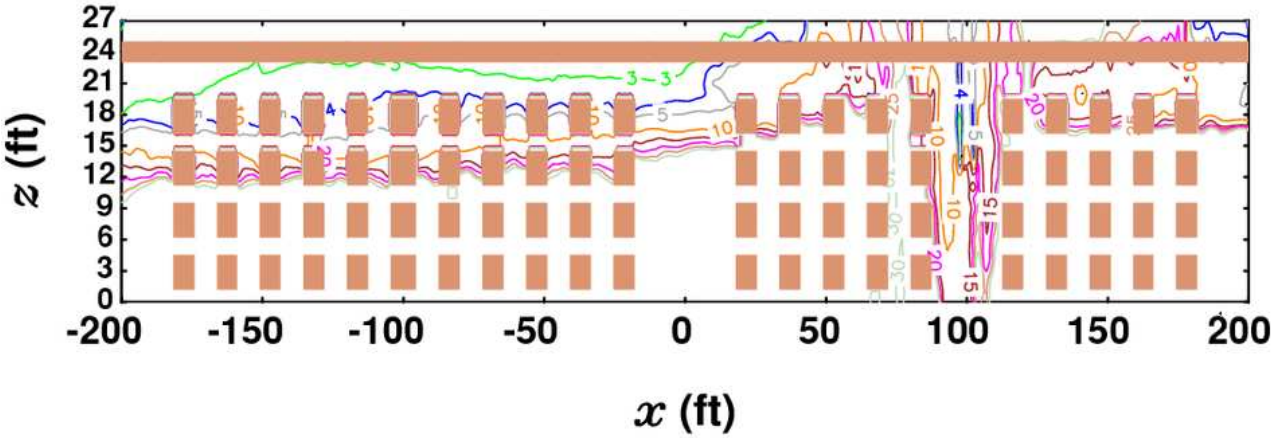

a) Run #4 (HRR2SHV0DC0): Without Smoke and Heat Vents and Without Draft Curtains

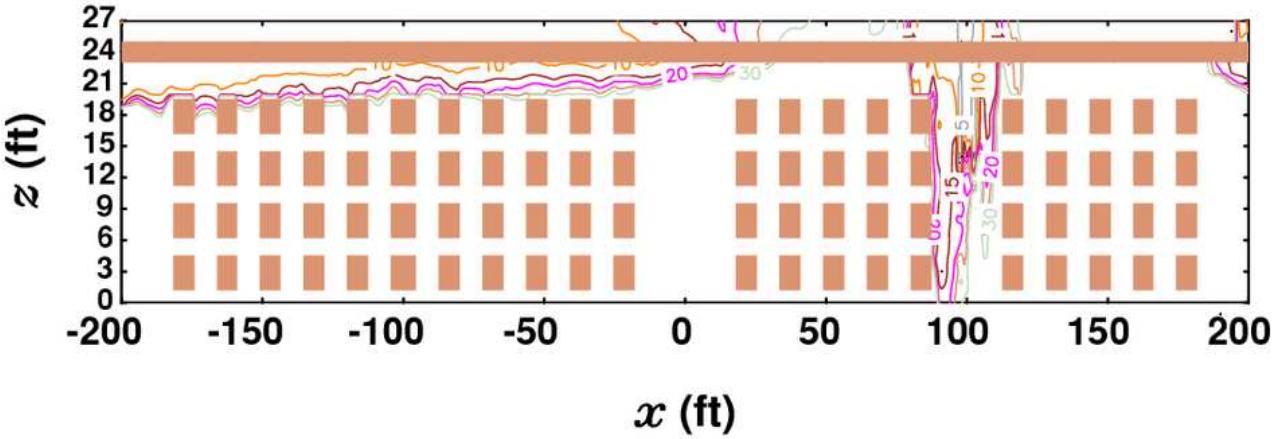

b) Run #5 (HRR2SHV1DC0): With Smoke and Heat Vents and Without Draft Curtains

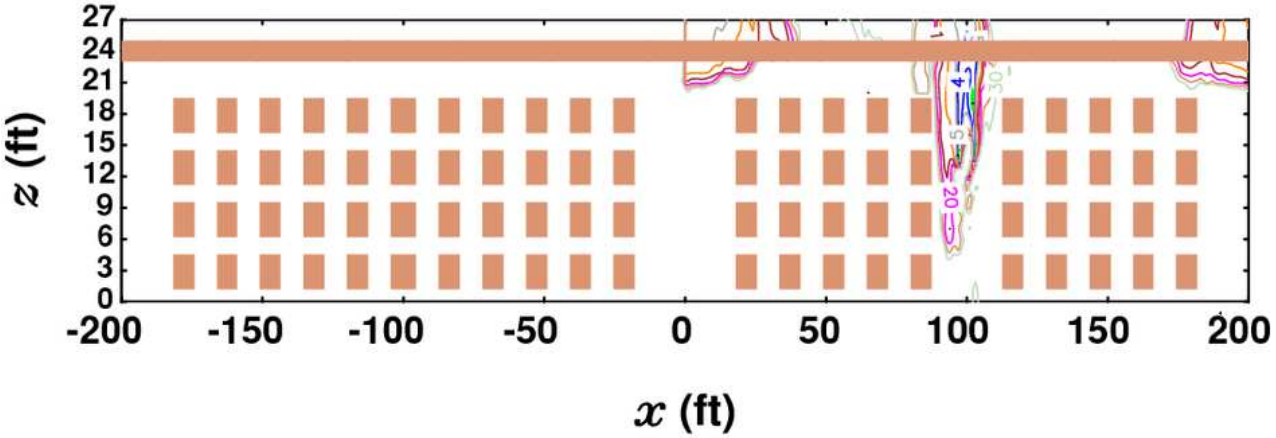

c) Run #6 (HRR2SHV1DC1): With Smoke and Heat Vents and With Draft Curtain

Figure 29. Visibility (in ft) along *y* = 0 ft at 360 s for HRR2 Runs 4 - 6. The vertical coordinate has been stretched.

Figures 27 - 29 show contours of the visibility (in ft) along the center of the warehouse ($y = 0$ plane). At 180 s, Figure 27 shows that the ceiling jet was still spreading along the length of the warehouse except for Run 6, where the draft curtain had already limited the ceiling jet's extent. At

270 s, Figure 28 shows a descending smoke layer for Run 4. The smoke and heat vents in Run 5 kept the smoke layer from descending. The partition provided by the draft curtain in Run 6 maintained an upper layer depth similar to that of Run 5 but with half the lateral extent. Figure 26 shows that this was possible because more smoke exited the warehouse with the vents-curtain combination. By 360 s, Figure 29 shows that for Run 4 the upper layer continued to descend. For Run 5, the zone that contains the vents was relatively clear of smoke. However, the remaining smoke in the rest of the warehouse would be traveling to this zone to exit. For Run 6, the zone without the fire was clear. The zone with the fire had residual traces of smoke that the vents continued to extract. For HRR2 the upper layer never drops to the 1.83 m (6′) level.

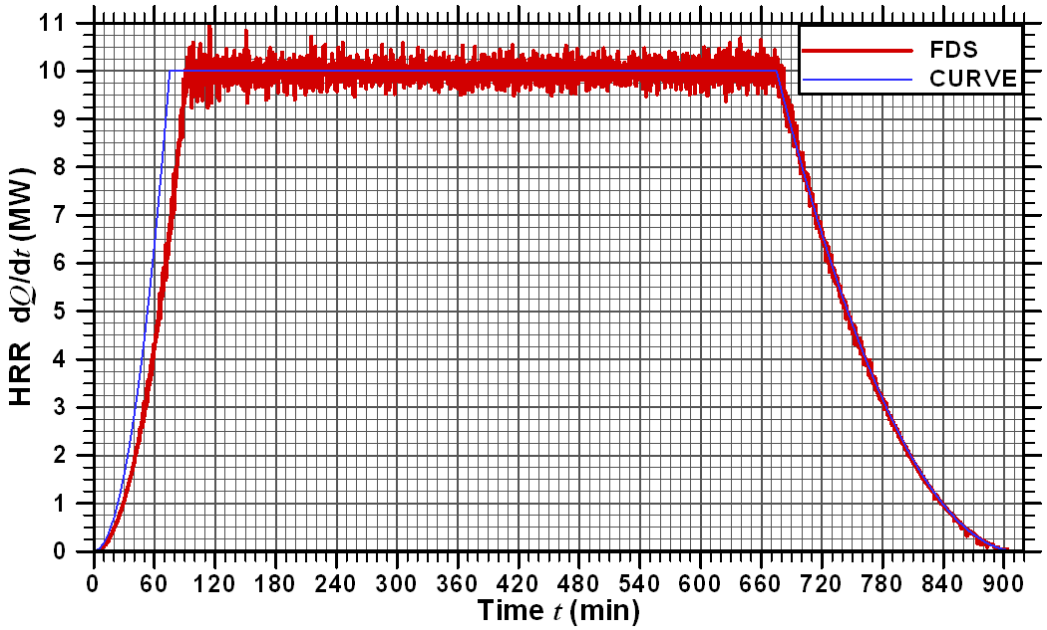

Figure 30. Comparison of the computed heat release rate for Run 7 (HRR3SHV0DC0) with the HRR3 curve.

3.4 HRR3 Fire Source

Runs 7 – 9 are based on HRR3. HRR3 is like HRR2 except with longer steady burn and decay periods as noted in Table 4. These features are directly based upon the plastic commodity tests performed by McGrattan et al [1998]. Like prior runs, Runs 7 – 9 utilized a fire originating from the center racks on the east side of the warehouse (Figures 1 and 2) and the simulations differed in the presence of curtains and/or vents. Figure 30 shows the HRR computed by Run 7. The output HRRs for Runs 8 and 9 are very similar. Comparison reveals good agreement with the target profile.

3.4.1 Run #7 (HRR3SHV0DC0): HRR3 without Smoke and Heat Vents and without Draft Curtains

Figure 31 compares the cumulative number of active sprinklers with the associated heat release rate for Run 7. Run 7 had a total of 21 sprinklers while Run 4 had 19. The sprinkler activation map in Figure 32 shows an orderly progression of sprinkler activations stemming from the center of the burning racks. Considering that the fire lasted so much longer than HRR2 it is at first surprising that only two more sprinklers operated. However, the experimental results in Table 6 indicate that an average of 21 sprinkler activations are associated with a 75 s t-squared rise to 10 MW. Cooling was being provided by the sprinklers (and the vents) so that the number of additional activations as the fire continued would be few in number.

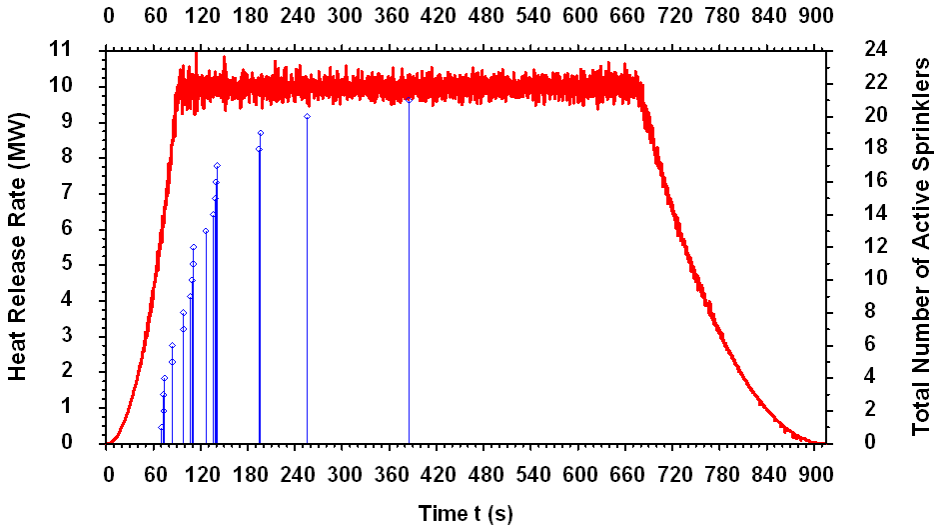

Figure 31. Comparison of the heat release rate and the sprinkler activation times for Run #7 (HRR3SHV0DC0): HRR3 without smoke and heat vents and without draft curtains.

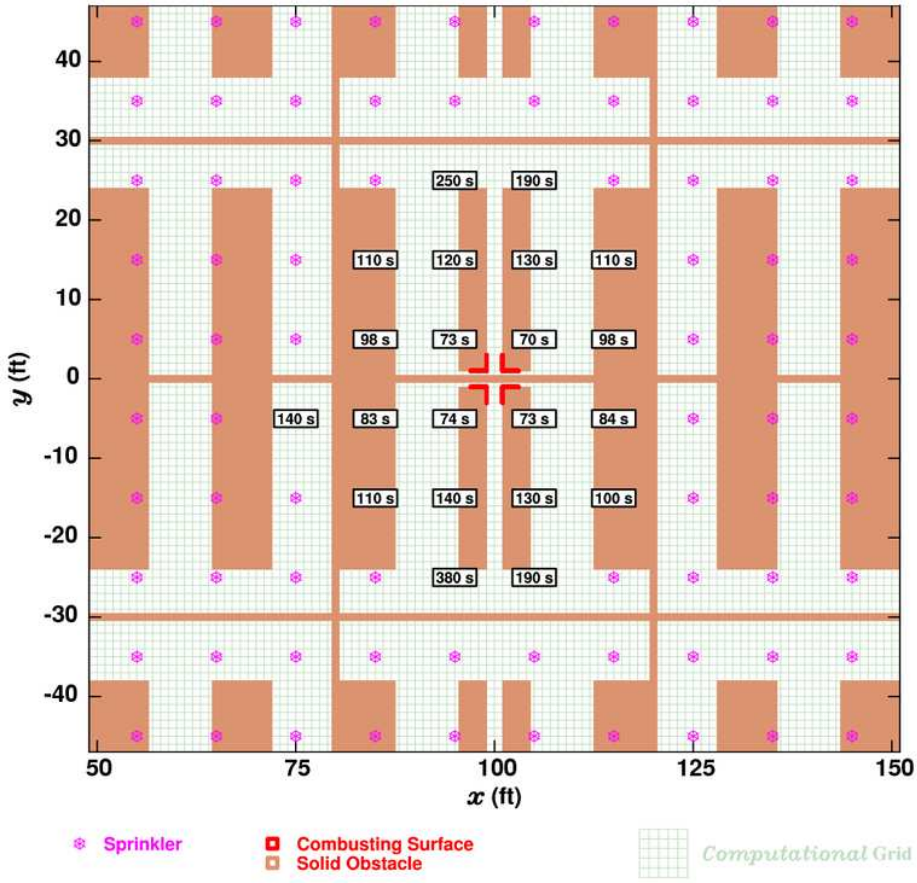

Figure 32. Sprinkler activation map for Run #7 (HRR3SHV0DC0): HRR3 without smoke and heat vents and without draft curtains.

3.4.2 Run #8 (HRR3SHV1DC0): HRR3 with Smoke and Heat Vents and without Draft Curtains

When the vents opened for Run 8, the rate of sprinkler activations in Figure 33 slowed down. This resulted in a total of 19 sprinkler activations. Again, the order of operation in Figure 34 is well behaved even after the vents opened.

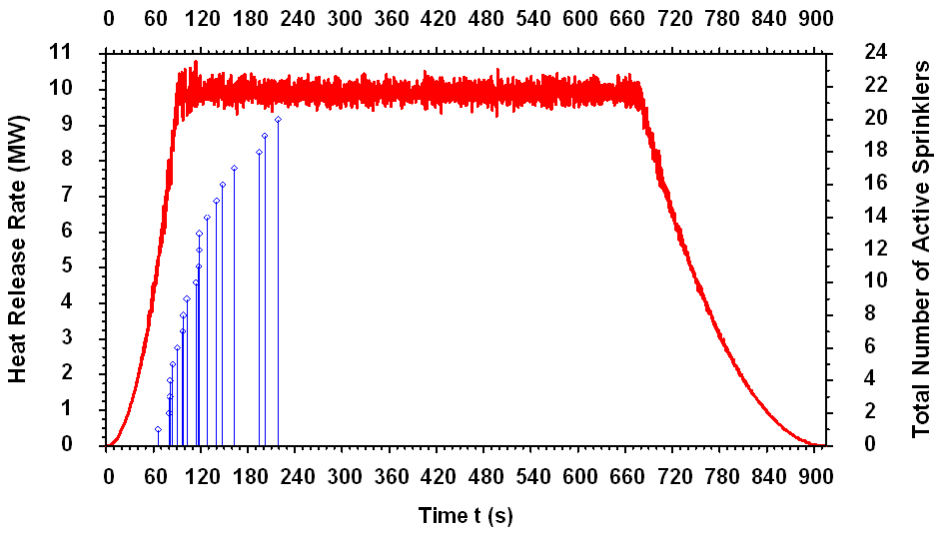

Figure 33. Comparison of the heat release rate and the sprinkler activation times for Run #8 (HRR3SHV1DC0): HRR3 with smoke and heat vents and without draft curtains.

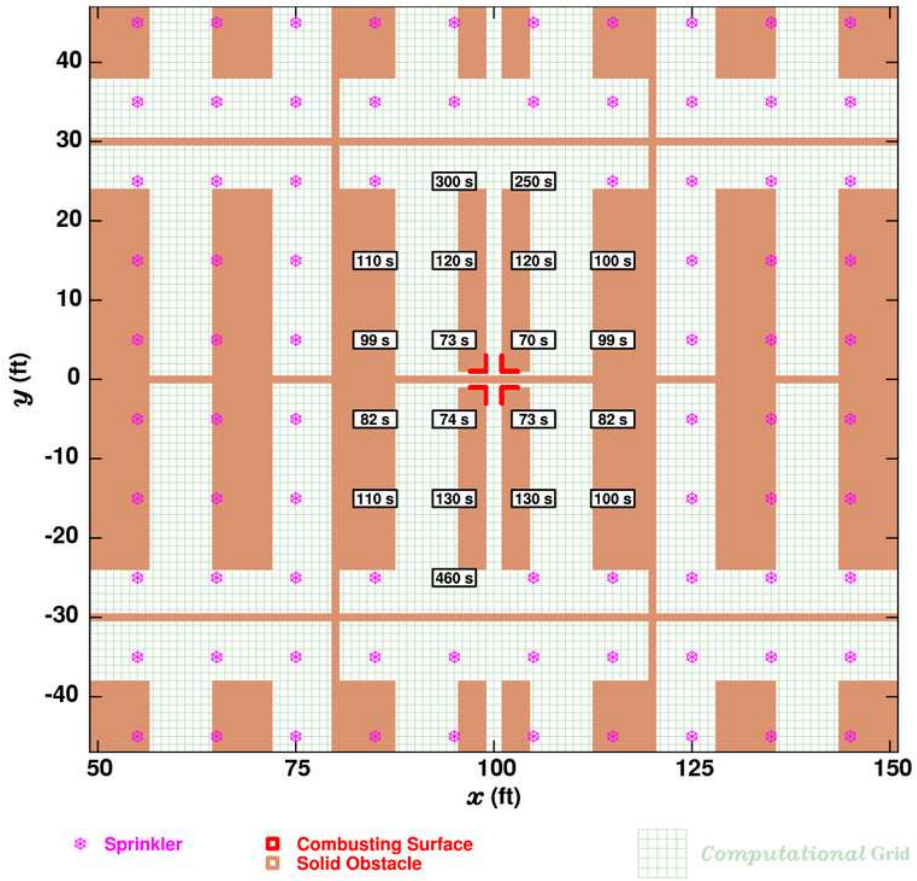

Figure 34. Sprinkler activation map for Run #8 (HRR3SHV1DC0): HRR3 with smoke and heat vents and without draft curtains.

3.4.3 Run #9 (HRR3SHV1DC1): HRR3 with Smoke and Heat Vents and with Draft Curtain

For Run 9, as Figure 35 shows, the addition of the draft curtain resulted in 20 sprinkler operations. This is one more than was the case for Run 8. The sprinkler activation pattern in Figure 36 is orderly.

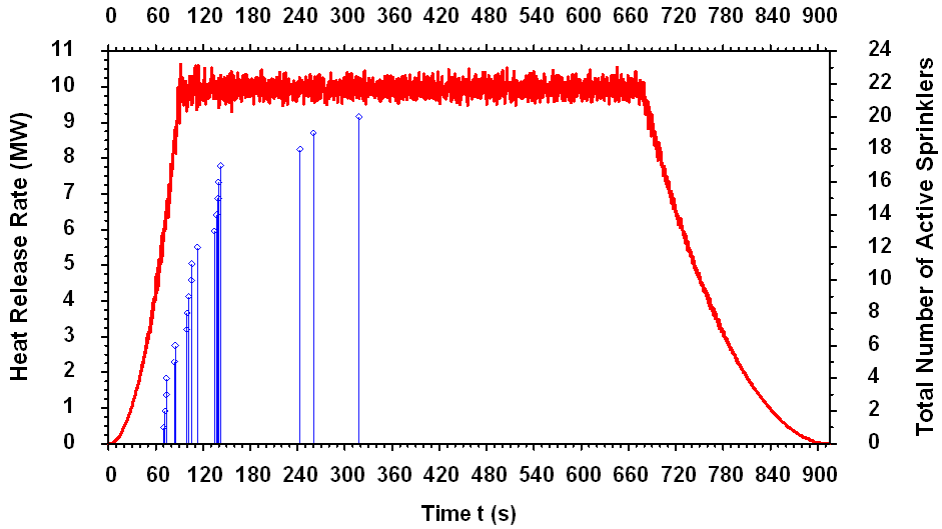

Figure 35. Comparison of the heat release rate and the sprinkler activation times for Run #9 (HRR3SHV1DC1): HRR3 with smoke and heat vents and with draft curtains.

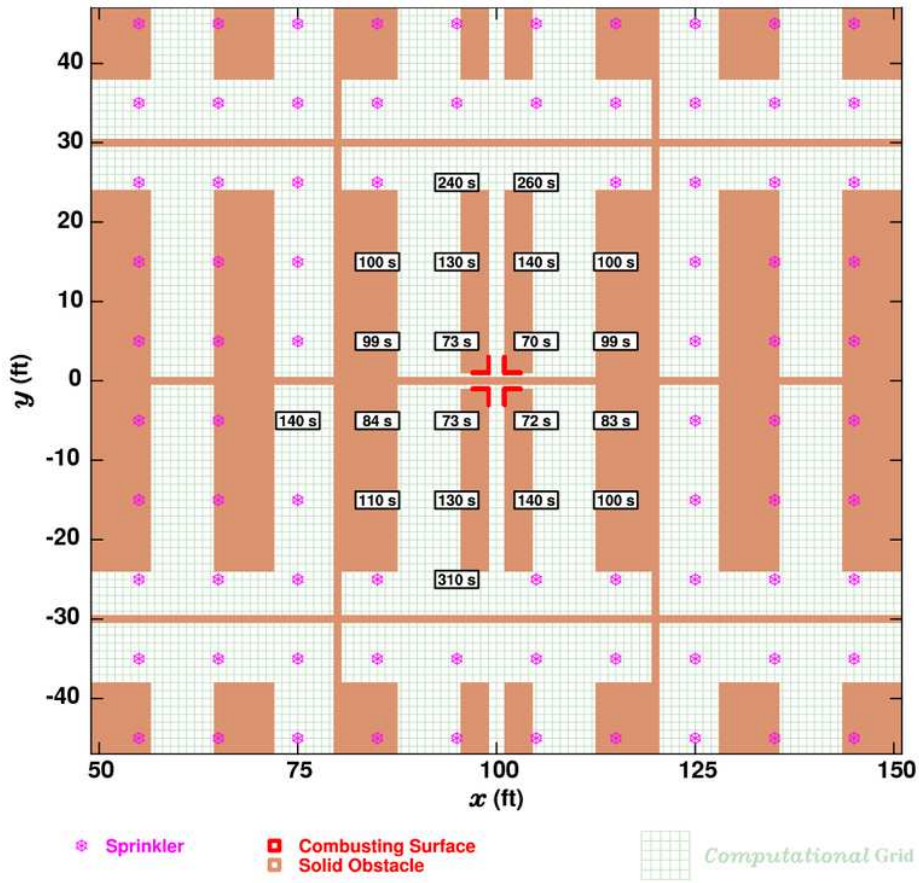

Figure 36. Sprinkler activation map for Run #9 (HRR3SHV1DC1): HRR3 with smoke and heat vents and with draft curtains.

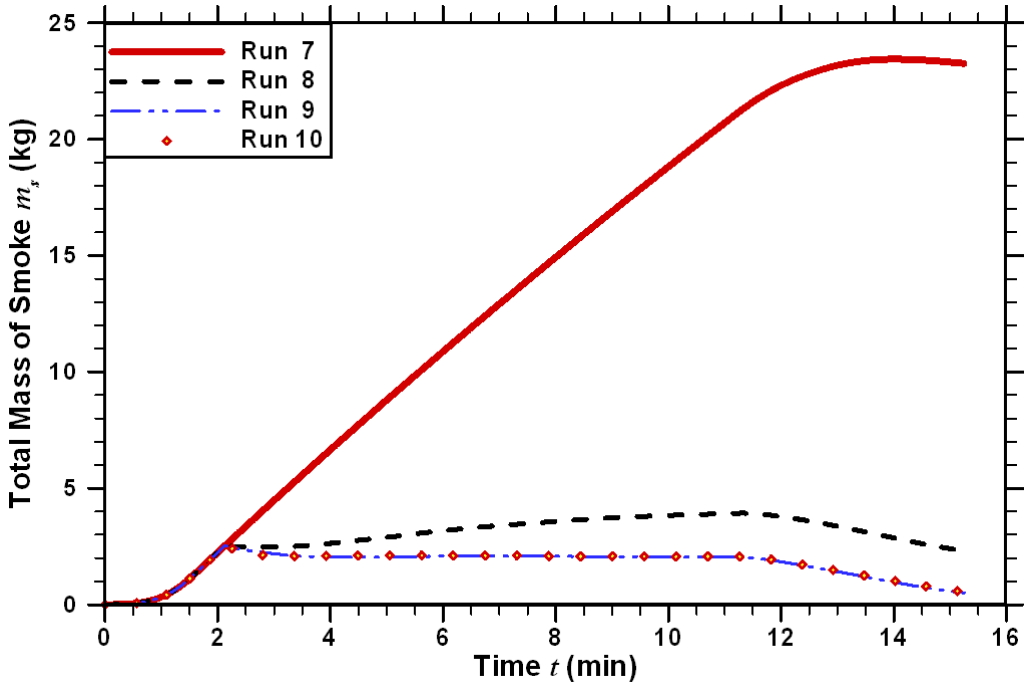

Figure 37. Comparison of the net building smoke masses remaining in the building for Runs 7 - 10 (HRR3SHV0DC0, HRR3SHV1DC0, HRR3SHV1DC1, HRR3SHV1DC1CB).

As illustrated in Figure 36, while the smoke mass in the unvented warehouse reached masses in excess of 23 kg, the net smoke masses remained at about the same levels as had been the case with HRR2 when curtains and/or vents were in use. Smoke and heat vent performance was, as before, improved by the presence of the draft curtain.

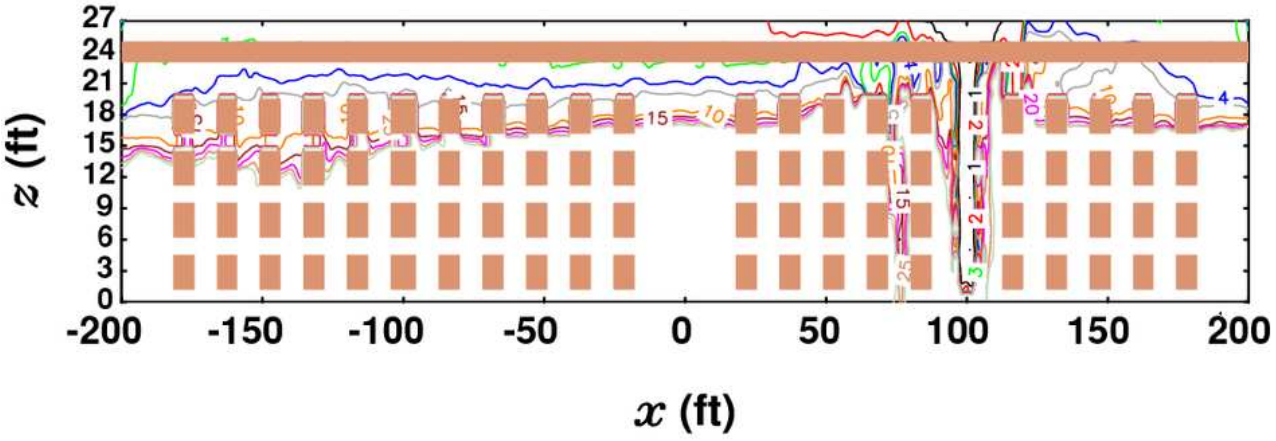

a) Run #7 (HRR3SHV0DC0): without smoke and heat vents and without draft curtains

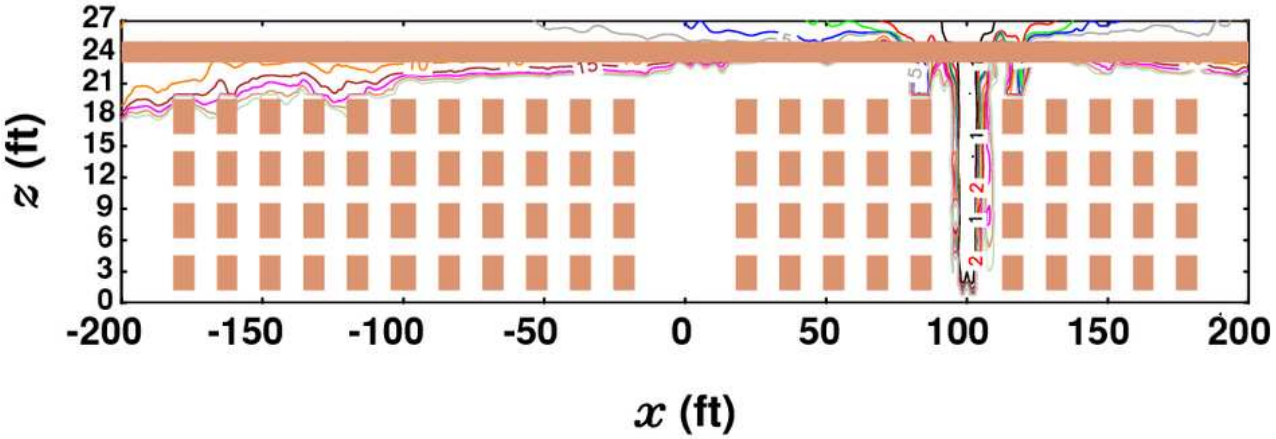

b) Run #8 (HRR3SHV1DC0): with smoke and heat vents and without draft curtains

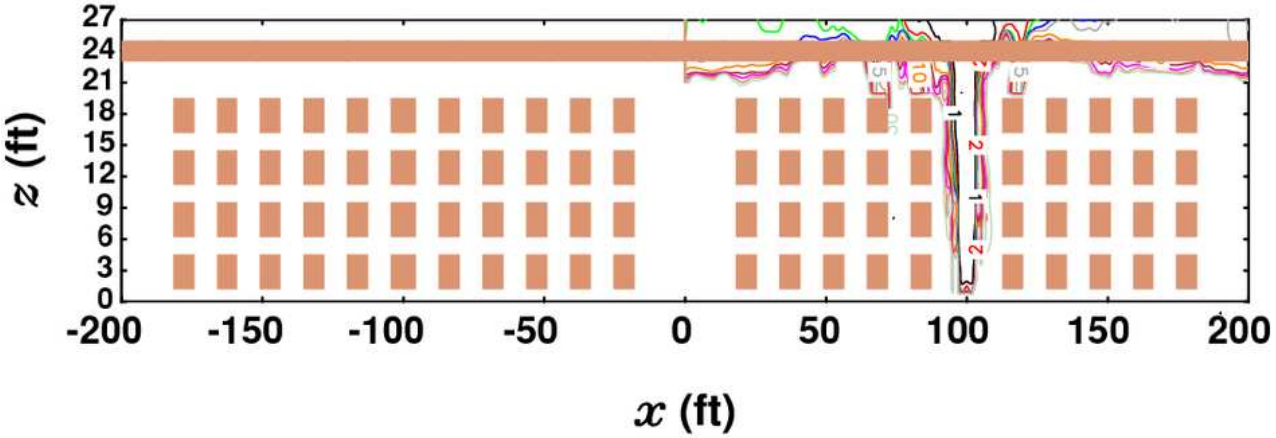

c) Run #9 (HRR3SHV1DC1): with smoke and heat vents and with draft curtains

Figure 38. Visibility (in ft) along *y* = 0 ft at 300 s for HRR3 Runs 7 - 9. The vertical coordinate has been stretched.

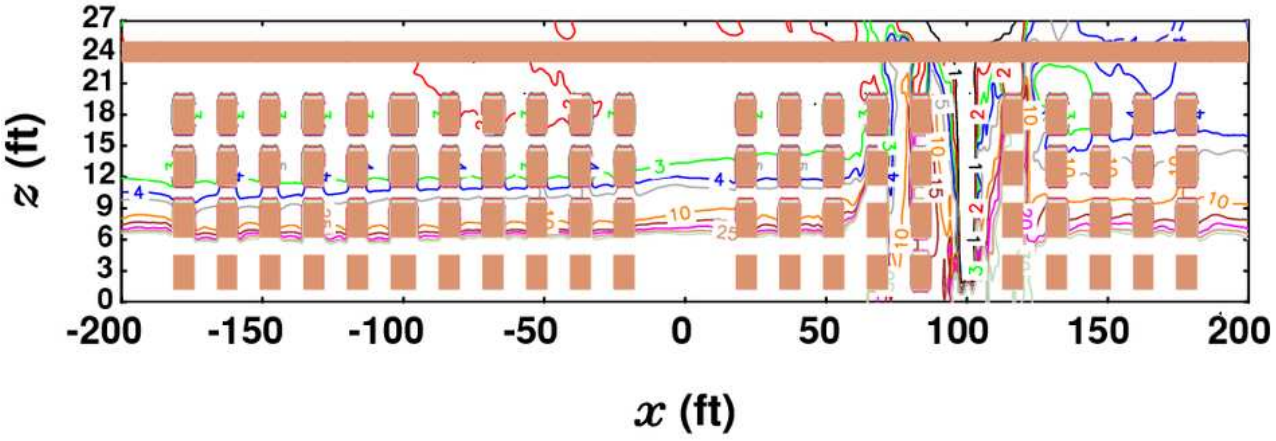

a) Run #7 (HRR3SHV0DC0): without smoke and heat vents and without draft curtains

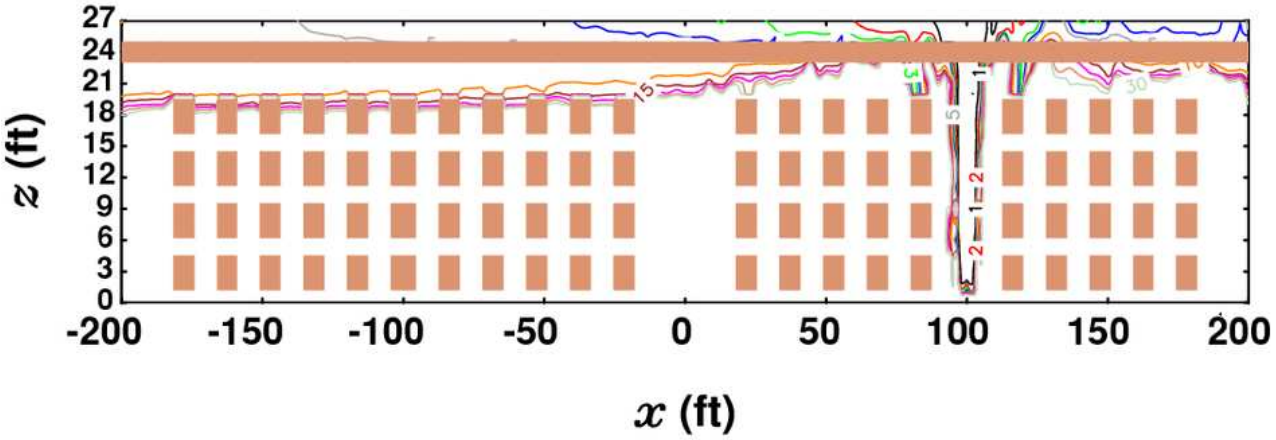

b) Run #8 (HRR3SHV1DC0): with smoke and heat vents and without draft curtains

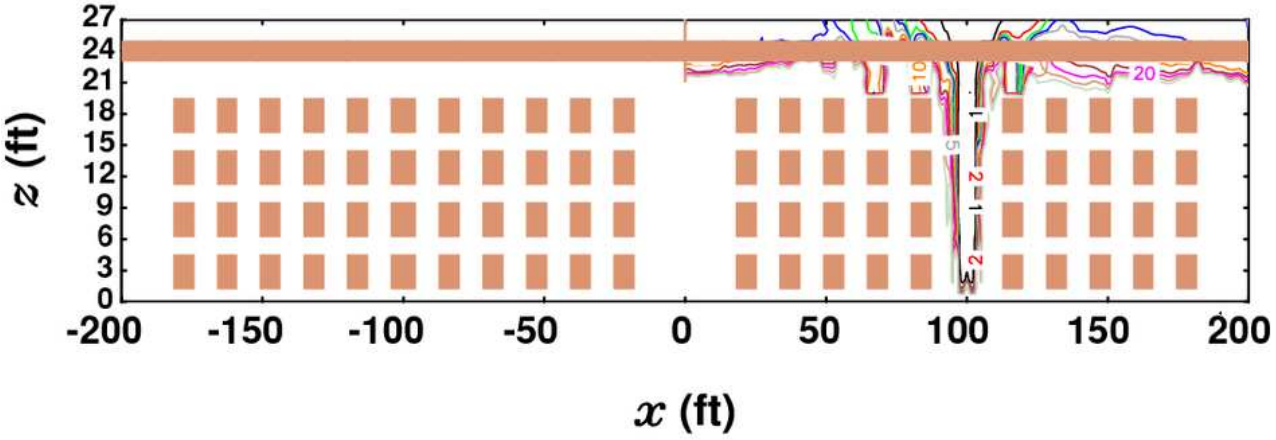

c) Run #9 (HRR3SHV1DC1): with smoke and heat vents and with draft curtains

Figure 39. Visibility (in ft) along *y* = 0 ft at 600 s for HRR3 Runs 7 - 9. The vertical coordinate has been stretched.

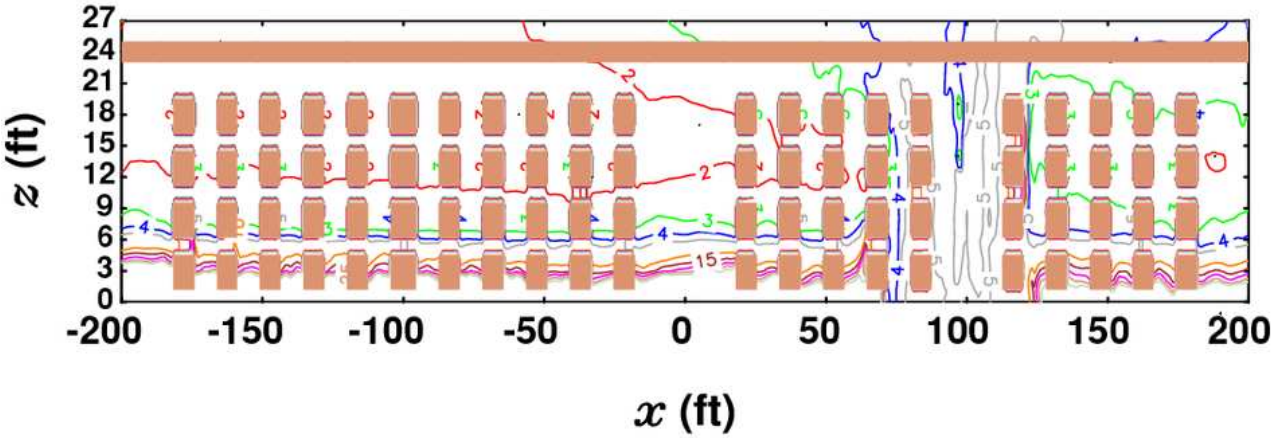

a) Run #7 (HRR3SHV0DC0): without smoke and heat vents and without draft curtains

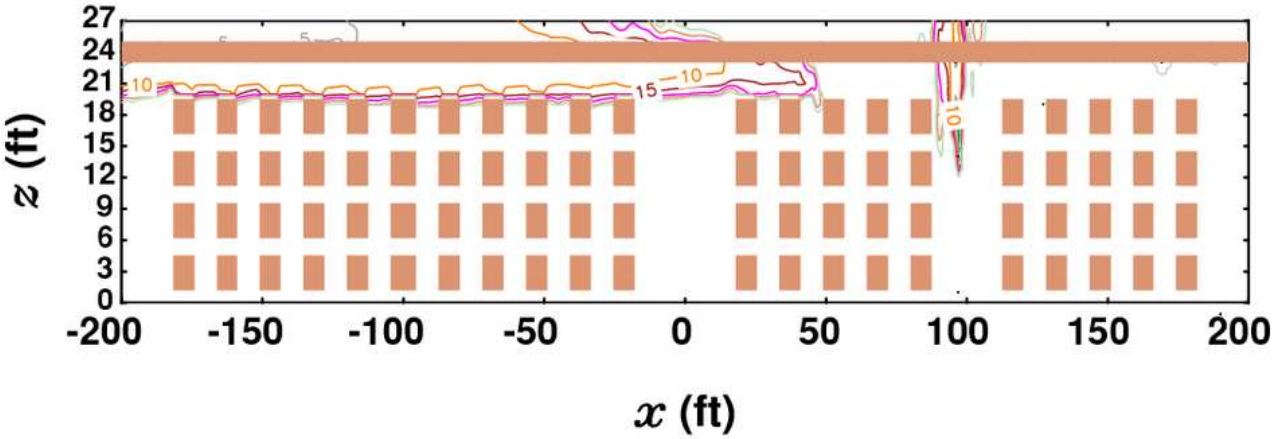

b) Run #8 (HRR3SHV1DC0): with smoke and heat vents and without draft curtains

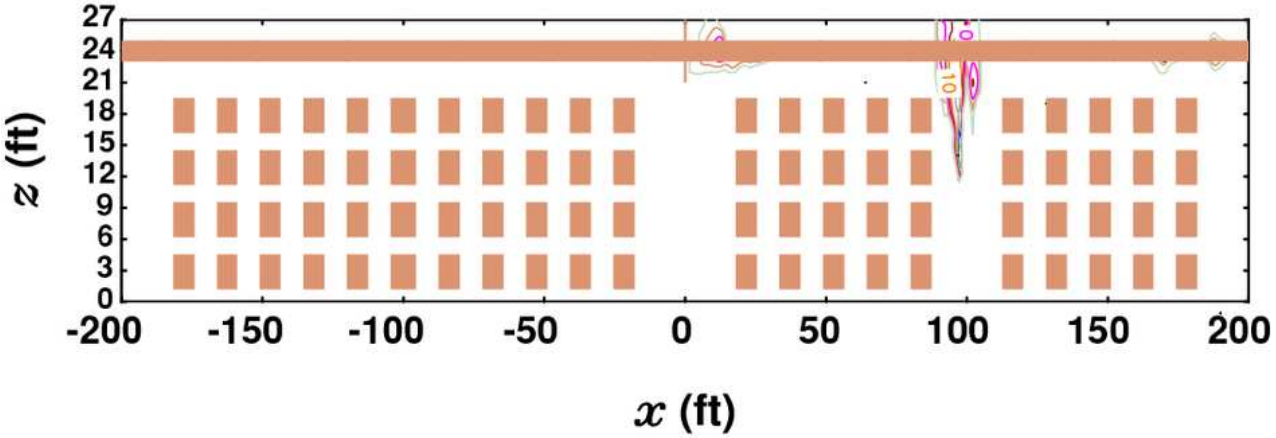

c) Run #9 (HRR3SHV1DC1): with smoke and heat vents and with draft curtains

Figure 40. Visibility (in ft) along *y* = 0 ft at 900 s for HRR3 Runs 7 - 9. The vertical coordinate has been stretched.

Figures 38 - 40 show contours of the visibility (in ft) for Runs 7 – 9 along the center of the warehouse (i.e., on the y = 0 plane). The unvented case was fully smoke logged while the vented cases were clear. Figure 38 shows the visibility contours at 300 s. For Run 7, a smoke layer which

was deeper at the west end of the warehouse was descending. Because of the lack of a draft curtain, the smoke layer was deeper at the west section as well for Run 8 even though the vents reduced the thickness of the smoke layer and provided improving conditions in sections removed from the west. For Run 9, the smoke was contained to the east roof vent zone. In Figures 39, by 600 s the smoke layer (i.e., the S = 30 ft (9.14 m) contour line) had descended to the critical level of 6 ft for Run 7. For Run 8, the smoke interface at the west section of the warehouse uniformly covered the top of the racks and was nowhere near the plane of concern for occupant and firefighter safety. Once again for Run 9, the smoke was contained to the east roof vent zone. Figure 40 shows the warehouse fully smoke logged for Run 7. On the other hand, for Run 8, which had smoke and heat vents but no draft curtain, the smoke in the unopened roof vent zone was traveling to the other zone with the open vents. For Run 9, which had vents and a draft curtain, the conditions were relatively clear throughout the warehouse.

3.5 Ceiling-Mounted Support Beams

In most runs support beams were offset from the ceiling in order to minimize any "draft curtain effects" that they might represent. Run 10 examines the impact of two foot deep support beams that were attached to the ceiling on smoke spread. Run 10 was based on HRR3 with the burning racks centered on the east roof vent zone. For Run 10, the warehouse was equipped with smoke and heat vents and a draft curtain. Thus Run 10 only differed from Run 9 in the separation distance of the support beams from the ceiling. Figure 41 shows a rapid succession of sprinkler activations that gradually slowed down once the heat release rate became steady. Twenty sprinklers operated instead of the twenty-two for Run 9. The sprinkler activation map in Figure 42 shows that the beams created two pockets about the center of burning racks. The sprinkler activations were confined to these pockets. Contrast this with Figure 36 for Run 9, where the 140 s activation occurs outside and to the west of the lower pocket. Even though the beams contained the sprinkler activations, Figure 37 shows that they had no noticeable impact on the vents ability to extract smoke.

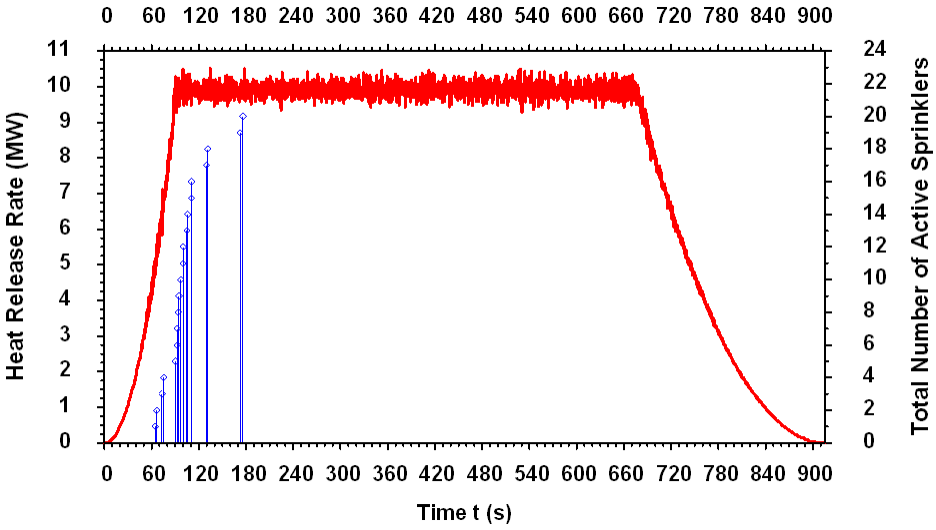

Figure 41. Comparison of the heat release rate and the sprinkler activation times for Run #10 (HRR3SHV1DC1CB): HRR3 with smoke and heat vents and with draft curtains and beams at the ceiling.

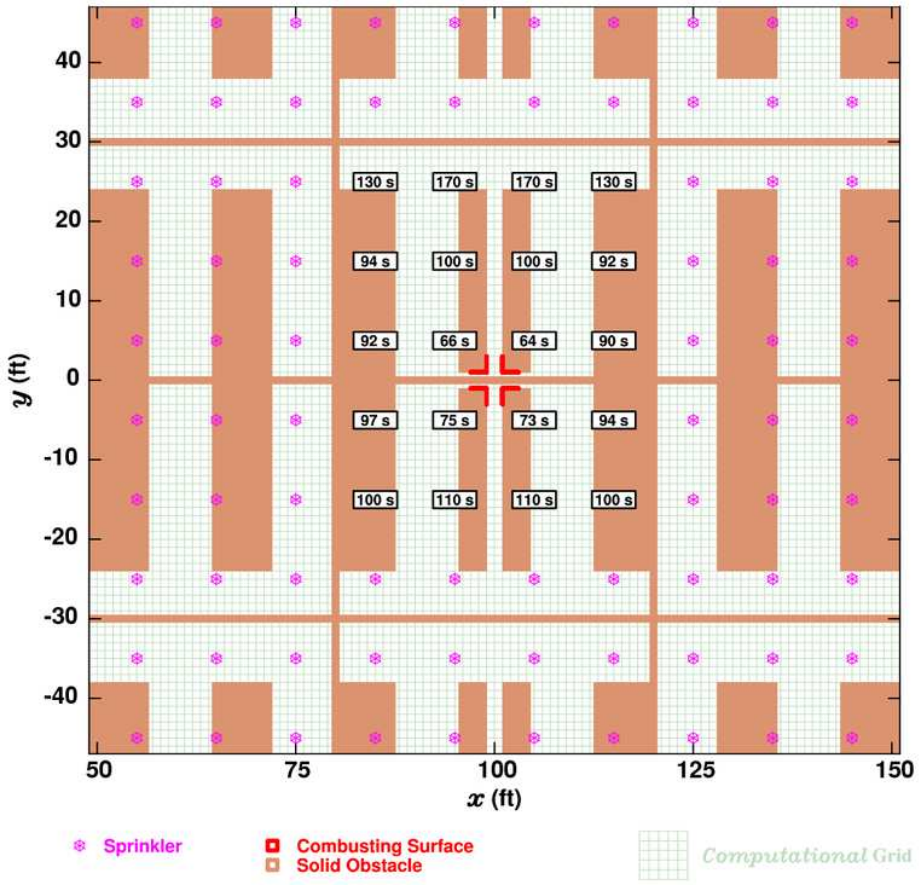

Figure 42. Sprinkler activation map for Run #10 (HRR3SHV1DC1CB): HRR3 with smoke and heat vents and with draft curtains and beams at the ceiling.

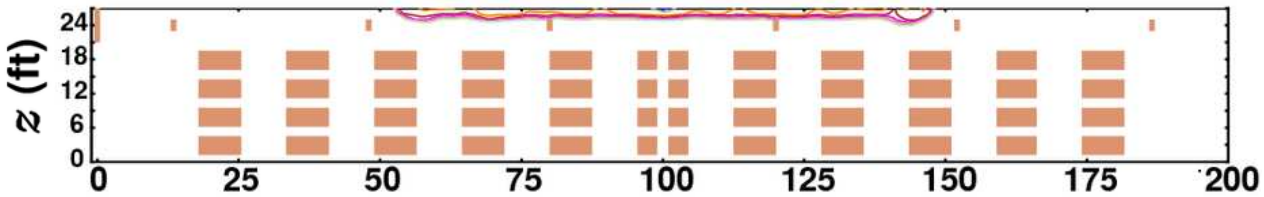

a) Run #9 (HRR3SHV1DC1): with smoke and heat vents and with draft curtains and without beams at the ceiling

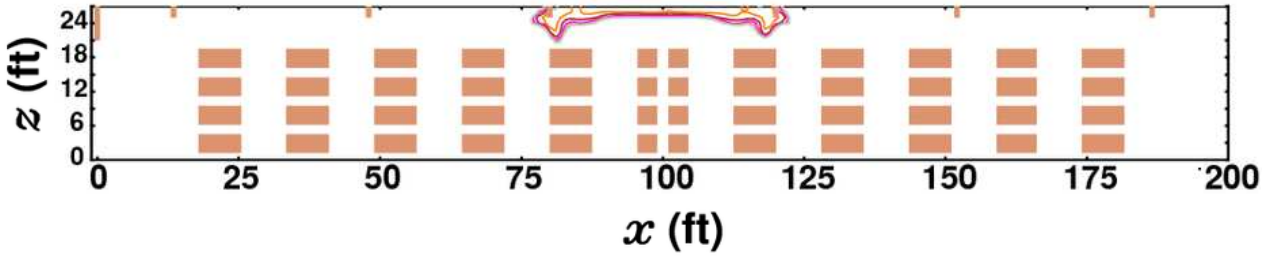

b) Run #10 (HRR3SHV1DC1CB): with smoke and heat vents and with draft curtains and with beams at the ceiling

Figure 43. Visibility (in ft) along *y* = -20 ft at 35 s for HRR3 Runs 9 and 10.

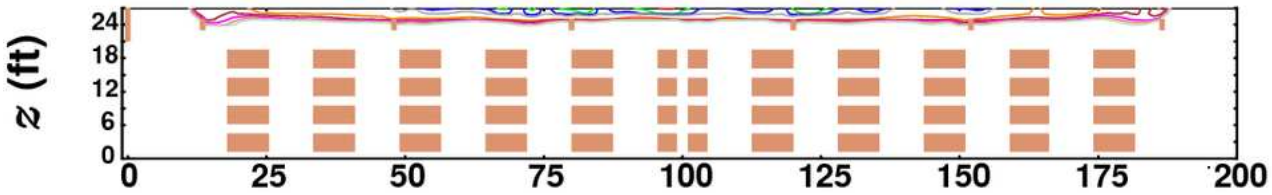

a) Run #9 (HRR3SHV1DC1): with smoke and heat vents and with draft curtains and without beams at the ceiling

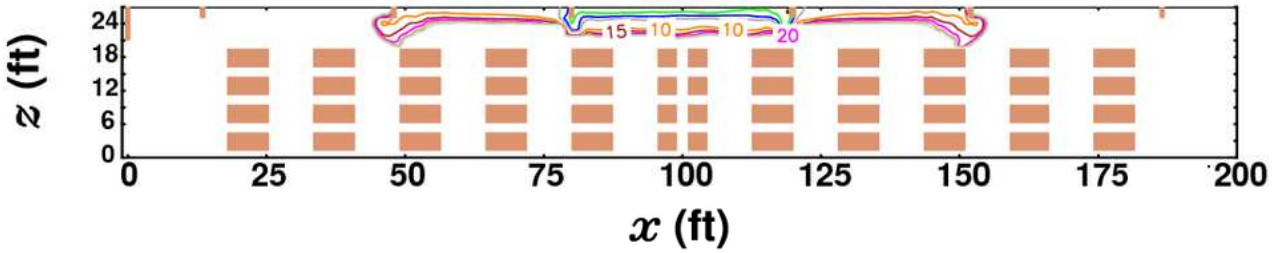

b) Run #10 (HRR3SHV1DC1CB): with smoke and heat vents and with draft curtains and with beams at the ceiling

Figure 44. Visibility (in ft) along *y* = -20 ft at 57 s for HRR3 Runs 9 and 10.

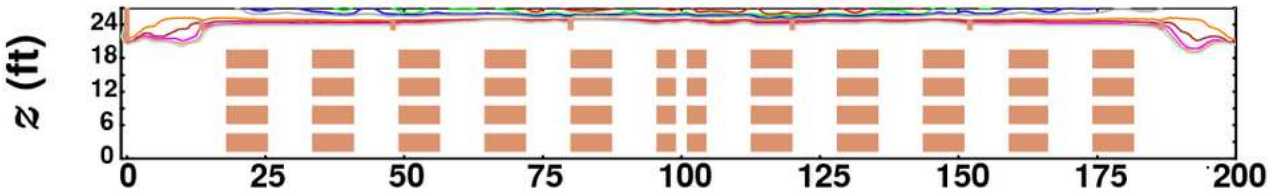

a) Run #9 (HRR3SHV1DC1): with smoke and heat vents and with draft curtains and without beams at the ceiling

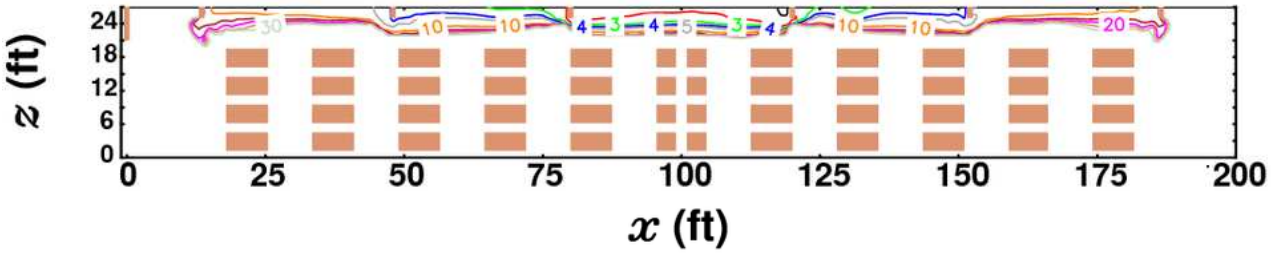

b) Run #10 (HRR3SHV1DC1CB): with smoke and heat vents and with draft curtains and with beams at the ceiling

Figure 45. Visibility (in ft) along *y* = -20 ft at 78 s for HRR3 Runs 9 and 10.

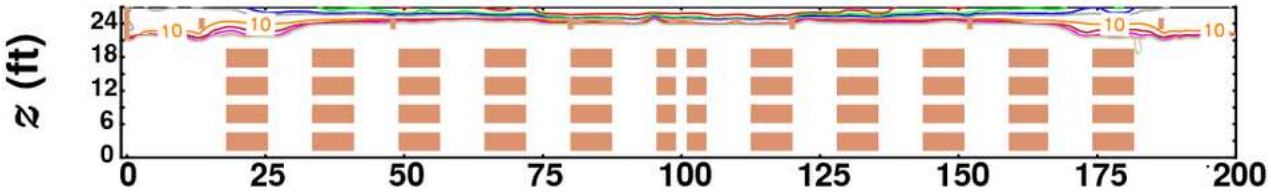

a) Run #9 (HRR3SHV1DC1): with smoke and heat vents and with draft curtains and without beams at the ceiling

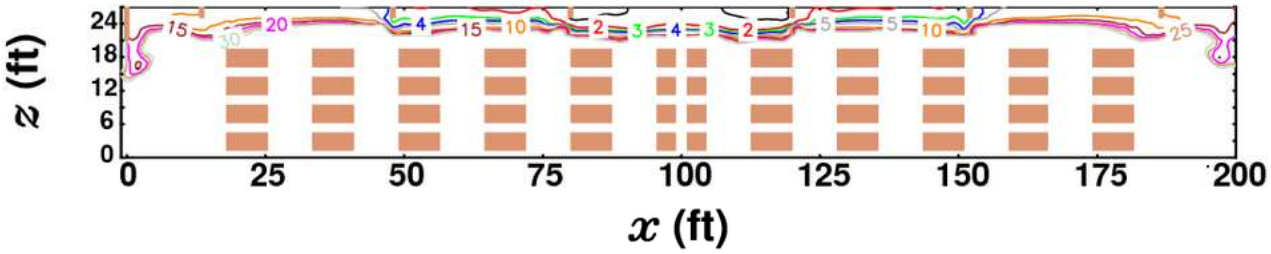

b) Run #10 (HRR3SHV1DC1CB): with smoke and heat vents and with draft curtains and with beams at the ceiling

Figure 46. Visibility (in ft) along *y* = -20 ft at 90 s for HRR3 Runs 9 and 10.

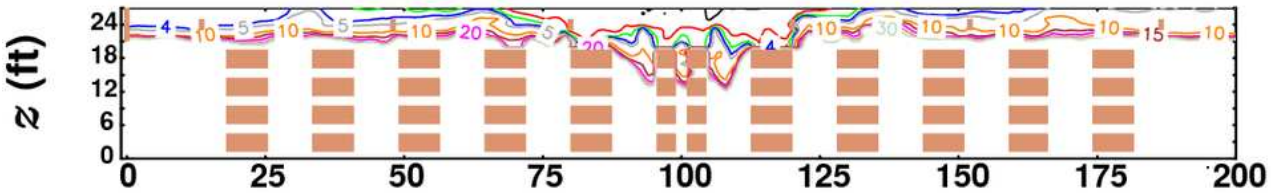

a) Run #9 (HRR3SHV1DC1): with smoke and heat vents and with draft curtains and without beams at the ceiling

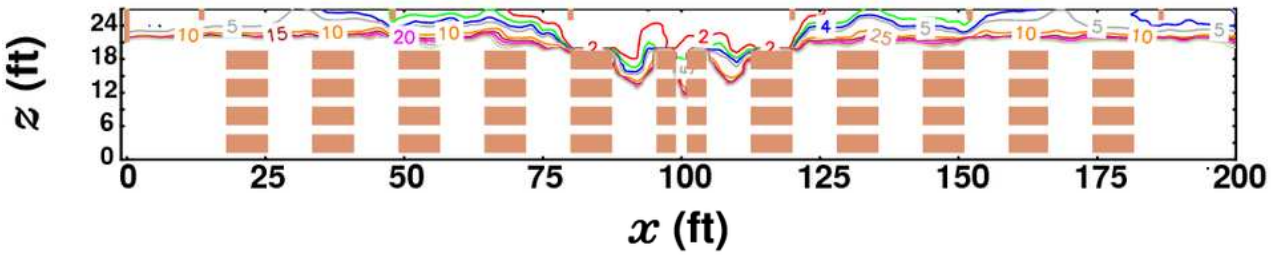

b) Run #10 (HRR3SHV1DC1CB): with smoke and heat vents and with draft curtains and with beams at the ceiling

Figure 47. Visibility (in ft) along *y* = -20 ft at 300 s for HRR3 Runs 9 and 10.

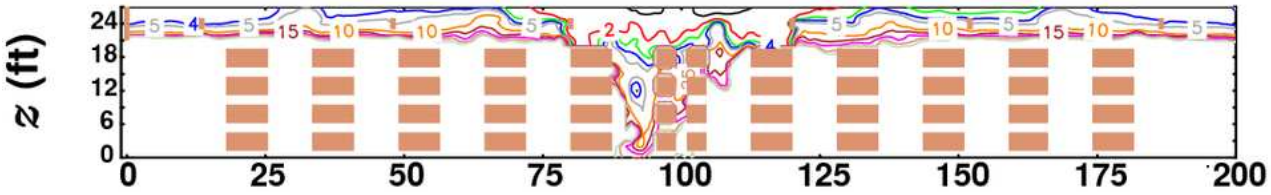

a) Run #9 (HRR3SHV1DC1): with smoke and heat vents and with draft curtains and without beams at the ceiling

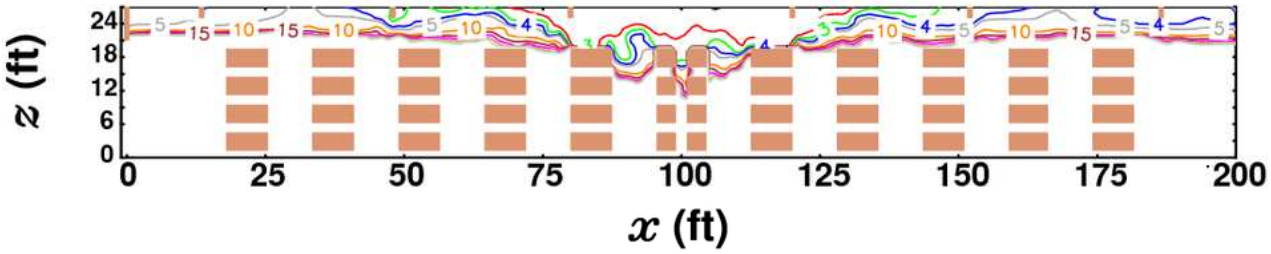

b) Run #10 (HRR3SHV1DC1CB): with smoke and heat vents and with draft curtains and with beams at the ceiling

Figure 48. Visibility (in ft) along *y* = -20 ft at 600 s for HRR3 Runs 9 and 10.

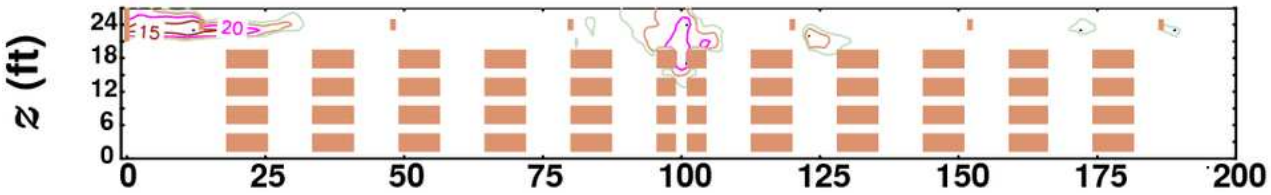

a) Run #9 (HRR3SHV1DC1): with smoke and heat vents and with draft curtains and without beams at the ceiling

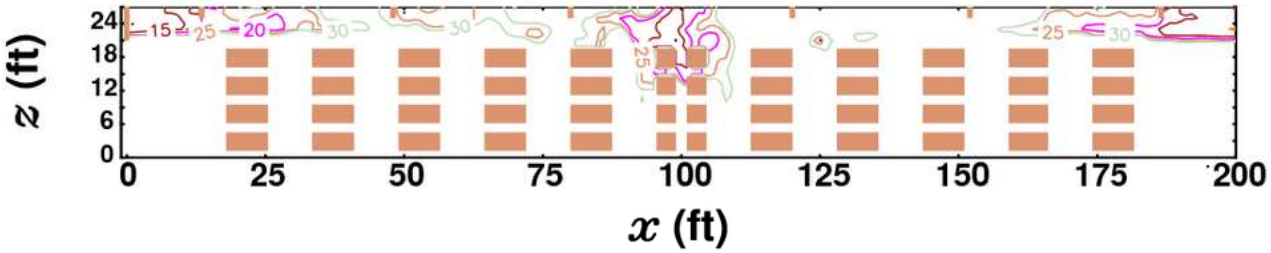

b) Run #10 (HRR3SHV1DC1CB): with smoke and heat vents and with draft curtains and with beams at the ceiling

Figure 49. Visibility (in ft) along *y* = -20 ft at 900 s for HRR3 Runs 9 and 10.

The visibility contour plots in Figures 43 - 49 correspond to the y = 20 ft plane because the support beam along the y = 0 plane obscures the smoke layer. The plots needed to go only as far west as the draft curtain in order to convey the effect. The resulting plots were clear enough so that one-to-one perspective could be used. At 35 s Figure 43 shows that the ceiling mounted support beams confined the ceiling jet that otherwise would be spreading as was the case for Run 9. At 57 s Figure 44 shows that for Run 10 the ceiling jet had reached the next set of beams while the ceiling jet continued to travel beyond the beam in Run 9. By 78 s the ceiling jet in Run 9 had reached the extent of the roof vent zone (Figure 45) while the ceiling jet in Run 10 was still moving to the edges. In Figures 44 - 45 the smoke layer depth was thicker for Run 10 than for Run 9. Run 10 reached the zone extents at 90 s (Figure 46). In Figures 47 - 49, though, the smoke depth was greater than four feet so the difference between the two cases centers around the disturbance imposed upon the interface by the two extra sprinklers that operated in Run 9. Hence, it has been shown that ceiling-mounted support beams retard the spread of the ceiling jet, but otherwise have minimal effect on the performance of sprinklers and smoke and heat vents. The remaining simulations make use of the offset support beam configuration.

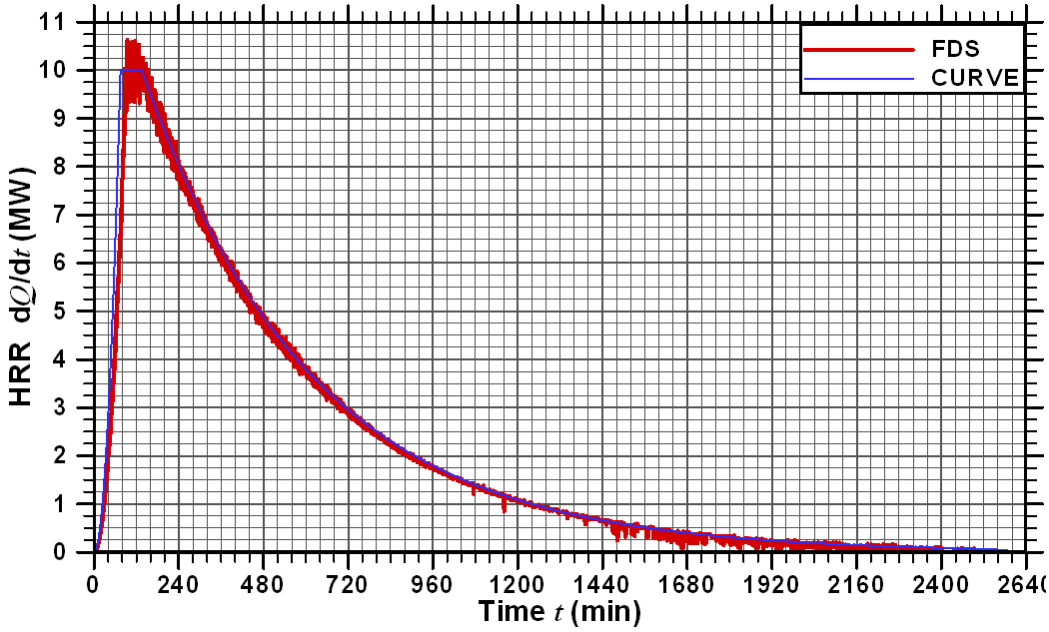

Figure 50. Comparison of the computed heat release rate for Run 11 (HRR4SHV1DC1) with the HRR4 curve.

3.6 HRR4 Fire Source

Since there is little data on the smoke and heat production from controlled fires, HRR1-HRR3 include no representation of this phase. To begin to address this phase, HRR4 with a long decay was used as a fire source.

Figure 50 shows the output heat release rate from Run 11. A comparison with Figure 5 shows that it matches the target profile well. The output HRR for Run 12 is very similar.

3.6.1 Run #11 (HRR4SHV0DC0): HRR4 without Smoke and Heat Vents and without Draft Curtains

Run 11 incorporated HRR4 in racks centered on the east roof vent zone within an unvented warehouse. Figure 51 shows that 18 sprinklers operated and sprinkler activations ended soon after the heat release rate started to decline. This was three less than had been the case with Run 7 (HRR3). Figure 52 shows the corresponding sprinkler activation map.

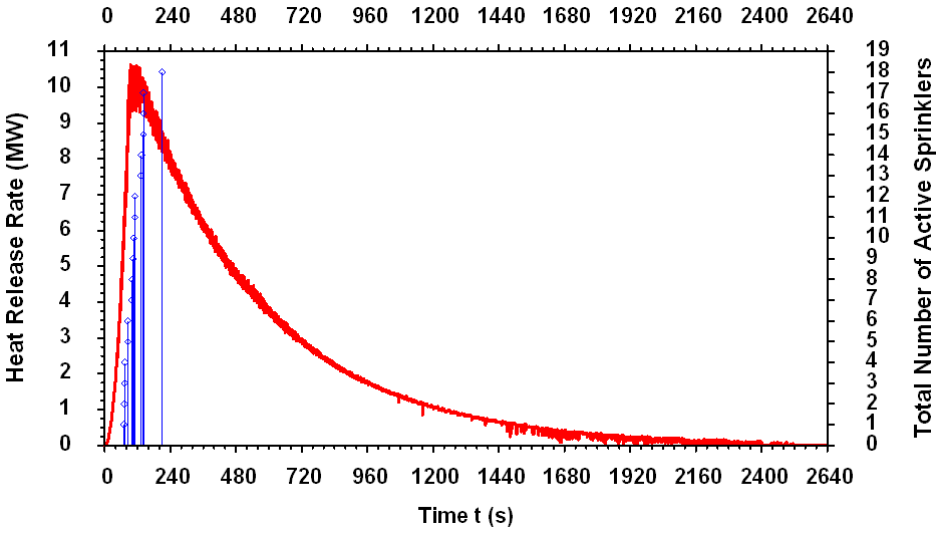

Figure 51. Comparison of the heat release rate and the sprinkler activation times for Run #11 (HRR4SHV0DC0): HRR4 Without Smoke and Heat Vents and Without Draft Curtains.

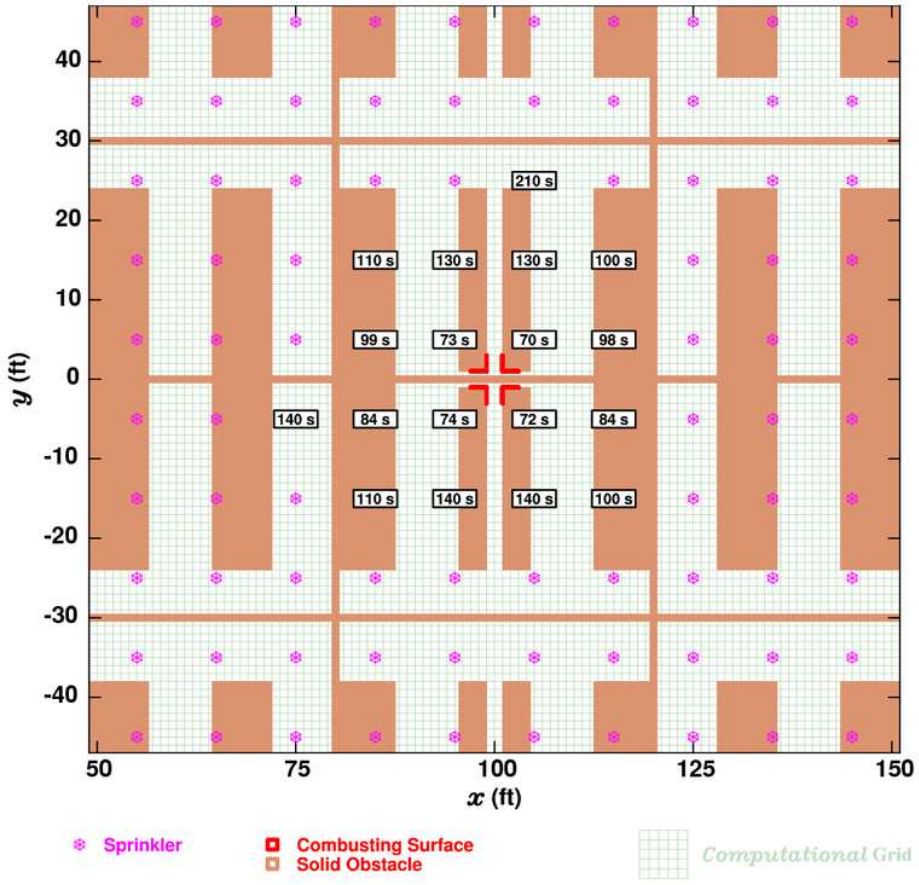

Figure 52. Sprinkler activation map for Run #11 (HRR4SHV0DC0): HRR4 without smoke and heat vents and without draft curtains.

3.6.2 Run #11 (HRR4SHV1DC1): HRR4 With Smoke and Heat Vents and Draft Curtain

Run 11 incorporated HRR4 in racks centered on the east roof vent zone within a warehouse with smoke and heat vents and a draft curtain. The results in Figure 53 are very similar to those of Figure 51: rapid sprinkler activations occurred until the heat release rate began to decline. Just one less sprinkler operated than had been the case in Run 10 (HRR3). The sprinkler activation pattern in Figure 54 is well behaved.

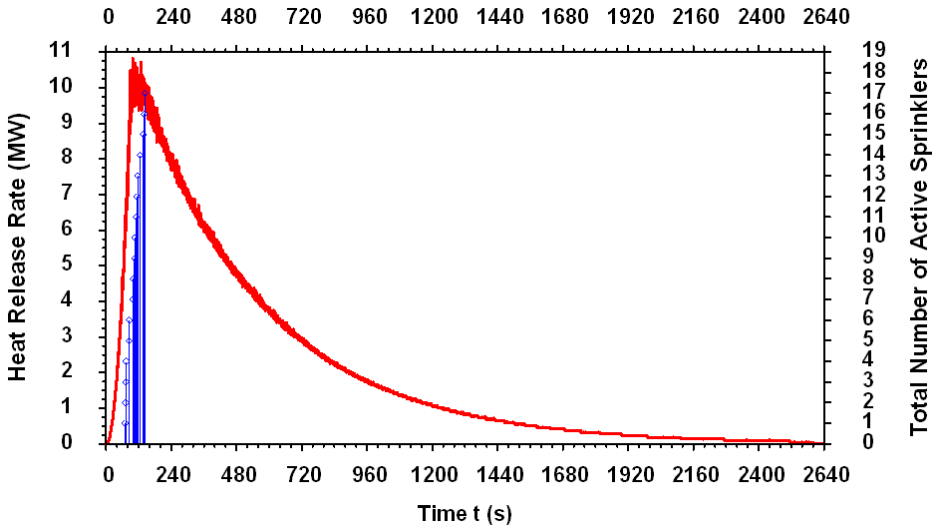

Figure 53. Comparison of the heat release rate and the sprinkler activation times for Run #12 (HRR4SHV1DC1): HRR4 with smoke and heat vents and with draft curtain.

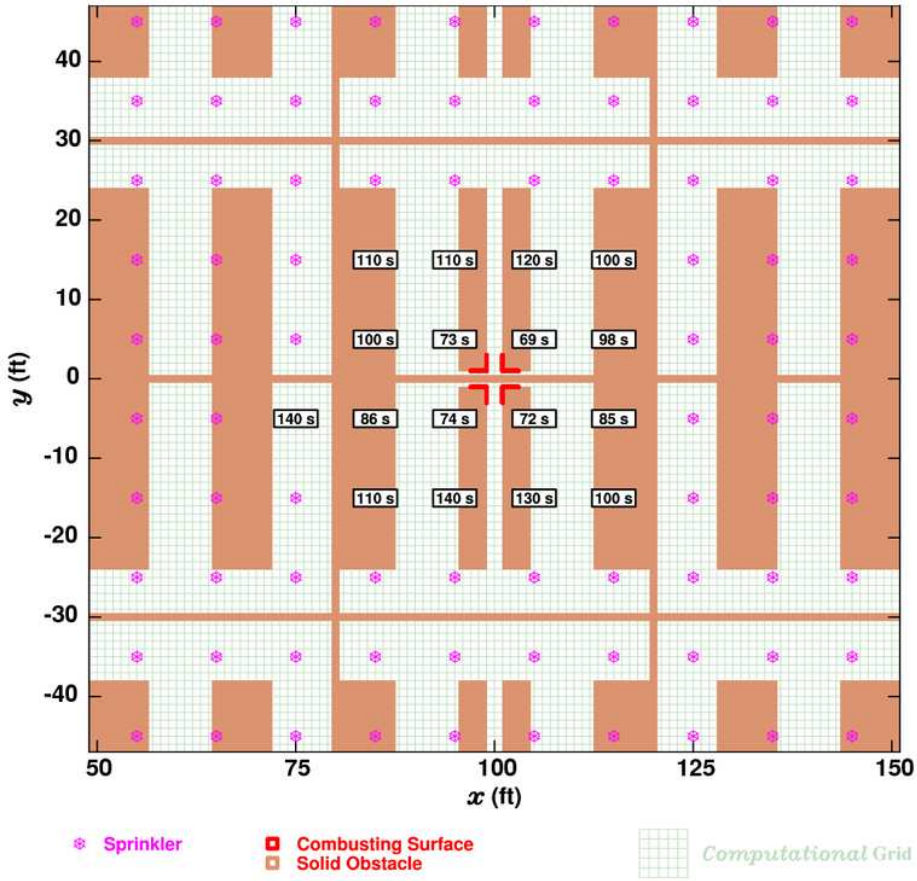

Figure 54. Sprinkler activation map for Run #12 (HRR4SHV1DC1): HRR4 with smoke and heat vents and with draft curtain.

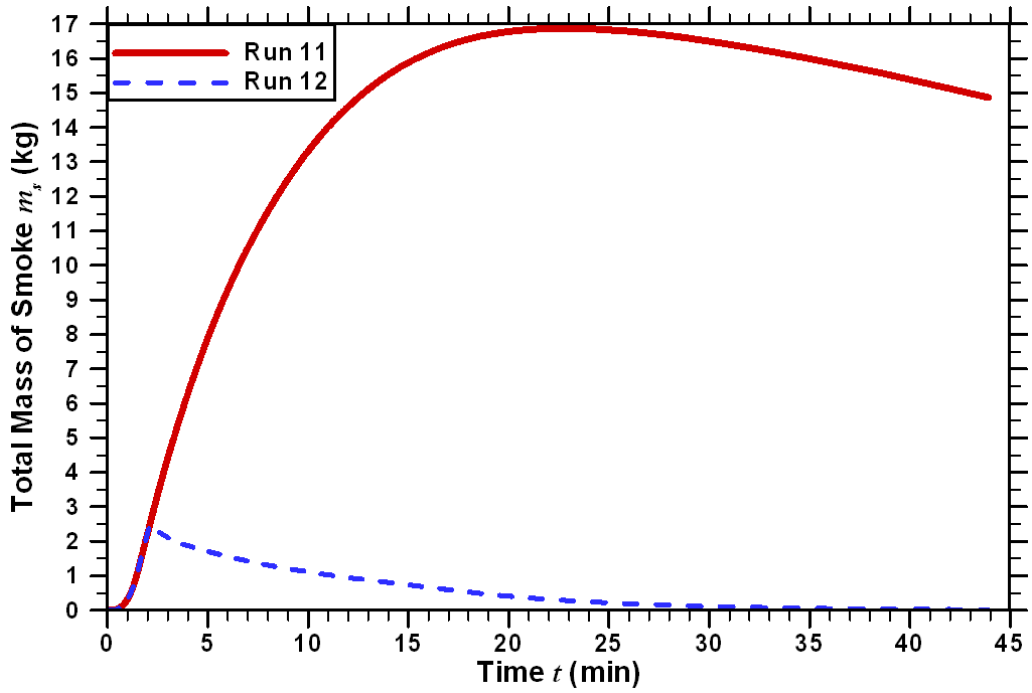

Figure 55. Comparison of the building net smoke masses for Runs 11 - 12 (HRR4SHV0DC0, HRR4SHV1DC1).

A comparison of the net smoke masses associated with Runs 11 and 12 is shown in Figure 55. Unlike the other cases without vents, the long duration of HRR4 along with its diminishing impact allowed the leaks in Run 11 to begin to reduce the smoke mass after 23 min. With smoke and heat vents and a draft curtain, the mass of smoke in Run 12 began to decrease as soon as the vents opened. The mass of smoke remaining by 43 min was insignificant.

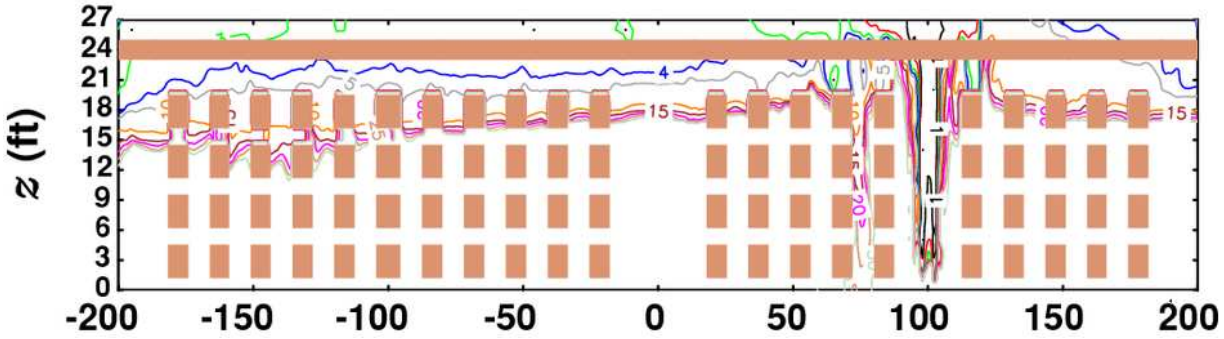

a) Run #11 (HRR4SHV0DC0): HRR4 without smoke and heat vents and without draft curtains

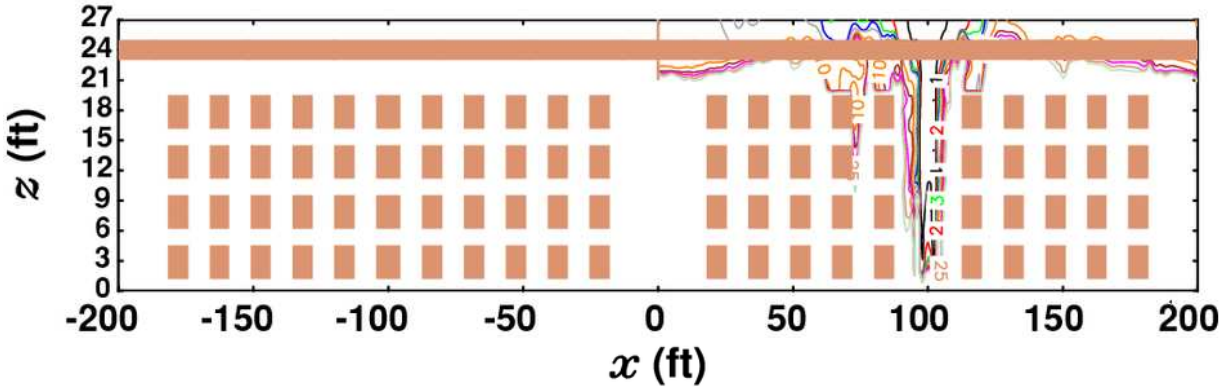

b) Run #12 (HRR4SHV1DC1): HRR4 with smoke and heat vents and with draft curtain

Figure 56. Visibility (in ft) along *y* = 0 ft at 300 s. The vertical coordinate has been stretched.

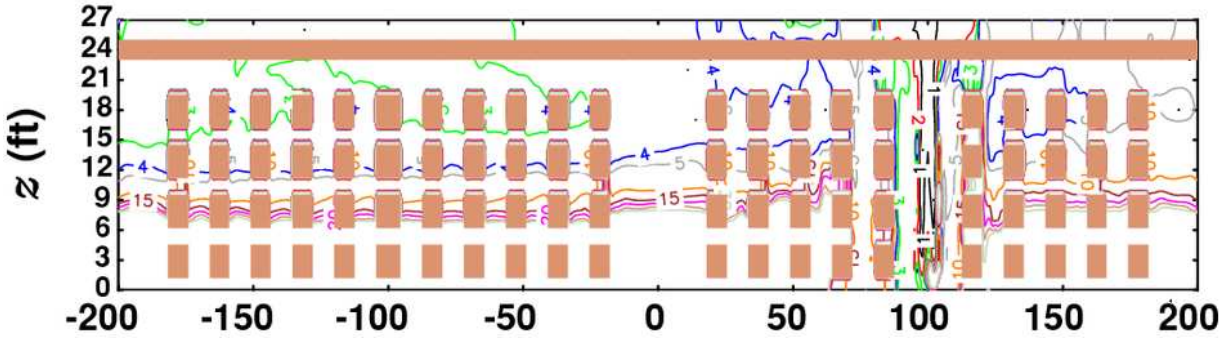

a) Run #11 (HRR4SHV0DC0): HRR4 without smoke and heat vents and without draft curtains

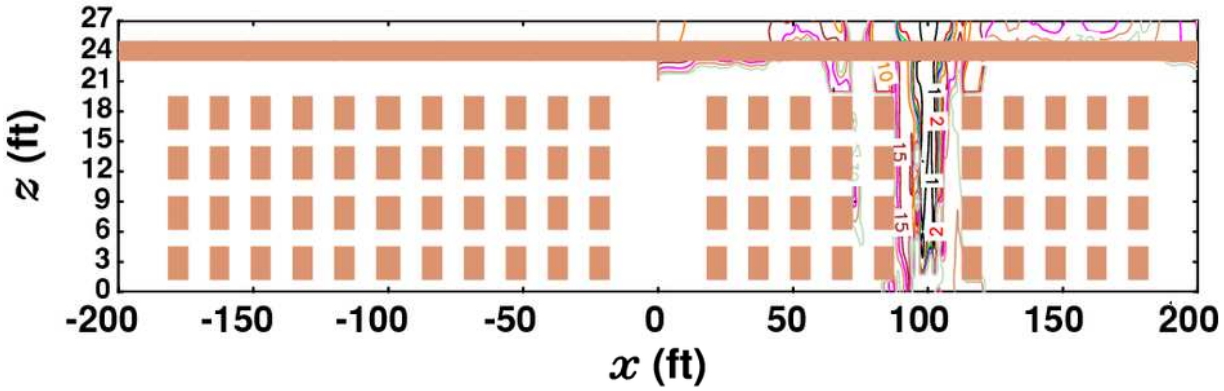

b) Run #12 (HRR4SHV1DC1): HRR4 with smoke and heat vents and with draft curtain

Figure 57. Visibility (in ft) along *y* = 0 ft at 600 s. The vertical coordinate has been stretched.

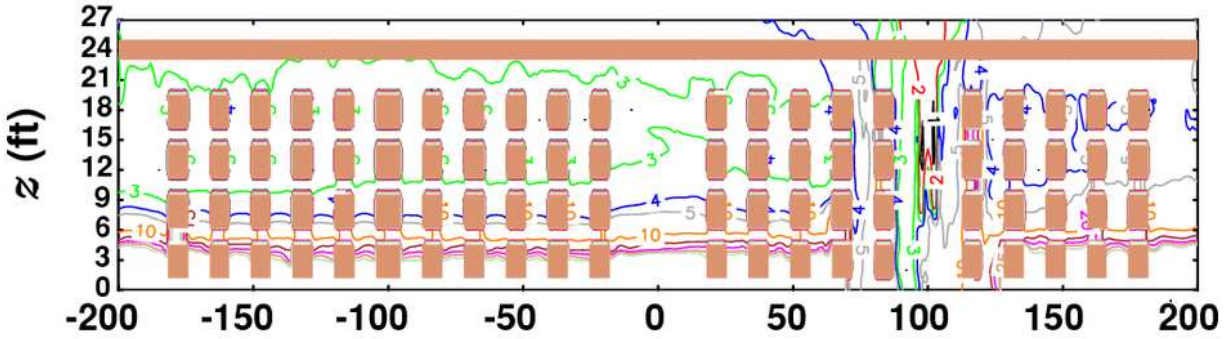

a) Run #11 (HRR4SHV0DC0): HRR4 without smoke and heat vents and without draft curtains

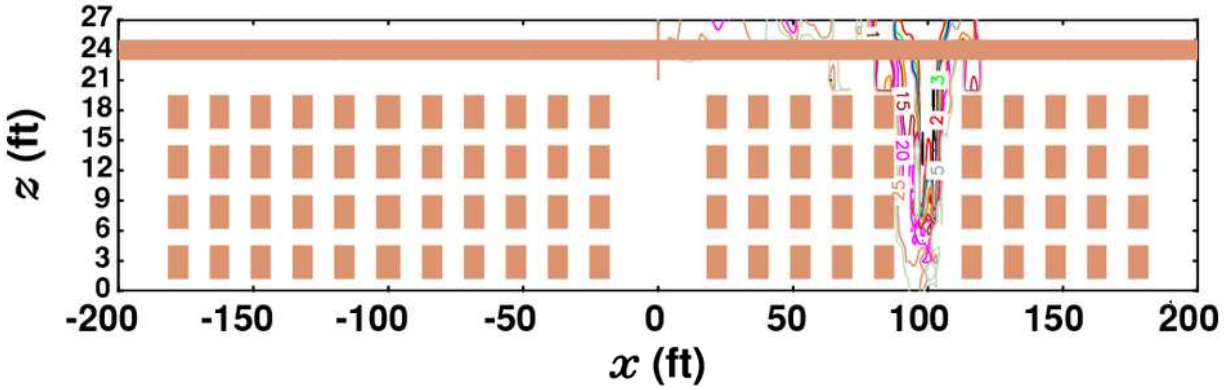

b) Run #12 (HRR4SHV1DC1): HRR4 with smoke and heat vents and with draft curtain

Figure 58. Visibility (in ft) along *y* = 0 ft at 900 s. The vertical coordinate has been stretched.

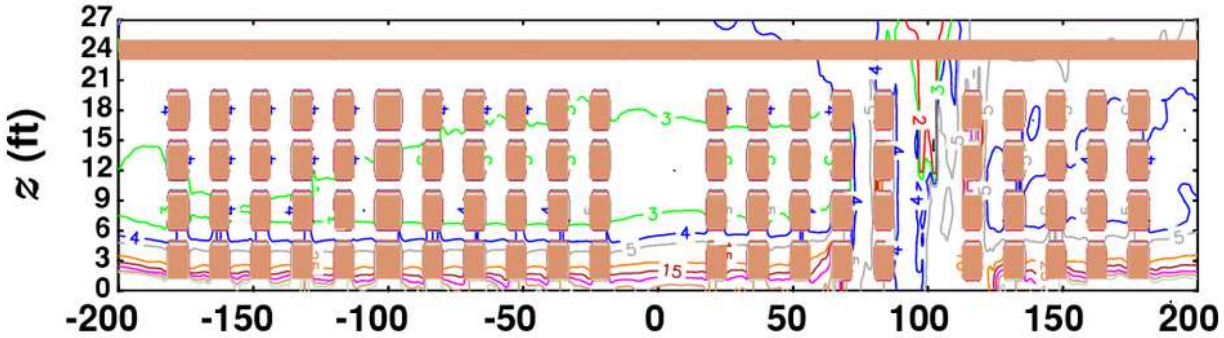

a) Run #11 (HRR4SHV0DC0): HRR4 without smoke and heat vents and without draft curtains

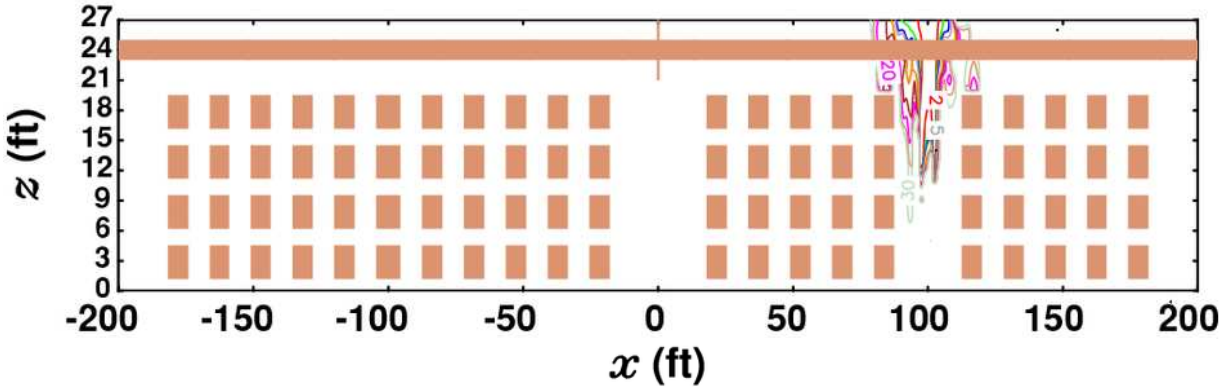

b) Run #12 (HRR4SHV1DC1): HRR4 with smoke and heat vents and with draft curtain

Figure 59. Visibility (in ft) along *y* = 0 ft at 1200 s. The vertical coordinate has been stretched.

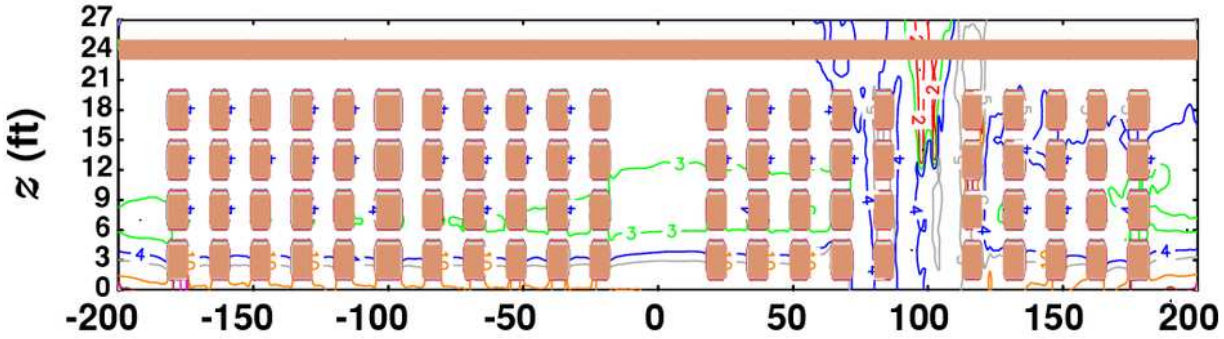

a) Run #11 (HRR4SHV0DC0): HRR4 without smoke and heat vents and without draft curtains

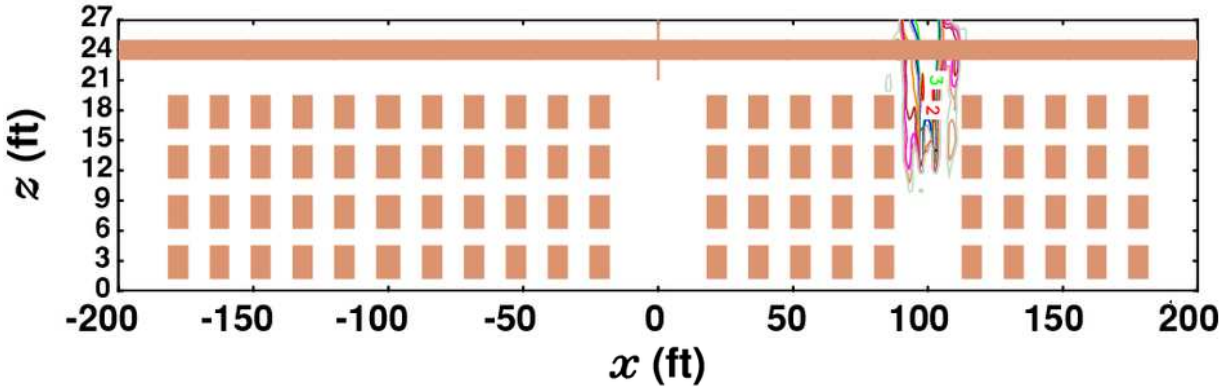

b) Run #12 (HRR4SHV1DC1): HRR4 with smoke and heat vents and with draft curtain

Figure 60. Visibility (in ft) along *y* = 0 ft at 1500 s. The vertical coordinate has been stretched.

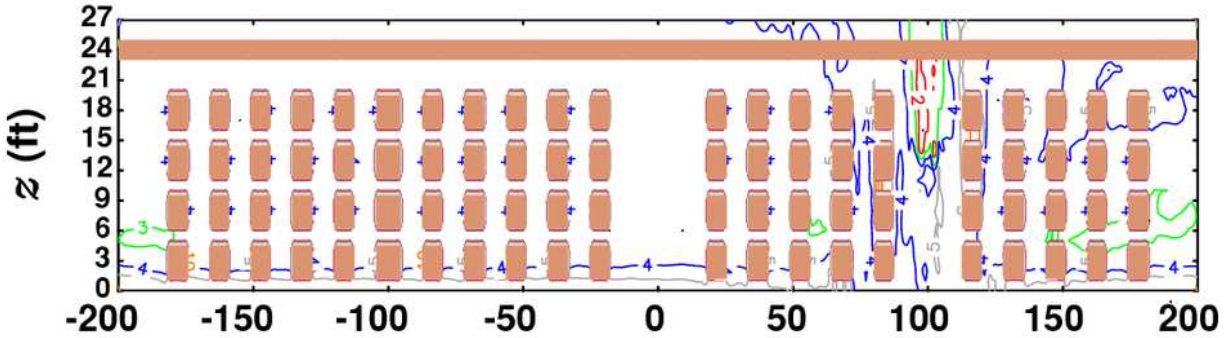

a) Run #11 (HRR4SHV0DC0): HRR4 without smoke and heat vents and without draft curtains

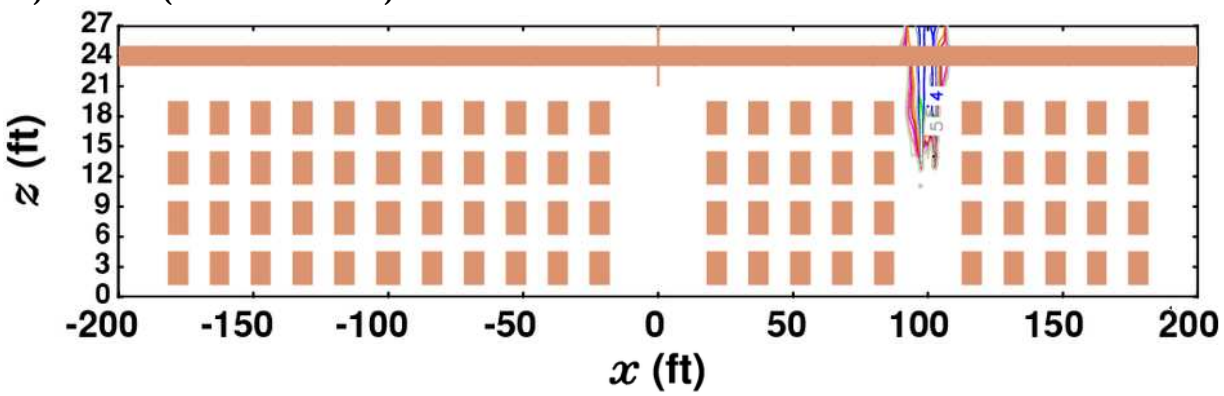

b) Run #12 (HRR4SHV1DC1): HRR4 with smoke and heat vents and with draft curtain

Figure 61. Visibility (in ft) along *y* = 0 ft at 1800 s. The vertical coordinate has been stretched.

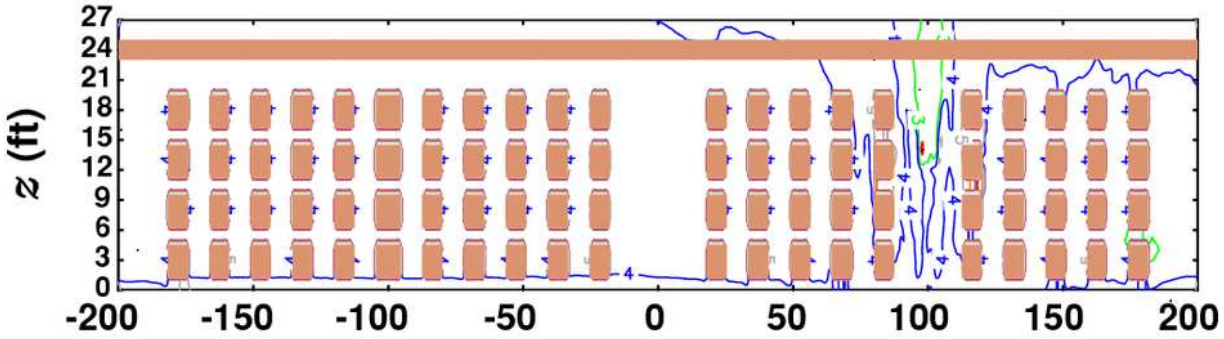

a) Run #11 (HRR4SHV0DC0): HRR4 without smoke and heat vents and without draft curtains

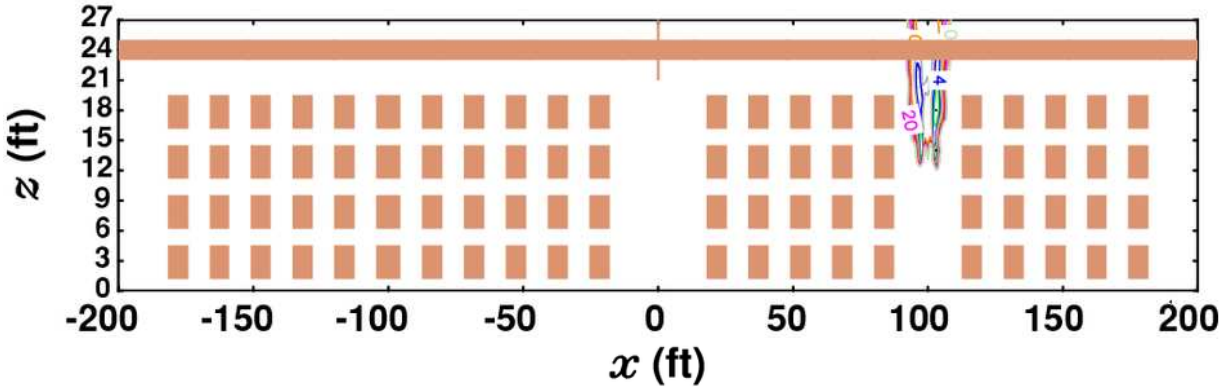

b) Run #12 (HRR4SHV1DC1): HRR4 with smoke and heat vents and with draft curtain

Figure 62. Visibility (in ft) along *y* = 0 ft at 2100 s. The vertical coordinate has been stretched.

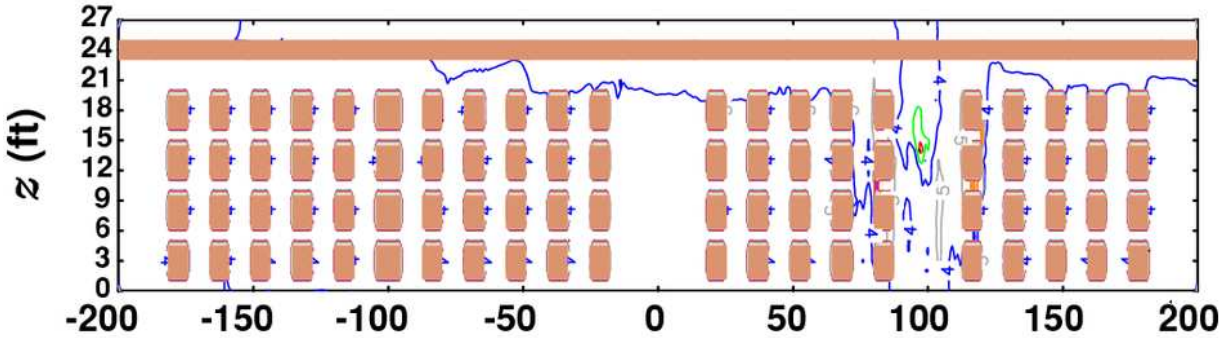

a) Run #11 (HRR4SHV0DC0): HRR4 without smoke and heat vents and without draft curtains

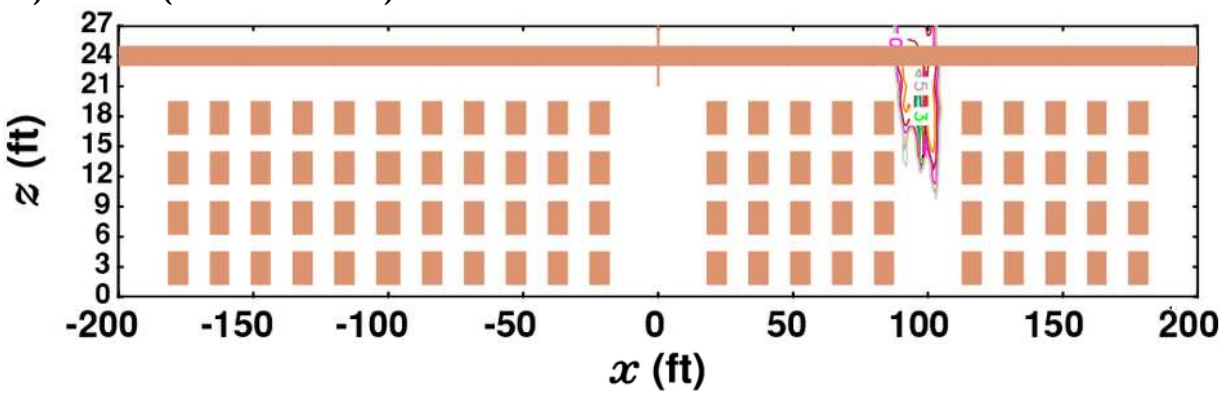

b) Run #12 (HRR4SHV1DC1): HRR4 with smoke and heat vents and with draft curtain

Figure 63. Visibility (in ft) along *y* = 0 ft at 2400 s. The vertical coordinate has been stretched.

At 300 s, the smoke layer in Figure 56a was descending while that in Figure 56b was contained within the east roof vent zone. Evidence of sprinkler spray smoke drag-down can be seen for both Runs 11 and 12 but it did not lead to smoke logging. By 600s, the smoke layer in Figure 57a continued to descend while the smoke in Figure 57b remained contained. For Run 11, the smoke level had dropped below occupant level by 900 s (Figure 58a). On the other hand, in Figure 58b the smoke layer had begun to clear out. From Figures 59 - 63 the situation remains the same: the warehouse in Run 11 was smoke logged while the warehouse in Run 12 was relatively clear. This comparison has shown that smoke and heat vents can improve conditions even with slowly decaying fires.

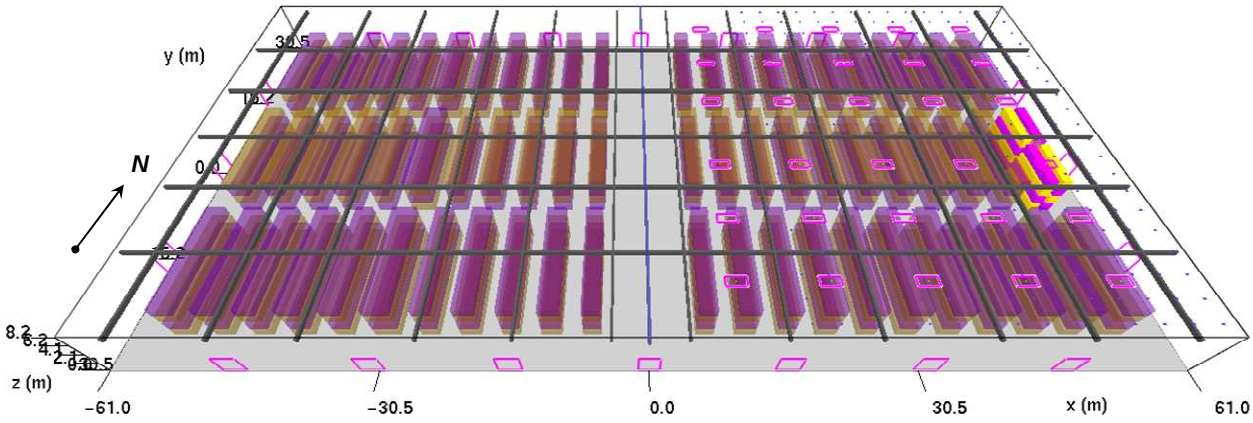

Figure 64. View of the computational domain for Run 13 (HRR3SHV1DC1R): burning racks centered on row farthest away from the draft curtain.

3.7 Run #13 (HRR3SHV1DC1R): Burning Racks Centered on Row Farthest away from the Draft Curtain

The previous twelve runs have dealt with four different heat release rate fires centered on the east roof vent zone. The remaining four simulations will use HRR3 but will move the fire to other locations within the east zone. For the centered rack fire runs, four vents and four sprinklers were symmetrically located around the center of the burning racks. With the last four simulations this was no longer the case. Unless otherwise indicated, the remaining runs have smoke and heat vents and one draft curtain. Figure 64 shows the computational domain for Run 13. The burning racks are centered along the east-most row of commodities. Figure 65 shows that 17 sprinklers activated before the vents opened and two additional sprinklers operated after the vents operated. The first sprinkler activated at 65 s, somewhat sooner than was the case for the centered fire. The reason for this and the fact that only 19 sprinklers operated are related to vent and sprinkler locations with respect to the fire location.

Figure 66 shows the sprinkler activation map. The view here is now different from that of the previous maps because the fire is in a new location. Once again the sprinkler activation map has been zoomed into the area of interest. The map shows that the sprinklers activated in a ring-like fashion about the center of the burning racks.

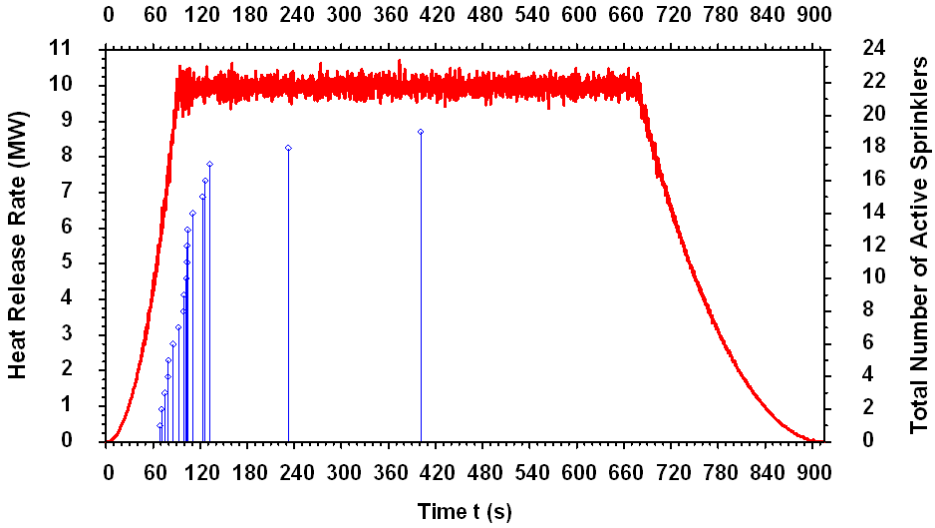

Figure 65. Comparison of the heat release rate and the sprinkler activation times for Run 13 (HRR3SHV1DC1R): burning racks centered on row farthest away from the draft curtain.

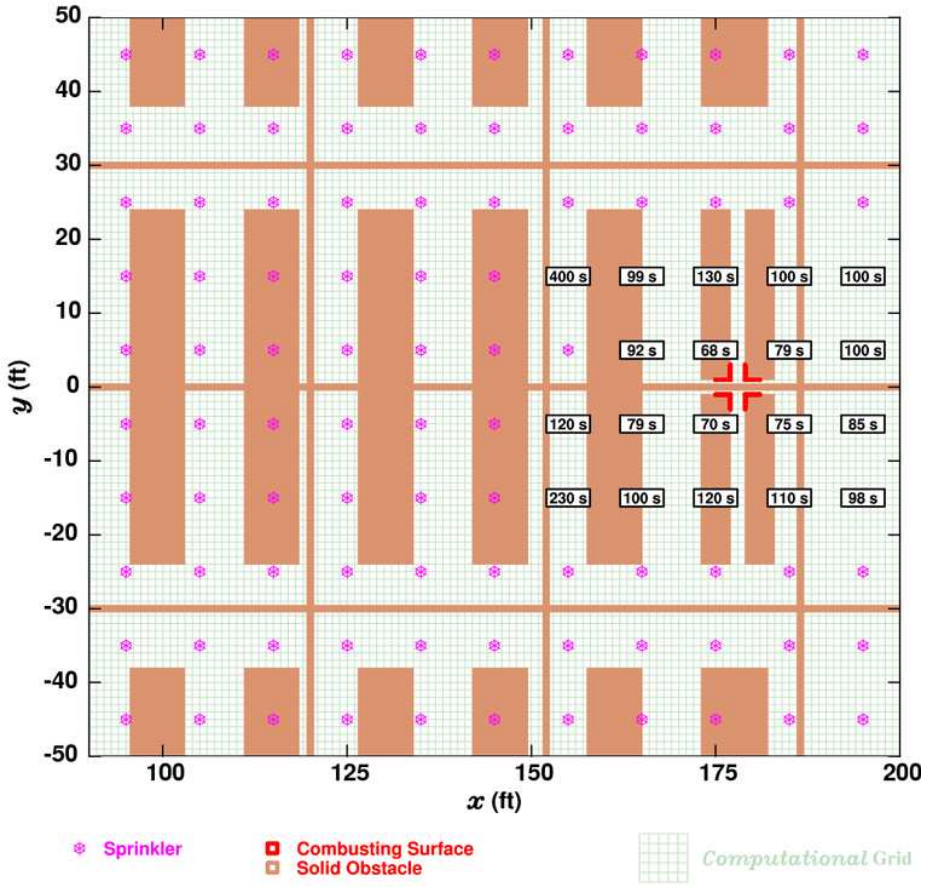

Figure 66. Sprinkler activation map for Run 13 (HRR3SHV1DC1R): burning racks centered on row farthest away from the draft curtain.

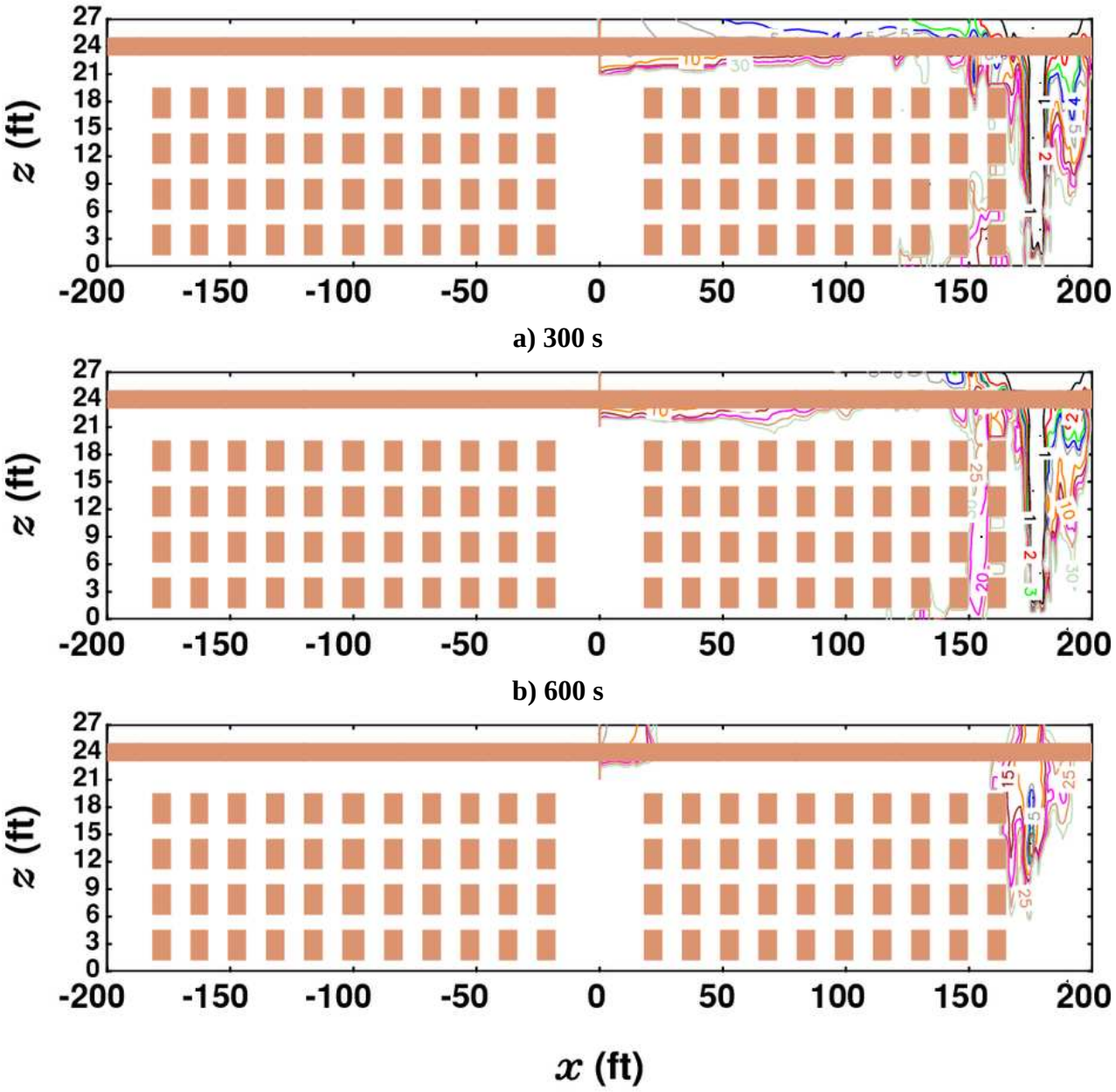

a) 300 s

b) 600 s

c) 900 s

Figure 67. Visibility (in ft) along y = 0 ft for Run 13 (HRR3SHV1DC1R): burning racks centered on row farthest away from the draft curtain. The vertical coordinate has been stretched.

The visibility contour plots in Figure 67 show that the vents-curtain combination is effective at containing and then eliminating the smoke for Run 13. Because of the absence of commodities, Figures67a and 67b show good examples of sprinkler-smoke layer interaction to the east of the burning racks. Notice how the 30 ft visibility contour line does not go down to the floor level in this passageway area.

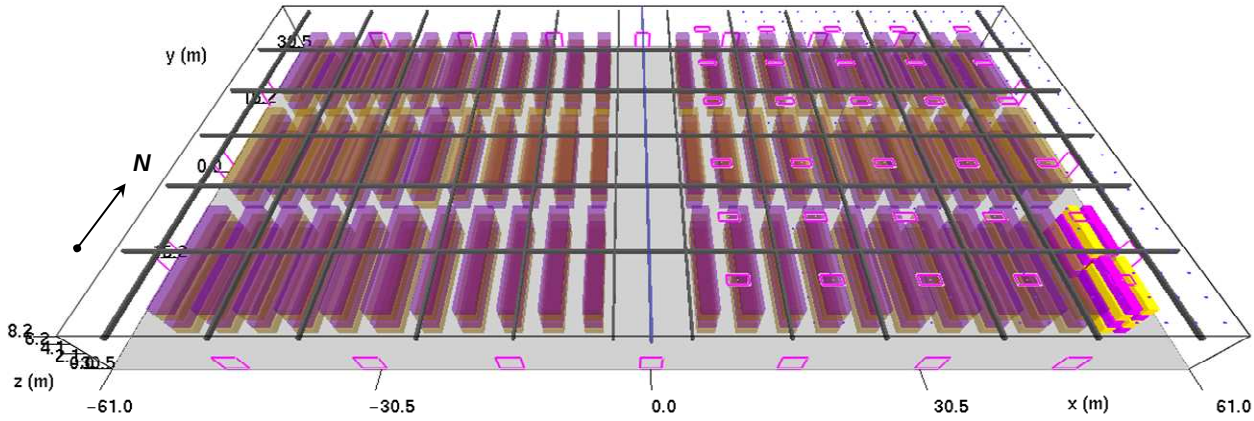

Figure 68. View of the computational domain for Run 14 (HRR3SHV1DC1RC): burning racks located on the corner farthest away from the draft curtain.

3.8 Run #14 (HRR3SHV1DC1RC): Burning Racks Located on Corner Farthest away from the Draft Curtain

Run 14 places the burning racks in the lower east corner of the warehouse. (See Figure 68.) As Figure 69 shows, this configuration resulted in 22 sprinkler activations, the largest of any of the simulations. Once again, the focus of the sprinkler activation map in Figure 70 has changed in accordance with the new location of the burning racks. Since Figure 70 shows no strange sprinkler activation pattern, it is concluded that having the fire near the corner allowed the ceiling jet that was reflected off the wall to activate a few more sprinklers.

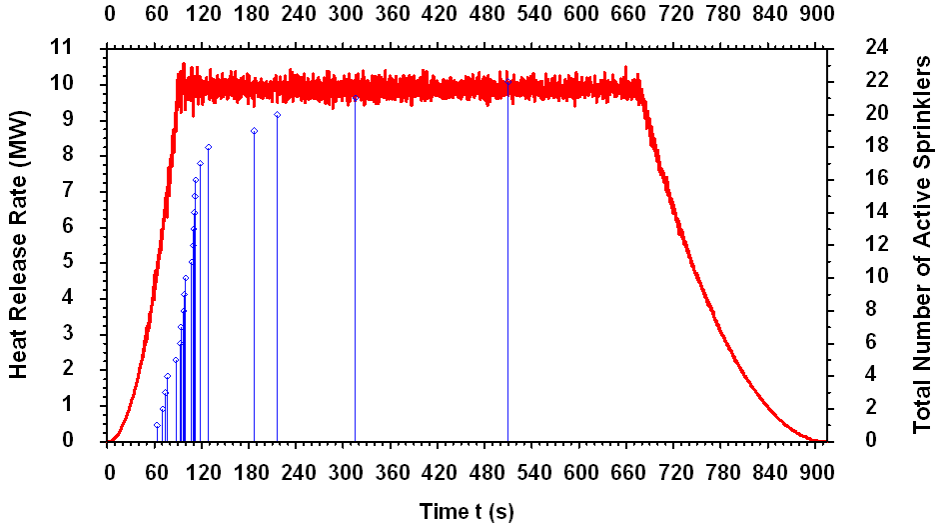

Figure 69. Comparison of the heat release rate and the sprinkler activation times for Run 14 (HRR3SHV1DC1RC): burning racks located on corner farthest away from the draft curtain.

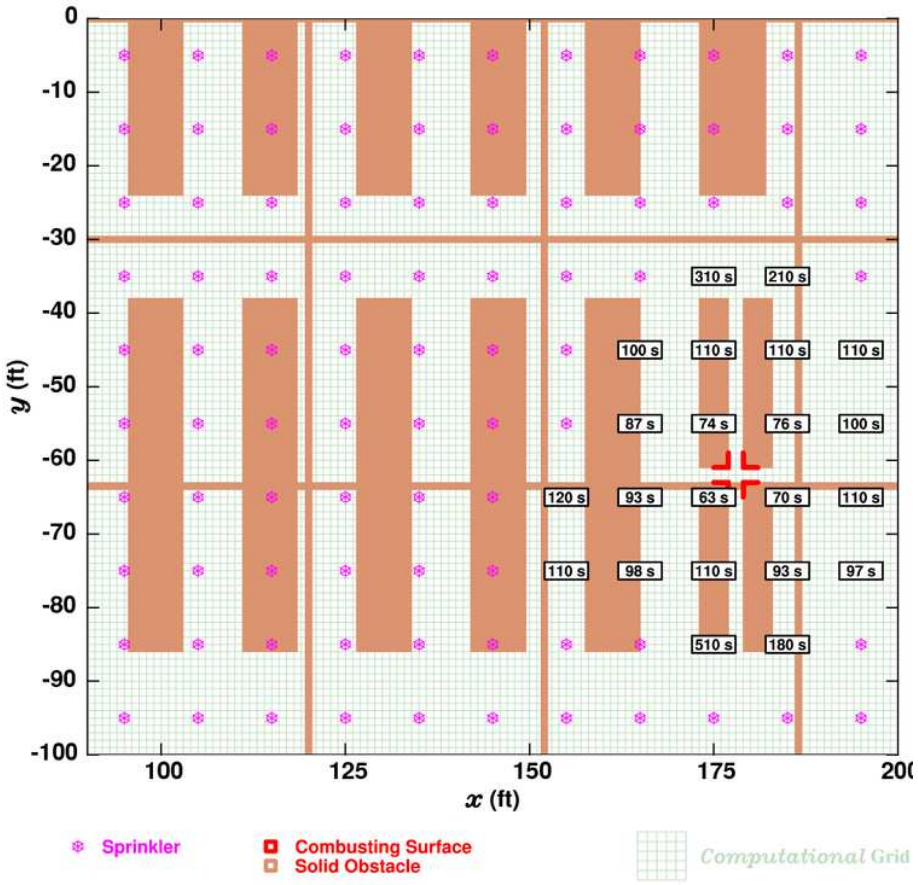

Figure 70. Sprinkler activation map for Run 14 (HRR3SHV1DC1RC): burning racks located on corner farthest away from the draft curtain.

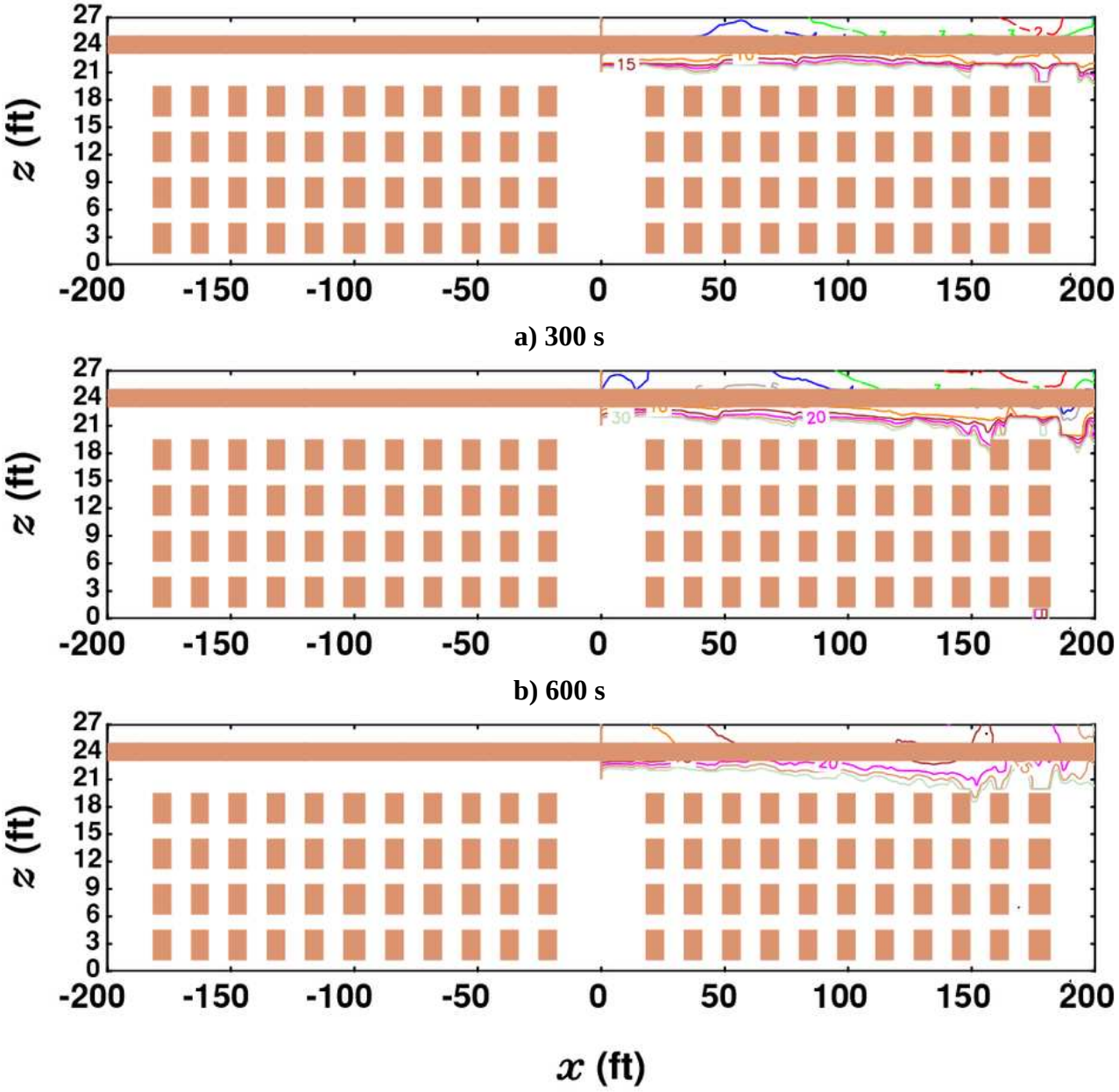

a) 300 s

b) 600 s

c) 900 s

Figure 71. Visibility (in ft) along y = 0 ft for Run 14 (HRR3SHV1DC1RC): burning racks located on corner farthest away from the draft curtain. The vertical coordinate has been stretched.

The visibility contour plots in Figure 71 are along the $y = 0$ plane. They show that for Run 14 the vents-curtain combination was again effective at containing and then eliminating the smoke.

3.9 Burning Racks Located on Corner Nearest to the Draft Curtain Location

The last two scenarios place the burning racks in the corner closest to the location of the

curtain. Both runs have smoke and heat vents. Run 15 has no draft curtain. Run 16 includes the draft curtain. The location of the burning racks is significant because it allows more smoke to escape into the west roof vent zone.

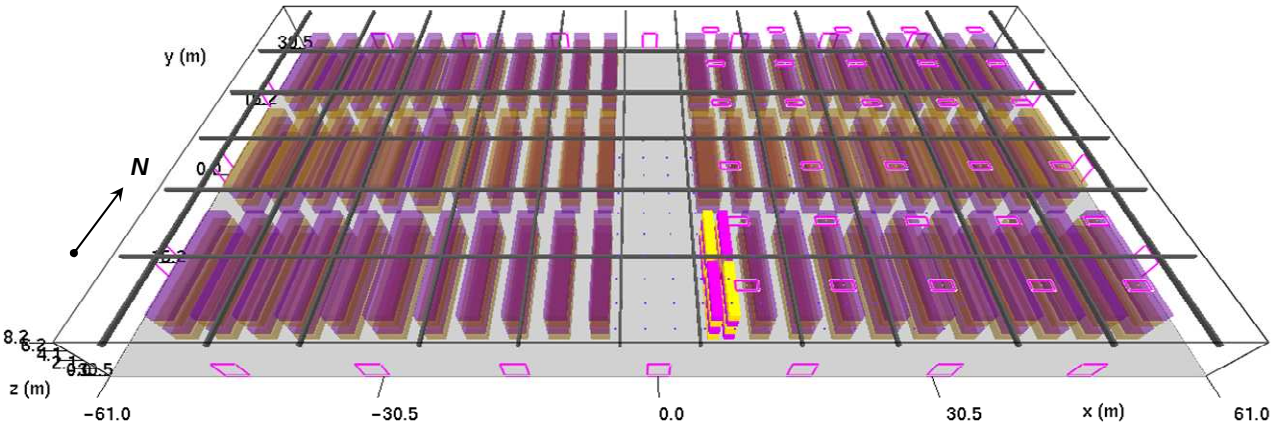

Figure 72. View of the computational domain for Run 15 (HRR3SHV1DC0FC): burning racks located on corner nearest to the draft curtain location with smoke and heat vents and without draft curtains.

3.9.1 Run #15 (HRR3SHV1DC0FC): With Smoke and Heat Vents and Without Draft Curtains

Figure 72 shows the computational domain for Run 15, which has no draft curtain. Figure 73 shows that for Run 15 the time frame for primary sprinkler activation was similar to that of Run 8 with only one later activation, resulting in a total of 20 operating sprinklers. The differences can be attributed again to relative sprinkler and vent spacing. The view for the sprinkler activation map in Figure 74 has been changed in order to zoom in on the new fire location. Figure 74 shows that no sprinklers in the western roof vent zone activated and that the sprinkler activation pattern was normal.

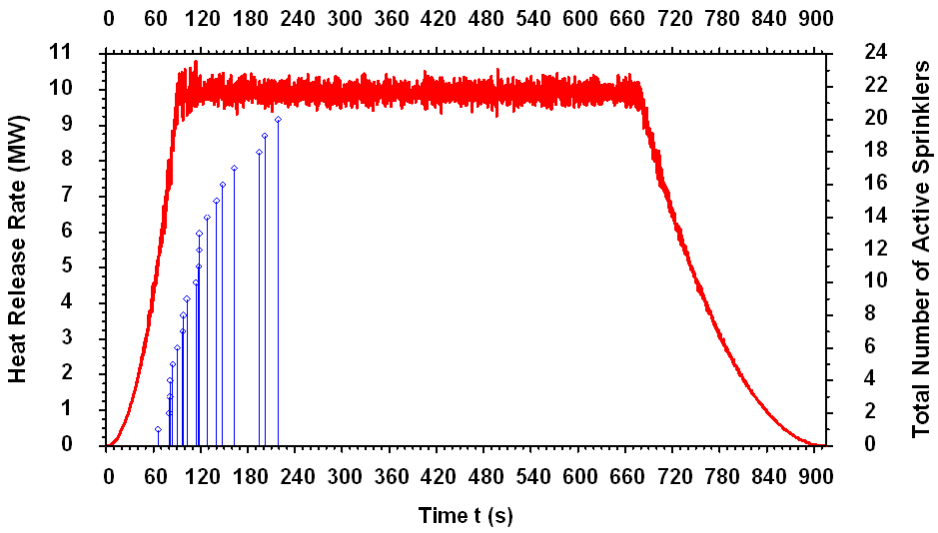

Figure 73. Comparison of the heat release rate and the sprinkler activation times for Run 15 (HRR3SHV1DC0FC): burning racks located on corner nearest to the draft curtain location with smoke and heat vents and without draft curtains.

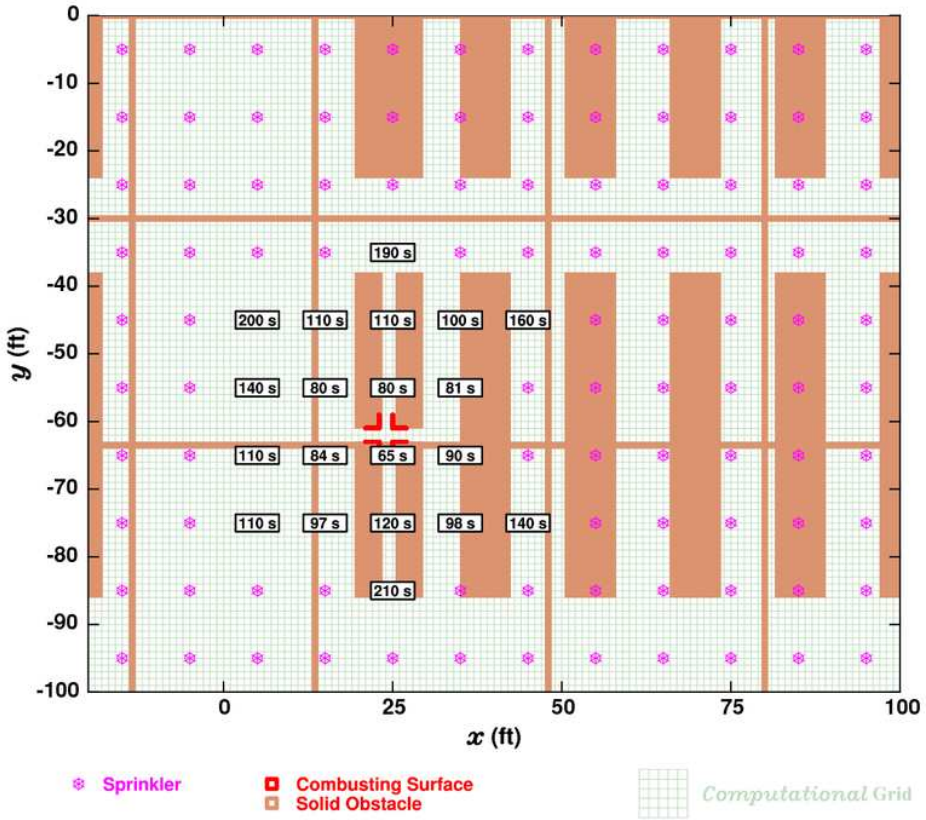

Figure 74. Sprinkler activation map for Run 15 (HRR3SHV1DC0FC): burning racks located on corner nearest to the draft curtain location with smoke and heat vents and without draft curtains.

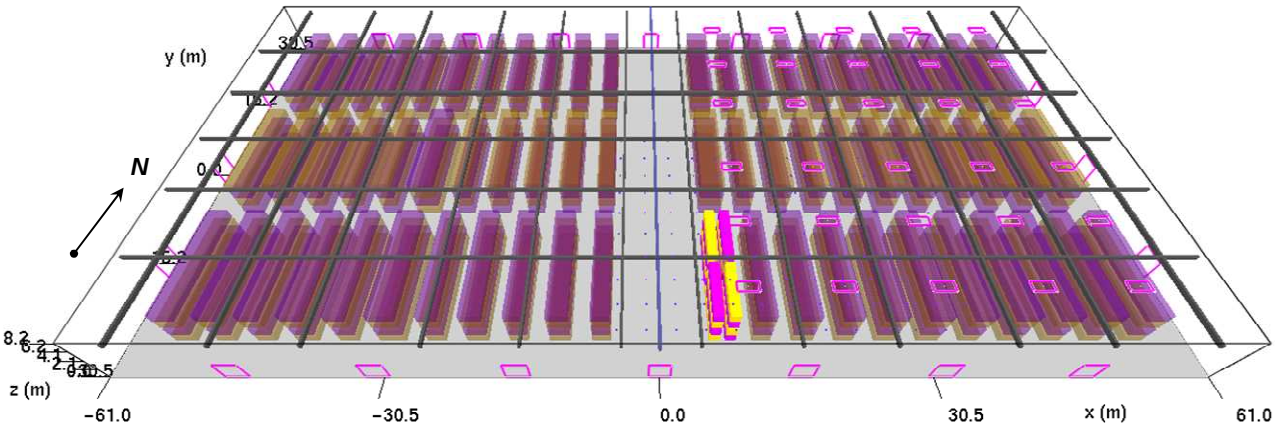

Figure 75. View of the computational domain for Run 16 (HRR3SHV1DC1FC): burning racks located on corner nearest to the draft curtain location with smoke and heat vents and with draft curtains.

3.9.2 Run #16 (HRR3SHV1DC1FC): With Smoke and Heat Vents and Draft Curtain

Figure 75 shows the computational domain for Run 16, which has a draft curtain. Figure 76 shows that the total number of operating sprinklers was 21. This is one more than was the case for Run 15. The addition of the draft curtain explains the difference between Runs 16 and 15. Figure 77 shows that no sprinklers activations occurred to the west of the draft curtain. The reason for this in both Runs 15 and 16 is the location of the draft curtain in the aisle. The expected ring-like activation pattern is present in Figure 77.

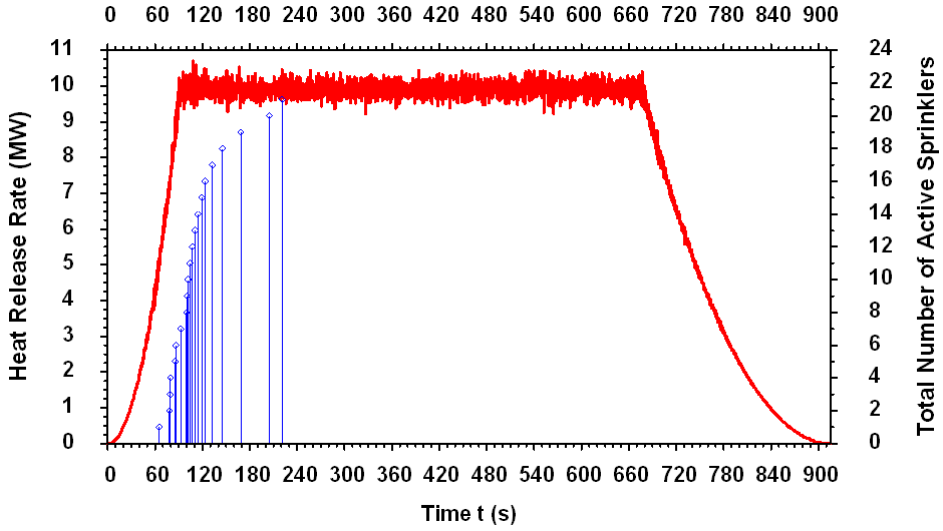

Figure 76. Comparison of the heat release rate and the sprinkler activation times for Run 16 (HRR3SHV1DC1FC): burning racks located on corner nearest to the draft curtain location with smoke and heat vents and with draft curtains.

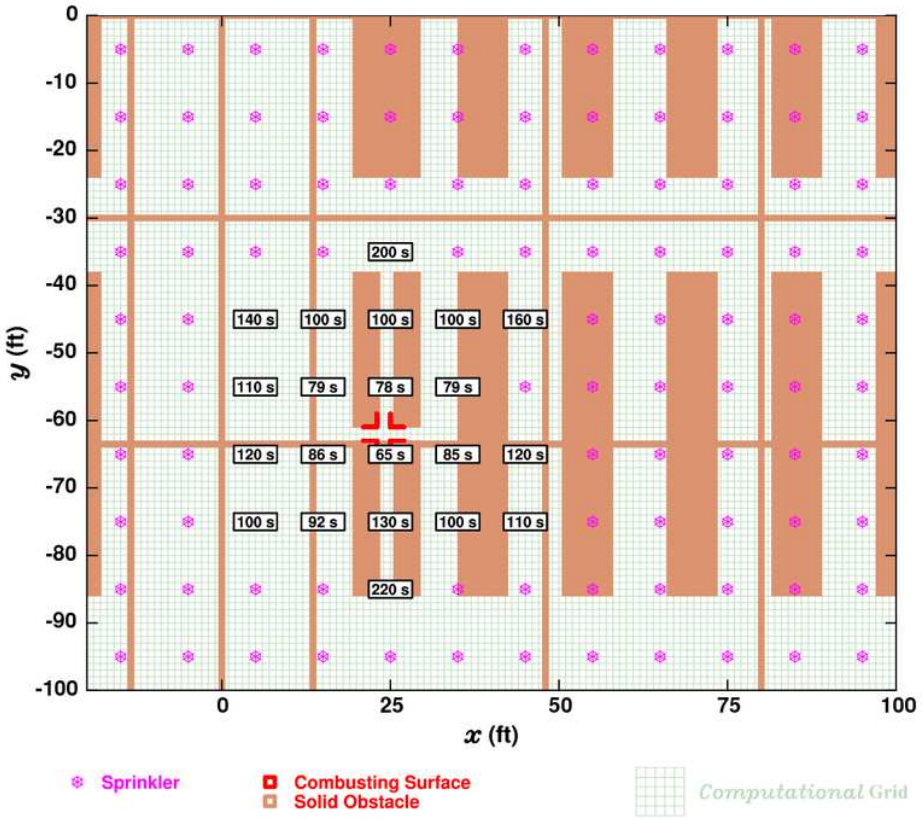

Figure 77. Sprinkler activation map for Run 16 (HRR3SHV1DC1FC): burning racks located on corner nearest to the draft curtain location with smoke and heat vents and with draft curtains.

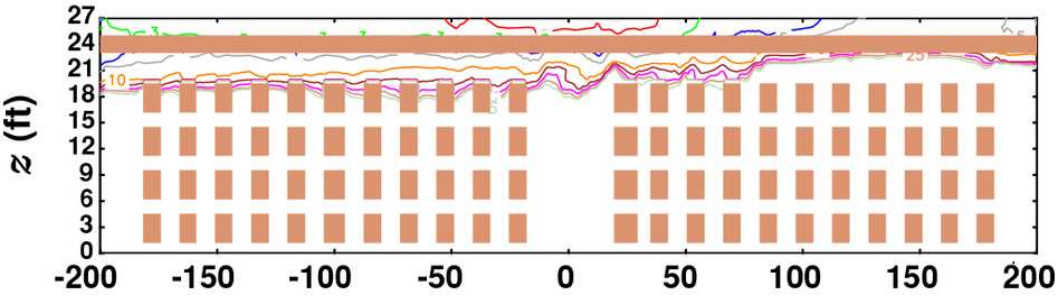

a) Run 15 (HRR3SHV1DC0FC): with smoke and heat vents and without draft curtains

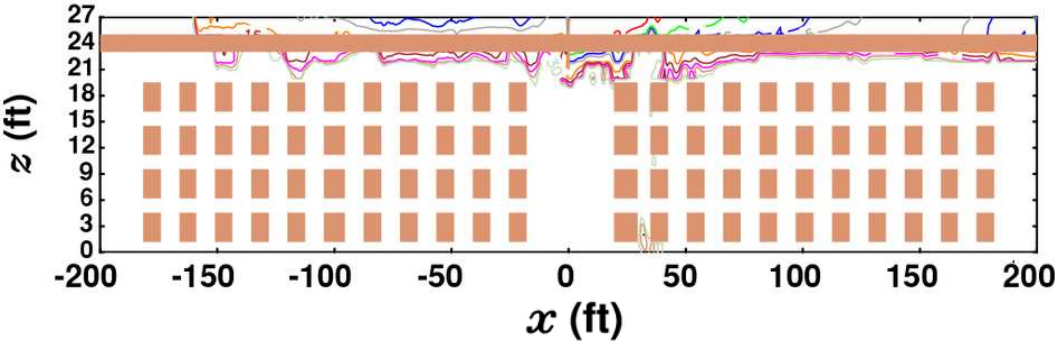

b) Run 16 (HRR3SHV1DC1FC): with smoke and heat vents and with draft curtains

Figure 78. Visibility (in ft) along *y* = 0 ft at 300 s for HRR3 Runs 15 and 16. The burning racks are located on the corner nearest to the draft curtain location. The vertical coordinate has been stretched.

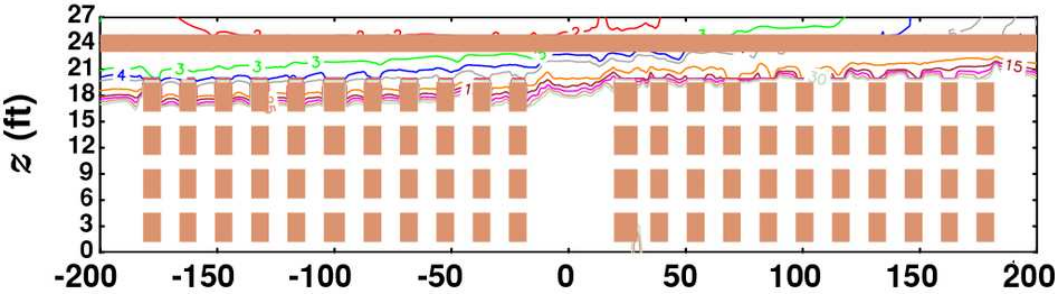

a) Run 15 (HRR3SHV1DC0FC): with smoke and heat vents and without draft curtains

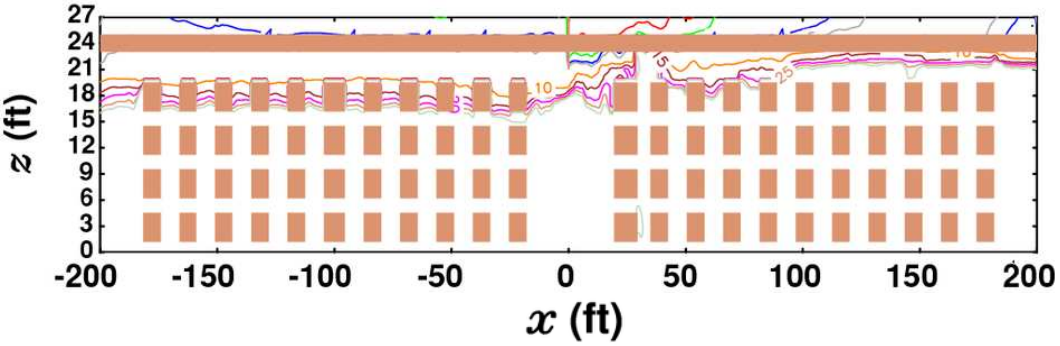

b) Run 16 (HRR3SHV1DC1FC): with smoke and heat vents and with draft curtains

Figure 79. Visibility (in ft) along *y* = 0 ft at 600 s for HRR3 Runs 15 and 16. The burning racks are located on the corner nearest to the draft curtain location. The vertical coordinate has been stretched.

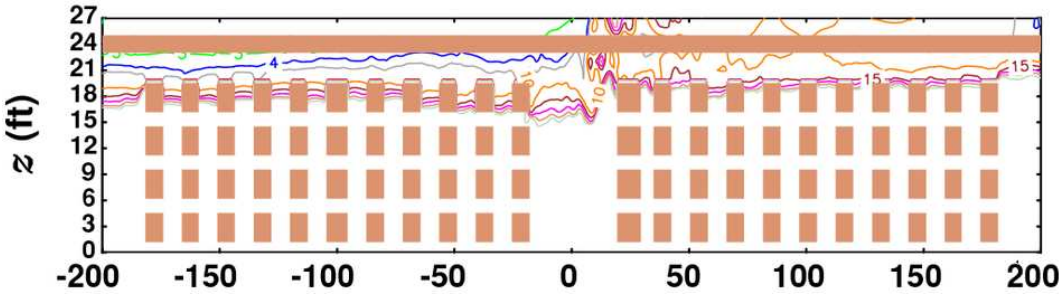

a) Run 15 (HRR3SHV1DC0FC): with smoke and heat vents and without draft curtains

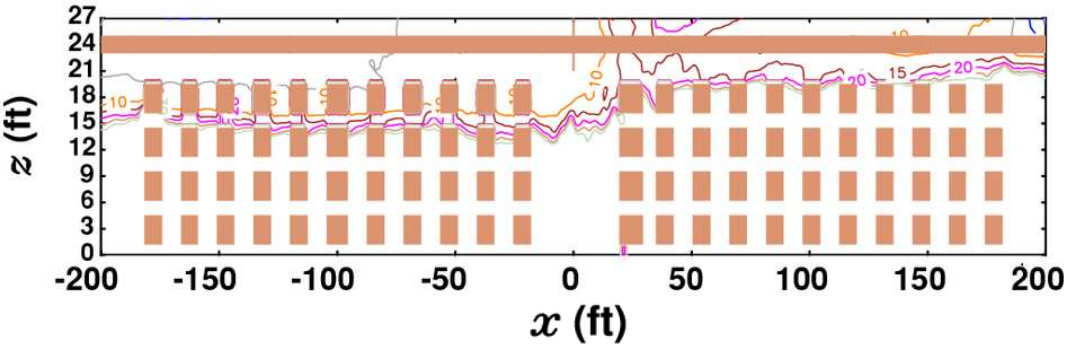

b) Run 16 (HRR3SHV1DC1FC): with smoke and heat vents and with draft curtains

Figure 80. Visibility (in ft) along *y* = 0 ft at 900 s for HRR3 Runs 15 and 16. The burning racks are located on the corner nearest to the draft curtain location. The vertical coordinate has been stretched.

Figure 78 shows that smoke had traveled to the western roof vent zone for both Runs 15 and 16. Because of the proximity of the burning racks to the curtain, the ceiling jet was able to travel under the draft curtain in appreciable amounts. However, the smoke layer interface at 300 s was greater for Run 15 than for Run 16. By 600 s, Figure 79 shows a deeper smoke layer in the western zone and a thinner smoke layer in the east zone for Run 16. It was relatively uniform for Run 15. Near the end of the runs at 900 s, the situation was much the same for Run 15 in Figure 80 but the western zone interface had dropped to the level of the top of the third commodity tier for Run 16 and the east interface was at the top of the fourth tier.

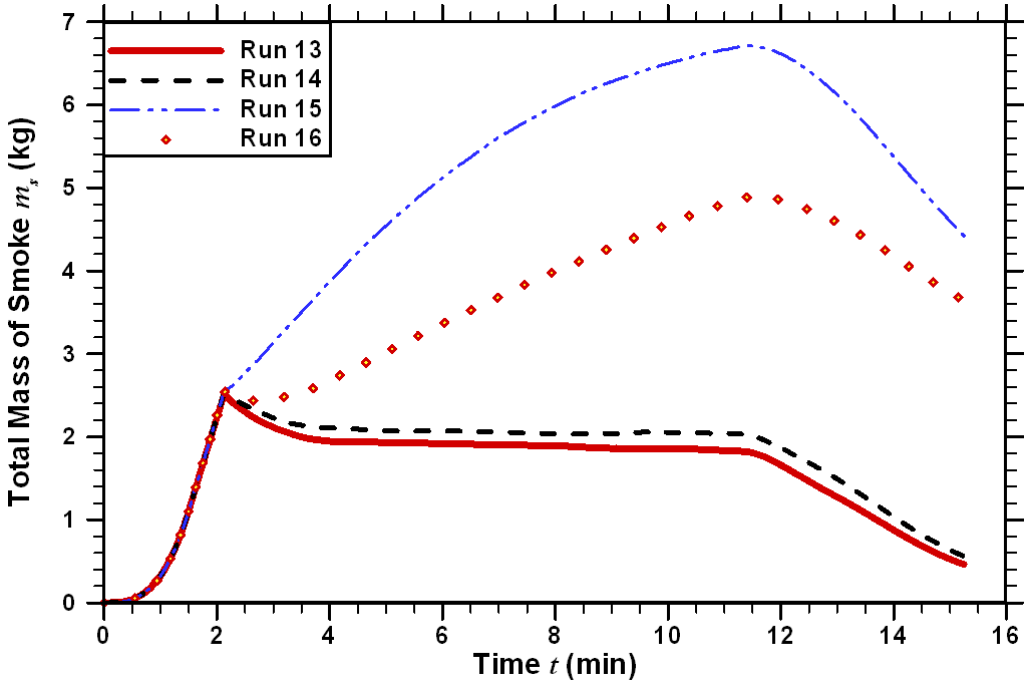

Figure 81. Comparison of the net building smoke masses for Runs 13 - 16 (HRR3SHV1DC1R, HRR3SHV1DC1RC, HRR3SHV1DC0FC, HRR3SHV1DC1FC).

Figure 81 compares the net building smoke mass time histories for Runs 13 – 16. The performance of Runs 13 and 14 is very similar to that of Runs 9 and 10. From this it can be concluded that this is the standard performance of smoke and heat vents with draft curtains when dealing with HRR3 in racks that are well within the roof vent zone. As was demonstrated in the visibility plots, because of the proximity of the burning racks to the western roof vent zone, more smoke accumulated in the western of the warehouse than had been the case for any other runs with vents. So, whereas for Run 8 the smoke mass was relatively constant after the vents opened, it continued to rise for Run 15 although at a reduced rate. Likewise, for Run 9 the smoke mass began to fall after the vents opened while for Run 16 it continued to rise, but at a lower rate still than Run 15. So, even with the burning racks adjacent to the curtain, draft curtains improve the performance of smoke and heat vents while the fire is active. Based on Figure 81 it can be estimated that the curve for Run 15 will drop below that of Run 16 at some time beyond 16 min. Because Run 15 has no draft curtain, the smoke in the western roof vent zone will be transported to the east zone to be exhausted. This will occur in Run 16 as well but, as Figure80 indicates, only for smoke below the six foot depth of the draft curtain. Smoke above this will remain in the western roof vent zone. If the system is equipped with a release switch then this can be used to manually open the vents in the western zone during overhaul. This would effectively clear out the smoke contained in the western zone.

4.0 Discussion

The simulations performed in this study were based upon the experimental work of McGrattan et al [1998]. The results with respect to sprinkler operation are consistent with that work both in terms of the time to first sprinkler operation and the total number of sprinklers operating. The simulations clearly span the range of performance that can be expected in practice with sprinkler operations numbering from four up to the number of sprinklers in the design area.

Comparison of sprinkler operations between vented and unvented cases clearly shows that the operation of sprinklers was not affected by smoke and heat vents or by smoke and heat vents with draft curtains. The time to first sprinkler operation, the number of sprinkler operations and the pattern of operation were not impacted by the venting system. The use of a one minute delay in vent operation allowed all sprinklers capable of applying water to the fire to operate before the vents operated, thus assuring that the sprinkler system performance would be unimpeded by the venting.

The use of ganged smoke and heat vents markedly reduced the smoke logging of the building. The visibility in the warehouse was measurably and qualitatively enhanced. The total quantity of smoke mass remaining in the building was found to be an effective metric for smoke and heat vent performance. Typically, venting reduced the total smoke load in the facility by an order of magnitude and drastically reduced the total exposure of goods to smoke.

The impact of smoke and heat venting upon the visibility and general environment for firefighting was significantly enhanced. For challenging fires without smoke and heat venting, loss of visibility was nearly complete. With smoke and heat venting, excellent visibility was maintained throughout the facility including in the area of actual sprinkler operation.

While excellent smoke and heat vent performance was realized even without draft curtains, the inclusion of draft curtains delineating sprinkler coverage areas enhanced smoke extraction and limited lateral movement of smoke to areas outside the sprinkler coverage area where the fire occurred. Lateral smoke movement was shown to have negative impacts upon goods stored high in the racks and upon every object from the top of the racks to the ceiling. For fires with sprinkler operations adjacent to draft curtains, smoke drag down allowed smoke to move under the draft curtain. While this allowed some smoke exposure for goods high in the racks in the adjacent zone, overall performance remained

quite satisfactory. The modeling results indicate that draft curtains offer value to owners and their insurers by limiting smoke damage to the building and contents outside the coverage area of the sprinkler system where the fire occurred.

While only limited data for smoke production from controlled fires is available in the literature, the modeling results show that smoke and heat venting is very effective in removing smoke even for heat release rates associated with controlled fires. This facilitates fire department operations to extinguish the controlled fire.

5.0 Conclusions

This investigation has shown that ganged operation of smoke and heat vents is highly effective in removing heat and smoke from the building. The action of the smoke and heat vent system markedly improved the visibility throughout the building and significantly reduced the exposure of the building and contents to smoke. Draft curtains, although not vital to the performance of the smoke and heat vents, did limit lateral spread of smoke to other zones and enhanced the extraction of smoke from the building. The operation of the smoke and heat vent system had no effect on the operation of sprinklers and as such maintained the operational effectiveness of the sprinkler system while improving the conditions within the building in support of fire department operations.

References

1. Baum, H.R., McGrattan, K.B., & Rehm, R.G. (1994), "Simulation of Smoke Plumes from Large Pool Fires", in *Proceedings of the 25th International Symposium on Combustion*, pages 1463—1469, The Combustion Institute, Pittsburgh, PA.

2. Baum, H. R., McGrattan, K. B., & Rehm, R. G. (1996), "Large Eddy Simulations of Smoke Movement in Three Dimensions," in C. Franks & S. Grayson (eds.), *Interflam '96* (pp. 189-198), London: Interscience Communications Ltd.

3. Baum, H. R., McGrattan, K. B., & Rehm, R. G. (1997), "Three Dimensional Simulation of Fire Plume Dynamics," in Y. Hasemi (ed.), *Fire Safety Science-Proceedings of the 5th International Symposium* (pp. 511-522), Boston, MA: International Association for Fire Safety Science.

4. Beyler, C. (1999), Smoke and Heat Venting in Sprinklered Buildings, Baltimore, MD: HAI Report to Code Transition Committee.

5. Beyler, C. (2006), Smoke and Heat Vents: A Review of the Technology and the Way Forward to the Next Generation, Baltimore, MD: HAI Report to Code Transition Committee.

6. Beyler, C. L., and Cooper, L. Y. (2001), "Interaction of Sprinklers with Smoke and Heat Vents," *Fire and Materials*, **37**:1, 9-35.

7. Bird, R. B., Stewart, W. E., & Lightfoot, E. N. (1960), *Transport Phenomena*, New York: John Wiley & Sons.

8. Cooper, L. Y. (2002), "Smoke and Heat Venting," in P. J. DiNenno, D. Drysdale, C. L. Beyler, W. D. Walton, R. L. P. Custer, J. R. Hall, & J. M. Watts (eds.), *SFPE Handbook of Fire Protection Engineering*, 3rd ed., (pp. 3-219–3-242), Quincy, MA: SFPE.

9. Drysdale, D. (1999), *An Introduction to Fire Dynamics*, 2nd ed., Chichester, UK: Wiley.

10. Floyd, J., & Lattimer, B.Y. (2004), "Validation of FDS V4 Boundary Heat Flux Predictions for a Corner Fire," *Interflam 2004*, S. Grayson, ed., London: Interscience Communications, pp. 1305-1292.

11. Golinveaux, J. E., & Hankins, H. B. (2003), "Sprinkler Systems for Storage Facilities," in Cote, A. E., ed., *Fire Protection Handbook*, 19th ed., Quincy, Massachusetts: National Fire Protection Association, 10-213-10-233.

12. Hamins, A., and McGrattan, K. B. (2006), Verification and Validation of Selected Fire Models for Nuclear Power Plant Applications, Volume 7: Experimental Uncertainty, U.S. Nuclear Regulatory Commission, Office of Nuclear Regulatory Research (RES), Rockville, MD, and Electric Power Research Institute (EPRI), Palo Alto, CA. NUREG-1824 and EPRI 1011999, Jan. 2006.

13. Heskestad, G. (2003), "Venting Practices," in Cote, A. E., ed., *Fire Protection Handbook*, 19th ed., Quincy, Massachusetts: National Fire Protection Association, 12-127-12-143.

14. Hinkley, P. L., Hansell, G. O., Marshall, N. R., & Harrison, R. (1993), "Large-Scale Experiments with Roof-Vents and Sprinklers. Part 1. Temperature and Velocity Measurements in Immersed Ceiling Jets Compared with a Simple Model," *Fire Science and Technology*, **13**:1/2, pp. 19–41.

15. Hinkley, P. L., Hansell, G. O., Marshall, N. R., & Harrison, R. (1993), "Large-Scale Experiments with Roof-Vents and Sprinklers. Part 2. The Operation of Sprinklers and the Effect of Venting with Growing Fires," *Fire Science and Technology*, **13**:1/2, pp. 43–59.

16. Holman, J. P. (1986), *Heat Transfer*, 6th ed., New York, McGraw Hill.

17. Jin, T. (2002), "Visibility and Human Behavior in Fire Smoke," in P. J. DiNenno, D. Drysdale, C. L. Beyler, W. D. Walton, R. L. P. Custer, J. R. Hall, & J. M. Watts (eds.), *SFPE Handbook of Fire Protection Engineering*, 3rd ed., (pp. 2-42–2-53), Quincy, MA: SFPE.

18. Klote, J. H., and Milke, J. A. (2002), *Principles of Smoke Management*, Atlanta, GA: American Society of Heating, Refrigerating, and Air-Conditioning Engineers, Inc. (ASHRAE).

19. Kung, H. C., Spaulding, R. D., and You, H-Z., (1984), Response of Sprinkler Links to Rack Storage Fires, JI 0G2E7.RA (2), Factory Mutual Research Corporation, (FMRC), Norwood, Massachusetts, November 1984.

20. Kung, H.-C., You, H.-Z., and Spaulding, R. (1986), "Ceiling Flows of Growing Rack Storage Fires," *Twenty-first Symposium (International) on Combustion*, The Combustion Institute, Pittsburgh, PA, pp. 121-128.

21. Lee, J. (1987), "Stored Commodity Fire Test Program, Part 1: Fire Products Collector Tests," Technical Report J.I. 0N0R4 RU/0N1J8 RU, prepared for The Society of the Plastics Industry, Factory Mutual Research Corporation, Norwood, MA.

22. Lienhard IV, J. H., & Lienhard V, J. H. (2006), *A Heat Transfer Textbook*, 3rd ed., Cambridge, MA: Phlogiston Press.

23. McGrattan, K. B., ed. (2005), Fire Dynamics Simulator (Version 4), Technical Reference Guide, NIST Special Publication 1018, National Institute of Standards and Technology, Gaithersburg, Maryland, September 2005.

24. McGrattan, K.B., Baum, H.R., & Rehm, R.G. (1996), "Numerical Simulation of Smoke Plumes from Large Oil Fires", *Atmospheric Environment*, 30(24):4125-4136.

25. McGrattan, K.B., Baum, H.R., Walton, W., & Trelles, J. (1997), Smoke Plume Trajectory from In Situ Burning of Crude Oil in Alaska--Field Experiments and Modeling of Complex Terrain, Technical Report NISTIR 5958, National Institute of Standards and Technology, Gaithersburg, Maryland.

26. McGrattan, K., and Dreisbach, J. (2006), Verification and Validation of Selected Fire Models for Nuclear Power Plant Applications, Volume 6: FDS, U.S. Nuclear Regulatory Commission, Office of Nuclear Regulatory Research (RES), Rockville, MD, and Electric Power Research Institute (EPRI), Palo Alto, CA. NUREG-1824 and EPRI 1011999, Jan. 2006.

27. McGrattan, K. B., and Forney, G. P. (2004), Fire Dynamics Simulator (Version 4), User's Guide, NIST Special Publication 1019, National Institute of Standards and Technology, Gaithersburg, Maryland, July 2004.

28. McGrattan, K. B., Hamins, A., & Stroup, D. (1998), Sprinkler, Smoke & Heat Vent, Draft Curtain Interaction - Large Scale Experiments and Model Development, Technical Report NISTIR 6196-1, National Institute of Standards and Technology, Gaithersburg, Maryland.

29. Mulholland, G. W. (2002), "Smoke Production and Properties," in P. J. DiNenno, D. Drysdale, C. L. Beyler, W. D. Walton, R. L. P. Custer, J. R. Hall, & J. M. Watts (eds.), *SFPE Handbook of Fire Protection Engineering*, 3rd ed., (pp. 2-258–2-268), Quincy, MA: SFPE.

30. Mulholland, G. W., and Croarkin, C. (2000), "Specific Extinction Coefficient of Flame Generated Smoke," *Fire and Materials*, **24**:5, 227-230.

31. Najafi, B., Salley, M.H., Joglar, F., and Dreisbach, J. (2006), Verification and Validation of Selected Fire Models for Nuclear Power Plant Applications, Volume 1: Main Report, U.S. Nuclear Regulatory Commission, Office of Nuclear Regulatory Research (RES), Rockville, MD, and Electric Power Research Institute (EPRI), Palo Alto, CA. NUREG-1824 and EPRI 1011999, Jan. 2006.

32. NFPA 92A (2006), *Standard for Smoke-Control Systems Utilizing Barriers and Pressure Differences*, Quincy, Massachusetts: National Fire Protection Association.

33. NFPA 92B (2005), *Standard for Smoke Management Systems in Malls, Atria, and Large Spaces*, Quincy, Massachusetts: National Fire Protection Association.

34. NFPA 204 (2007), *Guide for Smoke and Heat Venting*, Quincy, Massachusetts: National Fire Protection Association.

35. Press, W. H., Teukolsky, S. A., Vetterling, W. T., & Flannery, B. P. (1986), *Numerical Recipes in FORTRAN: the Art of Scientific Programming*, 2nd ed., Cambridge, England: Cambridge University Press.

36. Quintiere, J. G. (1998), *Principles of Fire Behavior*, Albany, New York: Delmar Publishers.

37. Rehm, R.G. & Baum, H.R. (1978), "The Equations of Motion for Thermally Driven, Buoyant Flows", *Journal of Research of the National Bureau of Standards*, 83(3):297--307.

38. Schulte, R. C. (2000), "Sprinklers and Roof Vents?" *Plumbing Engineer*, May, 10-15.

39. Spaulding, R. (1988), "Evaluation of Polyethylene and Polyethylene Terepthalate Commodities Using the Fire Products Collector," Technical Report J.I. 0P0J2 RA, Factory Mutual Research Corporation, Norwood, MA.

40. Tewarson, A. (2002), "Generation of Heat and Chemical Compounds in Fires," in DiNenno, P. J., et al. (eds.), *SFPE Handbook of Fire Protection Engineering*, 3rd ed., Quincy, MA: Society of Fire Protection Engineers, pp. 3-82—3-161.

41. Trelles, J., & Beyler, C. (1999a), The Impact of Smoke and Heat Vents with Curtains on Smoke and Heat Conditions in a Typical Warehouse – Modeling Results, Baltimore, MD: March-dated HAI Report to Code Transition Committee.

42. Trelles, J., & Beyler, C. (1999b), The Effect of Increased Activation Temperature on Vent Operation, Baltimore, MD: August-dated HAI Report to Code Transition Committee.

43. Trelles, J., & Beyler, C. (1999c), Exploratory Modeling in Support of the Design Method for Smoke and Heat Vents in a Sprinklered Facility, Baltimore, MD: August-dated HAI Report to Code Transition Committee.

44. Trelles, J., Mawhinney, J. R., & DiNenno, P.J. (2004), "Characterization of a High-Pressure Multi-jet Water Mist Nozzle for the Purposes of Computational Fluid Dynamics Modeling," in

J. A. Capote Abreu (ed.), *Computational Simulation Models in Fire Engineering and Research*, Santander, Spain: GIDAI, October 20, 2004, pp. 261-270.

45. Van Wylen, G. J., & Sonntag, R. E. (1986), *Fundamentals of Classical Thermodynamics*, 3rd ed., New York: John Wiley & Sons.

46. Yao, C. (1997), "Overview of Sprinkler Technology Research," *Fire Safety Science-Proceedings of the Fifth International Symposium*, Y. Hasemi (Ed.), International Association for Fire Safety Science, Boston, MA, pp. 93-110.

47. You, H.-Z., and Kung, H.-C. (1984), "Strong Buoyant Plumes of Growing Rack Storage Fires," *Twentieth Symposium (International) Symposium on Combustion*, The Combustion Institute, Pittsburgh, PA, pp. 1547-1554.

48. Yu, H.-Z., Lee, J. L., & Kung, H.-C. (1994), "Suppression of Rack-Storage Fires by Water," *Fire Safety Science-Proceedings of the Fourth International Symposium*, T. Kashiwagi (Ed.), International Association for Fire Safety Science, Boston, MA, pp. 901-912.

49. Yu, H.-Z., and Stavrianidis, P. (1994), "The Transient Ceiling Flows of Growing Rack Storage Fires" *Fire Safety Science-Proceedings of the Fourth International Symposium*, T. Kashiwagi (Ed.), International Association for Fire Safety Science, Boston, MA, pp. 281-290.

50. Zalosh, R. G. (2003), *Industrial Fire Protection Engineering*, Chichester, UK: Wiley.

Nomenclature

Roman

A	Area [m^2]
C	Concentration [ ]
C_D	Discharge coefficient [ ]
c	Specific heat (of a solid) [J/(kg·K)]
c_c	Contrast [ ]
c_p	Specific heat at constant pressure [J/(kg·K)]
c_v	Specific heat at constant pressure [J/(kg·K)]
d	Diameter [m]
g	Acceleration of gravity [9.81 m/s^2]
I	Intensity [W/m^2]
K	Extinction coefficient [m^{-1}]
K_m	Specific extinction coefficient [m^2/kg]
k	Thermal conductivity [W/(m·K)]
L	Length [m]
$\mathcal{M}$	Molar mass [kg/kmol]
m	Mass [kg]
p	Pressure [Pa]
Q	Total heat (energy) [J]
q	Local heat (energy) [J]
R	Ideal gas constant [J/(kg·K)]
S	Visibility [m]
T	Temperature [°C]
t	Time [s]
u	Velocity [m/s]
V	Volume [m^3]
$\mathbf{x}$	The Cartesian position vector, equal to (x , y , z) [(m,m,m)]
x	The first Cartesian coordinate [m]
y	The second Cartesian coordinate [m]

y	A yield based on the fuel mass [kg/kg]
z	The third Cartesian coordinate [m]

Greek

α	Thermal diffusivity [m^2/s]
γ	Rossin-Rammler exponent [ ]
Δ	The difference operator [ ]
ΔH_C	Heat of combustion [J/kg]
ρ	Density [kg/m^3]
σ	Log-normal variance [ ]

Superscripts

—	Denotes a quantity on a molar basis
$*$	Denotes a dimensionless quantity
$\bullet$	Quantity per unit time [s^{-1}]
$''$	Quantity per unit area [m^{-2}]
$'''$	Quantity per unit volume [m^{-3}]

Subscripts

0	Denotes an initial quantity
F	Refers to a fuel quantity
i	An index for a member of a sequence, array, or vector
j	An index for a member of a sequence, array, or vector
m	Refers to a mean quantity
s	Refers to a smoke quantity
T	Denotes a total quantity
∞	Denotes an ambient quantity

List of Abreviations

AAMA	American Architectural Manufacturers Association
BFRL	Building and Fire Research Laboratory
CFD	Computational Fluid Dynamics
HRR	Heat release rate
IBC	International Building Code
FDS	Fire Dynamics Simulator
FM	Factory Mutual
FMRC	Factory Mutual Research Corporation
IFS	Industrial Fire Simulator
LES3D	Three dimensional large eddy simulation
NFPA	National Fire Protection Association
NFPARF	NFPA Research Foundation
NIST	National Institutie of Standards and Technology
SFPE	Society of Fire Protection Engineers
US	United States